Fall 2004

Layer-by-layer nanoassembly combined with microfabrication techniques for microelectronics and microelectromechanical systems

Jingshi Shi
Louisiana Tech University

Recommended Citation

NOTE TO USERS

This reproduction is the best copy available.

UMI®

LAYER-BY-LAYER NANOASSEMBLY COMBINED WITH

MICROFABRICATION TECHNIQUES FOR

MICROELECTRONICS AND MICROELECTROMECHANICAL

SYSTEMS

By

Jingshi Shi, B. S.

A Dissertation Presented in Partial Fulfillment
of the Requirement for the Degree
Doctor of Philosophy in Engineering

COLLEGE OF ENGINEERING AND SCIENCE
LOUISIANA TECH UNIVERSITY

November 2004

UMI Number: 3148960

INFORMATION TO USERS

The quality of this reproduction is dependent upon the quality of the copy submitted. Broken or indistinct print, colored or poor quality illustrations and photographs, print bleed-through, substandard margins, and improper alignment can adversely affect reproduction.

In the unlikely event that the author did not send a complete manuscript and there are missing pages, these will be noted. Also, if unauthorized copyright material had to be removed, a note will indicate the deletion.

UMI®

LOUISIANA TECH UNIVERSITY

THE GRADUATE SCHOOL

Nov. 12, 2004
Date

We hereby recommend that the dissertation prepared under our supervision

by _____ JINGSHI SHI _____

entitled LAYER-BY-LAYER NANOASSEMBLY COMBINED WITH MICROFABRICATION

TECHNIQUES FOR MICROELECTRONICS AND MICROELECTROMECHANICAL SYSTEMS

be accepted in partial fulfillment of the requirements for the Degree of

DOCTOR OF PHILOSOPHY IN ENGINEERING

Yuri Lvov
Supervisor of Dissertation Research

Ray Sterling
Head of Department

Engineering
Department

Recommendation concurred in:

Andrei Poun / DSM

Hai

S. Schmit

Ji Fang   YL.

Advisory Committee

Approved:
Bala Ramachandaa
Director of Graduate Studies

Sven Nagy
Dean of the College

Approved:
_____
Dean of the Graduate School

GS Form 13
(5/03)

ABSTRACT

The objective of this work is to investigate the combination of layer-by-layer self-assembly with microfabrication technology and its applications in microelectronics and MEMS.

One can assemble, on a standard silicon wafer, needed multilayers containing different nanoparticles and polymers and then apply various micromanufacturing techniques to form microdevices with nanostructured elements.

Alternate layer-by-layer self-assembly of linear polyions and colloidal silica at elevated temperatures have been firstly studied by QCM and SEM. LbL self-assembly and photolithography were combined to fabricate an indium resistor. The RTA method was employed in the fabrication. Hot-embossing technique as a reasonably fast and moderately expensive technique was used to replicate mold structures into thermoplastics. Microstamps with nanofeatures formed by this method can be applied on LbL nanoassembled multilayers. Finally, multiple ultrathin microcantilevers were developed by integrating LbL self-assembly, photolithography, wet etching, and ICP techniques. The purpose is to develop chemical/biosensor arrays for parallel, massive data gathering.

APPROVAL FOR SCHOLARLY DISSEMINATION

The author grants to the Prescott Memorial Library of Louisiana Tech University the right to reproduce, by appropriate methods, upon request, any or all portions of this Dissertation. It is understood that "proper request" consists of the agreement, on the part of the requesting party, that said reproduction is for his personal use and that subsequent reproduction will not occur without written approval of the author of this Dissertation. Further, any portions of the Dissertation used in books, papers, and other works must be appropriately referenced to this Dissertation.

Finally, the author of this Dissertation reserves the right to publish freely, in the literature, at any time, any or all portions of this Dissertation.

Author _____

Date _____

GS Form 14
(5/03)

TABLE OF CONTENTS

LIST OF TABLES

LIST OF FIGURES

ACKNOWLEDGMENTS

I would like to express my sincere gratitude and thanks to my advisor, Dr. Yuri Lvov, who has instructed me in the scientific method and honest attitude, and my co-advisor, Dr. Tianhong Cui, for his discussion and support. Their invaluable advice, continuous guidance, encouragement, and assistance have been necessary for completion of this dissertation. Special acknowledgments are extended to Dr. Frank Ji, Dr. Sandra Selmic, Mr. Ji Fang and Dr. Andrei Paun for their advice and for serving as advisory committee members for this dissertation.

The author would like to thank the staff at Institute for Micromanufacturing for their help and support on the process. Much gratitude is extended to Feng Hua, Xiaodong Yan, and Malcolm Prouty for their valuable discussion, support, and contributions.

Finally, I dedicate this dissertation to my parents whose love and encouragement accompanied me through this research.

CHAPTER ONE

INTRODUCTION

1.1 Nanotechnology and Nanofabrication

The semiconductor industry has seen a remarkable miniaturization trend, driven by many scientific and technological innovations. It is widely believed that these trends are likely to continue for at least another several years (Figure 1-1), but if the trend is to continue and provide even faster and cheaper computers, the size of microelectronic circuit components will soon need to reach the scale of atoms or molecules [1].

"Moore's Law" continues to drive semiconductor roadmap
- ~ 30% reduction in transistor size with each new technology
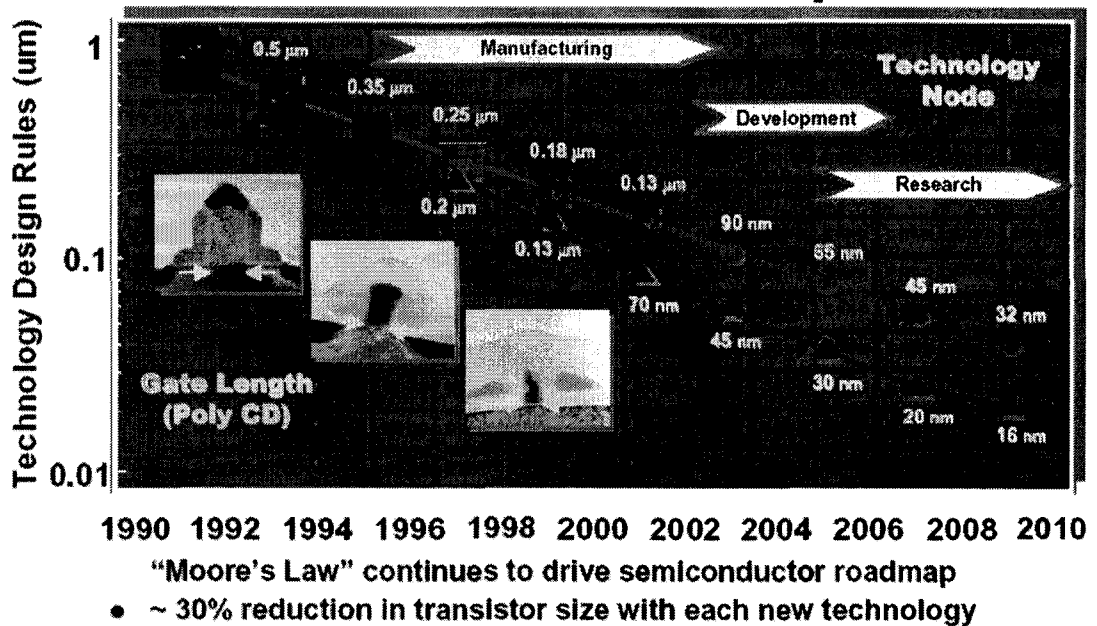
Figure 1-1 Overview of semiconductor manufacturing[2]

1

Photolithography, the technology used to manufacture computer chips and virtually all other microelectronic systems, can be refined to make structures smaller than 100 nanometers, but doing so is very difficult, expensive and inconvenient. The electronics industry is deeply interested in developing new methods for nanofabrication so that it can continue its long-term trend of building even smaller, faster and cheaper devices.

Therefore, we will have to develop a new "post-lithographic" manufacturing technology that will let us inexpensively build computer systems with mole quantities of logic elements that are molecular in both size and precision and are interconnected in complex and highly idiosyncratic patterns. Nanotechnology will let us do this.

Nanotechnology is concerned with materials and systems whose structures and components exhibit novel and significantly improved physical, chemical, and biological properties, phenomena, and processes due to their nanoscale size. The aim is to exploit these properties by gaining control of structures and devices at atomic, molecular, and supermolecular levels and to learn to efficiently manufacture and use these devices [3].

1.2 Nanofabrication

1.2.1 Top Down and Bottom Up

The potential benefits of nanotechnology are pervasive and impact materials and manufacturing, nanoelectronics and computer technology, medicine and health, aeronautics and space exploration, environment and energy, biotechnology and agriculture, even national security and some other government applications [4].

However, in order for this potential of nanotechnology to be realized, novel manufacturing methods deviating from scaled-down versions of currently practiced

technologies are required at the nanoscale. Originally, nanofabrication is defined as the design and manufacture of devices with dimensions measured in nanometers. One nanometer is 10^{-9} meter, or a millionth of a millimeter.

The two opposite approaches to nanofabrication have been labeled "top down" and "bottom up". In order to extend the macroscale properties effectively down to the nanoscale, traditional manufacturing techniques have been miniaturized for fabrication of nanostructures as in nanoelectronics, in a top–down approach such as "machining" or etching techniques. On the other hand, mono-atomic or molecular units, with their well known subatomic structure in isolation, offer the ultimate building blocks for a bottom–up, atom-by-atom manufacturing (Figure1-2). They illustrate the evolution of nanotechnology's sophistication.

Nanostructured Material

Assemble from Nano- building Blocks

- powder/aerosol compaction
- chemical synthesis

'Sculpt' from Bulk

- mechanical attrition (ball milling)
- lithography/etching...
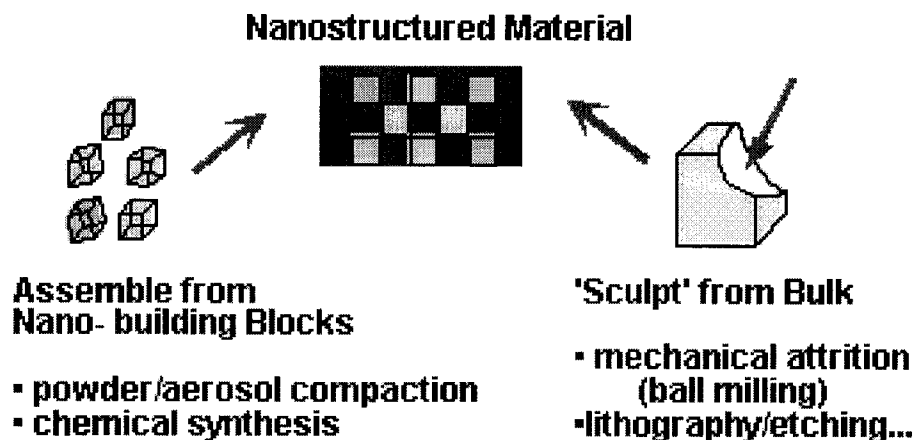
Figure 1-2 Schematic of variety of nanostructure synthesis and assembly approaches. Bottom-up method (left), Top-down method (right)[5]

Now, this concept was extended as a combination of both theoretical (analytical and computational) and experimental methodologies including the synthesis of nanomaterials and nanoparticles, fabrication and analysis processes; instrumentation and equipment for characterization and processing; theory, modeling, simulation and control; design and integration of nanodevices and systems [6].

1.2.2 Fabrication of Ultrathin Film

Driven by the large number of potential applications, in the last decade a lot of effort has been put in the study of ultrathin film formation. The current methods used for the design of ultrathin films include spin coating and solution casting, thermal deposition, polyion layer-by-layer assembly, chemical self-assembly, the Langmuir-Blodgett technique, and others. The optimal combination of molecular order and stability of films determines the practical usefulness of these technologies [7].

1.2.3 Spin-coating

Spin coating is generally regarded as the best way to deposit a uniform coating for many applications such as photoresist coating and dielectric/insulating layer coating. It gives optimal coverage with minimum material usage. This deposition technique is extremely desirable because the process is simple, safe, and inexpensive. In practice, spin coating involves four stages as shown in Figure 1-3 [8]. In the first stage, gravitational forces dominate. The surface is first wetted with excess polymer solution. In the second stage, rotational forces dominate. Film uniformity is often not present at this stage. In the third stage, viscous forces dominate. The film continues to get thinner but at a slower rate, and excess liquid continues to be expelled. In the final stage, evaporative forces dominate. Eventually, the film's thickness begins to stabilize as the evaporation of the solvent causes the viscosity of the liquid to rise sharply and overcome the centrifugal forces. What remains is an extremely thin and uniform film that is ready to be further processed.

1.2.4 Self-assembly

The self-assembly process, defined as the autonomous organization of components into structurally well-defined aggregates, is characterized by numerous beneficial attributes; it is cost-effective, versatile, and facile. The process occurs towards the system's thermodynamic minima, resulting in stable and robust structures [9]. As the name suggests, it is a process whereby the organization or the assembly into desired structures occurs through nature intended phenomena, either through physical or chemical processes or assisted by biomolecules to promote molecular selectivity and specificity. It is also a process in which defects are rejected energetically, and, therefore, the degree of perfection is relatively high [10][11]. There are numerous different mechanisms by which self-assembly of molecules and nanoclusters can be accomplished.

1.2.5 The Langmuir–Blodgett (LB) Technique

The Langmuir–Blodgett (LB) technique is one of the most conventional methods of nano-film fabrication in which organized systems of moieties are efficiently built one monolayer at a time. The method involves the monolayer transfer of the desired substance, originally adsorbed at the gas-liquid interface, to the substrate of choice [12]. The LB apparatus includes a Langmuir trough with a dipping device to lower or raise the substrate through the gas-liquid interface, an automated movable barrier, which moves during the deposition process in order to maintain a controlled surface pressure, and a surface pressure sensor that controls the movable barrier [13]. Unlike the traditional LB films of amphiphiles, which displayed poor thermal and mechanical stability, there has been progress reported on the robust monolayer fabrication of ligand-stabilized gold nanoclusters [14], semiconducting quantum dots [15], and polymeric films [16].

Although the LB technique has proven to yield consistently near-perfect long range ordering of monolayers and multilayers [17] of species that self-assemble at the liquid surface, it is cumbersome and time consuming. Additionally, the required apparatus comes at great cost and maintenance.

(a) First stage of spin-coating	(b) Second stage of spin-coating
(c) Third stage of spin-coating	(d) Fourth stage of spin-coating
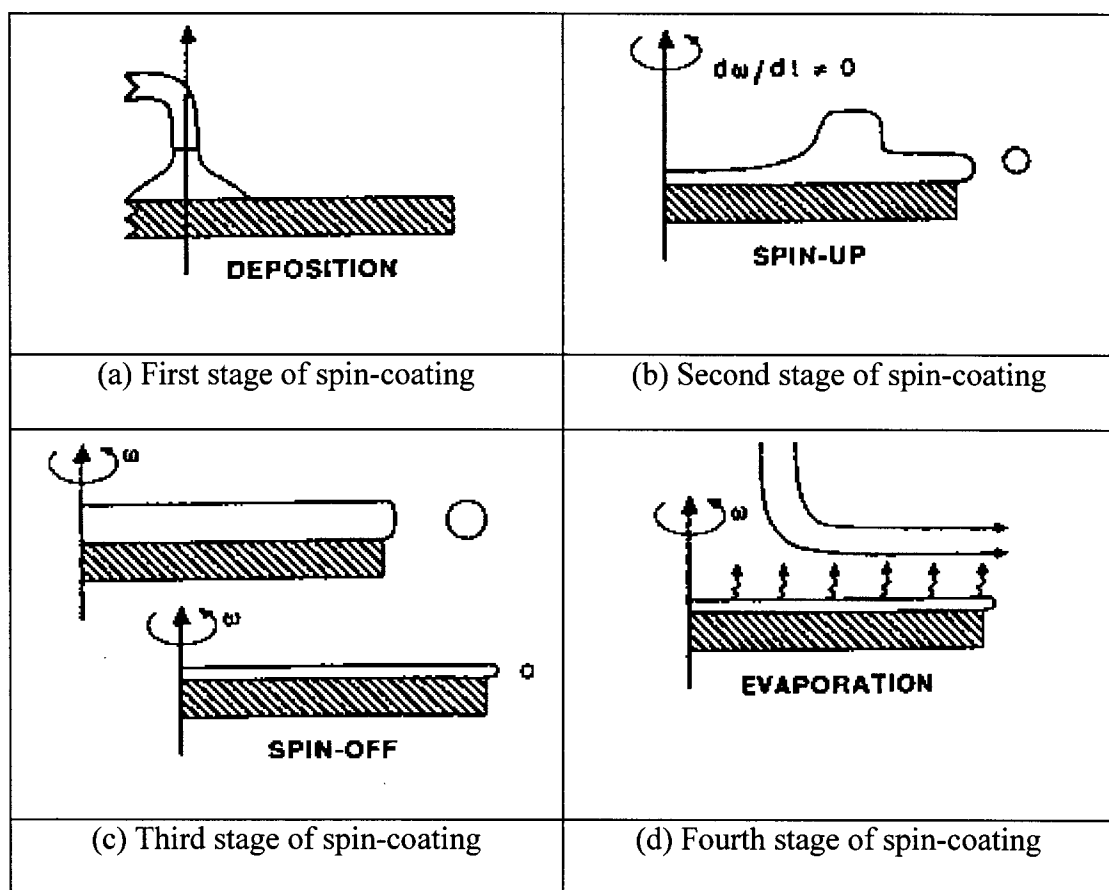
Figure 1-3 Four stages of spin-coating process[8]

1.2.6 Surface Forces

Surface forces could contribute directly as routes by which molecular self-assembly is realized; solvent evaporation in a controlled manner can bring colloids together into an ordered array, just as surface active agents can promote periodic network structures [18]. Moreover nanotemplates can be directly obtained utilizing microphase separation of block copolymers at various concentrations, based on the immiscibility of

the two polymer blocks [19]. With respect to the former, nanoparticles and other molecules can self-assemble in the presence of a thin liquid layer when its thickness is suitably controlled. For the case of colloids, it has been hypothesized that particles are assembled either by the convective flow at the boundary of the array or by the attractive force acting between particles due to surface tension at the film surface [20].

1.2.7 Chemical Self-assembly

Primary chemical bonding, namely covalent, serves as another interaction in the self-assembly of molecules and nanoclusters. Since covalent bonding is specific in fixating functional groups, robust and permanent structures will be yielded. Chemical self-assembly thus provides a method of achieving less dynamic self-assembled films.

The fabrication process is relatively easy, involving alternate immersions of the substrate into different solutions containing materials to be deposited, followed by a rinse in the appropriate solvent to remove the unbound species. It can be repeated until the desired structure is assembled, like the method of electrostatic self-assembly. Through molecular engineering and sensible selection of functional spacers/surfactants, we can promote molecular level self-assembly through covalent bonding.

1.2.8 Biomolecule-assisted Self-assembly

Currently, there is an escalating awareness in exploiting biomolecules, such as DNA and proteins, as construction materials for biomimetic synthesis of nanostructures. Numerous research groups have successfully developed protocols to employ DNA oligomers, proteins and other biomolecules as self-assembly promoters. Biological systems are characterized by complex structures, yet the assembly is dictated by highly

selective, non-covalent interactions, such as hydrogen bonding and van der Waals attractions.

Protein molecules have contributed as self-assembly promoters, especially with nanoparticulates. Biological molecules as self-assembly promoters allow systematic understanding and fabrication of complex yet functional structures at the molecular level. Microfabrication is an indispensable tool in the microelectronics and optoelectronics industry today.

Other mechanistic interactions for mediating self-assembly are hydration forces (hydrophilic and hydrophobic interactions), van der Waals forces, temperature control, and capillary forces.

1.3 LbL Self-assembly

1.3.1 General Principles

The most ordered macromolecular films are free-standing liquid crystalline films, but they are very unstable. The Langmuir-Blodgett method allows constructing lipid multilayers with a thickness from 5 to 500 nm, but only flat substrates can be covered by this film, and it has intrinsic defects at the lipid grain borders. Another method that can be applied to surface modification is a monolayer self-assembly, based on thiol or silane compounds [7]. By this method, one can achieve self-assembly of 2-5 nm thick organic layers on silicon or gold surfaces, but there is no simple means for thicker film construction. Other widely used methods for the industrial manufacture of thin films are spin coating and thermal deposition of macromolecules onto a substrate. Unfortunately, unlike the methods considered above, these methods do not allow one to control a film composition in the direction perpendicular to the surface.

One prevalent mechanism by which self-assembly processes occur is through electrostatic interactions between nanoparticles or molecules. This method was first introduced and reported by Iler in 1966 [21], who published the original technique of constructing multilayer films composed of positively and negatively charged colloidal particles, such as silica and alumina.

The assembly of alternating layers of oppositely charged linear or branched polyions and nanoparticles is simple and provides the means to form 5–500 nm thick films with monolayers of various substances growing in a pre-set sequence on any substrate at a growth step of about 1 nm. Mallouk [22] has called this technique "molecular beaker epitaxy," meaning that with simple instruments (exploiting the materials self-assembly tendency) one can produce molecularly organized films similar to the ones obtained with sophisticated and expensive molecular beam epitaxy technology.

1.3.2 Polycation / Polyanion Layer-by-Layer Assembly

A cleaned substrate of any shape and dimension is immersed into a dilute solution of a cationic polyelectrolyte, for a time optimized for the adsorption of a single monolayer (ca 1 nm thick). Afterwards, it is rinsed and dried. The next step is the immersion of the polycation-covered substrate into a dilute dispersion of polyanions or negatively charged nanoparticles (or any other nanosize charged species), also for a time optimized for the adsorption of a monolayer. Next, it is rinsed and dried. These operations complete the self-assembly of a polyelectrolyte monolayer and monoparticulate layer sandwich unit onto the substrate (Figure 1-4). Subsequent sandwich units are self-assembled analogously. Different nanoparticles, enzymes, and polyions may be assembled in a pre-planned order in a single film.
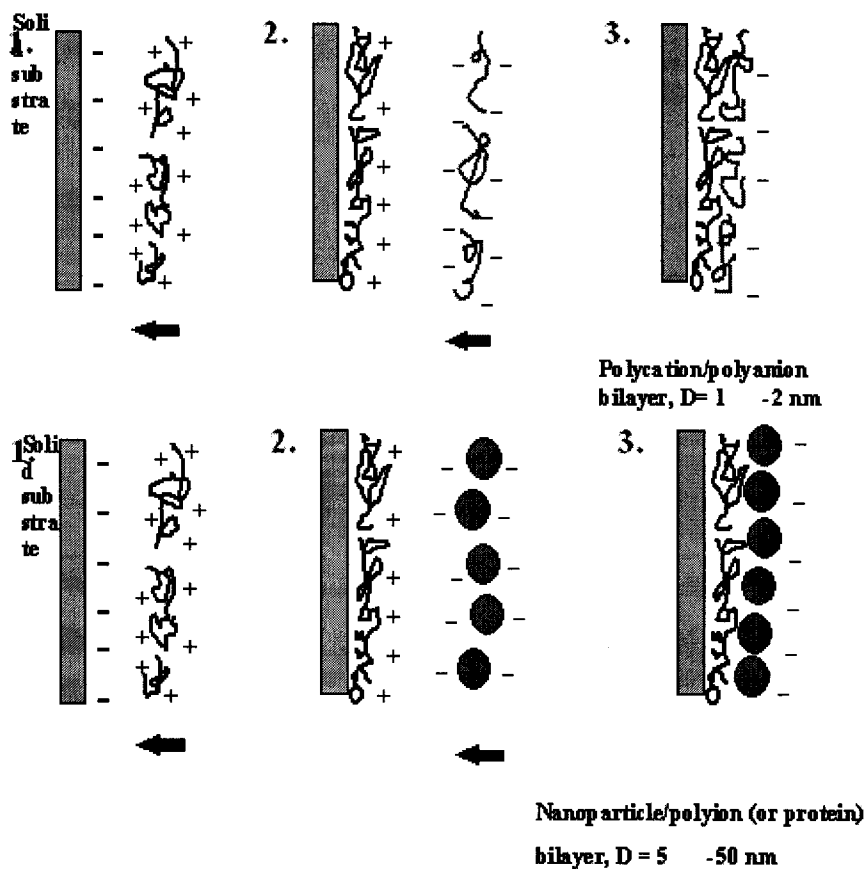
Figure 1-4 A scheme of the layer-by-layer assembly

The forces between nanoparticles and binder layers govern the spontaneous layer-by-layer self-assembly of ultrathin films. These forces are primarily electrostatic and covalent in nature, but they can also involve hydrogen bonding, hydrophobic, and other types of interactions. The properties of the self-assembled multilayers depend on the choice of building blocks used and their rational organization and integration along the axis perpendicular to the substrate.

The sequential adsorption of oppositely charged colloids was reported in a seminal paper in 1966 by Iler [21]. The electrostatic self-assembly was subsequently

"rediscovered" in the mid-nineties and extended to the preparation of multilayers of polycations and phosphonate ions, as well as to the layering of linear polyions, proteins and nanoparticles by Decher, Mallouk, Möhwald, Lvov, Rubner, Fendler, Hammond, Kunitake, Schlenoff, Kotov, and others. This self-assembly is now employed in the fabrication of ultrathin films from charged polymers (polyions) [23]-[35]; dyes [36][37]; nanoparticles (metallic, semiconducting, magnetic, insulating); clay nanoplates [38]-[40]; proteins [41]-[46]; and other supramolecular species [43]. The greatest advantage of this self-assembly is that any of these species can be absorbed layer-by-layer in any order. The oppositely charged species are held together by strong ionic bonds, and they form long-lasting, uniform and stable films. Self-assembly is economical and readily amenable to scaling-up for the fabrication of large-area defect-free devices on any kind and shape of surfaces.

The main idea of this method consists of the resaturation of polyion adsorption, which results in the alternation of the terminal charge after each layer is deposited. This idea is general and implies that there are no major restrictions in the choice of polyelectrolytes. It is possible to design composite polymeric films in the range of 5 to 1000 nm, with a definite knowledge of their composition. For the successful assembly of nanoparticle or protein multilayers, the alternation with linear polyion layers is important. Flexible linear polyions penetrate between nanoparticles and act as electrostatic glue. The concept of "electrostatic polyion glue," which keeps together neighboring arrays of nanoparticles, is central to this approach [42][43]. The self-assembled film contains amorphous polyion interlayers, and this organization "heals"

defects that arise because of the introduction of foreign particles during the process of film formation (dust, microbes) [26][43].

Linear polyions predominately used in the assembly are: polycations - poly(ethylenimine) (PEI), poly(dimethyldiallylammonium chloride) (PDDA), poly(allylamine) (PAH), polylysine, chitosan, polyanions - poly(styrenesulfonate) (PSS), poly(vinylsulfate), poly(acrylic acid), dextran sulfate, sodium alginate, heparin, and DNA. One can grow polymer nanocomposite films by means of the sequential adsorption of different material monolayers that employ hundreds of commercially available polyions. The only requirement is that there be a proper (positive/negative) alternation of the component charges.

1.3.3 Kinetics of Polyion Adsorption

For the time-dependent control of adsorption and monitoring of the assembly in situ, the quartz crystal microbalance method is quite suitable [47]. The kinetics of the adsorption process could be delineated by the QCM-technique, which is indispensable for establishing proper assembly conditions (e.g., a saturation adsorption time).

The multilayer assemblies are characterized by means of quartz crystal microbalance technique in two ways: 1) after drying a sample in a nitrogen stream we measured the resonance frequency shift and calculated an adsorbed mass by the Sauerbrey equation; or 2) by monitoring the resonator frequency during the adsorption process onto one side of the resonator which was in permanent contact with polyion solutions. While performing experiments in permanent contact with the polyion solution, we touched the surface of solutions with one side of the resonator, while the upper

electrode was kept open to air and the upper contact wire was insulated from the solution by a silicone paint covering.

The fitting of adsorption to an exponential law yields a first-order rate of adsorption for poly (styrenesulfonate) (PSS) $\tau = 2.5 \pm 0.2$ minutes and for polyallylamine (PAH) $\tau = 2.1 \pm 0.2$ minutes. This means that during the first 5 minutes about 87% of the material is adsorbed onto the charged support and $t = 8$ minutes ($t = 3\tau$) gives 95% full coverage. Typically, in most publications on polyion assembly, adsorption times of 5 to 20 minutes are used. One does not need to maintain an adsorption time with great precision: a minute more or less does not influence the layer thickness if we are at the saturation region. For other species, poly(dimethyldiallylammonium chloride) (PDDA), polyethyleneimine (PEI), montmorillonite clay, myoglobin, lysozyme, and glucose oxidase, the first-order rate of adsorption onto an oppositely charged surface was found to be 2, 3, 1.8, 3, 4 and 5 minutes respectively. Interestingly, 5 - 20 minutes is essentially greater than the diffusion-limited time (mass transport limitation), which is necessary for complete surface covering (for the used linear polyion concentrations it is a few seconds). Only for 45-nm silica/PDDA assembly do we have an example when 2 seconds time corresponds to the diffusion limited time for the SiO_2 monolayer adsorption.

One could suppose that linear polyion adsorption occurs in two stages: quick anchoring to a surface and slow relaxation. To reach a surface charge reversion during linear polyion adsorption one needs a concentration greater than 10^{-5} M [47]. The dependence of polyion layer thickness on concentration is not great: thus, in the concentration range of 0.1 - 5 mg/ml poly(styrenesulfonate)/poly(allylamine) (PSS/PAH) pair yielded a similar bilayer thickness. A further decrease in polyion

concentration (using 0.01 mg/ml) decreases the layer thickness of the adsorbed polyion. An increase in the component concentrations to 20-30 mg/ml may result in the non-linear (exponential) enlargement of the growth rate with adsorption steps, especially if an intermediate sample rinsing is not long enough.

1.3.4 First Layers and Precursor Film

At the very beginning of the alternate assembly process one often sees non-linear film growth. At the first 2 - 3 layers, smaller amounts of polyion are adsorbed as compared with further assembly, when the film mass and thickness increase linearly with the number of adsorption cycles. Tsukruk et al [48] explained this as an island-type adsorption of the first polyion layer on a weakly charged solid support. In the following two-three adsorption cycles these islands spread and cover the entire surface, and further multilayer growth occurs linearly. If a substrate is well charged then a linear growth with repeatable steps begins earlier.

In studying the possibility of using new compounds in the assembly, a precursor film approach was used. On a substrate (silver electrode of QCM resonator or quartz slide) we deposited 2 - 3 layers of polyions, and on this "polyion blanket", with a well defined charge of the outermost layer, an assembly of proteins, nanoparticles, or other compounds was produced. In a typical procedure, precursor films were assembled by repeating two or three alternate adsorptions of PEI and PSS. The outermost layer became "negative" or "positive", respectively.

QCM monitoring of multilayer growth was often the first stage of the assembly procedure elaboration. Initially, we estimated the time needed for a component's saturated adsorption in a kinetic experiment. Then, we performed the assembly typically

with 10 min alternate adsorption. After every other adsorption step, a layer was dried by a nitrogen stream and the QCM resonator frequency was registered. The frequency shift with adsorption cycles gave us the adsorbed mass at every assembly step. A linear film mass increase with the number of assembly steps indicated a successful procedure.

The following relationship is obtained between adsorbed mass M (g) and frequency shift ΔF (Hz) by taking into account the characteristics of the 9 MHz quartz resonators used [47]: $\Delta F = -1.83 \times 10^8 \, M/A$, where $A = 0.16 \pm 0.01$ cm^2 is the surface area of the resonator. One finds that a 1 Hz change in ΔF corresponds to 0.9 ng, and the thickness of a film may be calculated from its mass. The adsorbed film thickness at both faces of the electrodes (d) is obtainable from the density of the protein / polyion film (ca 1.3 g/cm^3) and the real film area: $d(nm) = -(0.016 \pm 0.02) \, \Delta F \, (Hz)$. The scanning electron microscopy data from a number of protein / polyion and linear polycation / polyanion film cross-sections permitted us to confirm the validity of this equation. Another powerful method for polyion film characterization was small-angle X-ray and neutron reflectivity.

1.3.5 Multilayer Structure

X-ray or neutron reflectivity measurements of polyion films show patterns with profound intensity oscillations, as demonstrated in Figure 1-5. They are so-called Kiessig fringes, due to the interference of radiation beams reflected from interfaces solid support/film and air/film. From the periodicity of these oscillations one can calculate the film thickness (with the help of the Bragg-like equation and taking into account refraction phenomena which are essential at small-angles). Growth steps for a bilayer of 1.1 - 2.0 nm are typical for alternate linear polyion assembly, and a thickness of one layer often

equals to half of this value [1]-[27]. These values correspond to a polyion cross-section and show that in one cycle of excessive adsorption we have approximately one monolayer coverage of the substrate. The nanoparticle/polyion bilayer thickness is determined by the diameter of the particle. Model fitting of X-ray data gives a surface roughness of the polyion film on an order of 1 nm. Atomic force microscopy and scanning electron microscopy data revealed a surface roughness of 1 - 2 nm [34]. Polyion films are insoluble in water and in many organic solvents and are stable to 280°C [33] [44][45].

Neutron reflectivity analysis of the films composed of alternate layers of deuterated PSS and hydrogen containing PAH has proved that polyanion/polycation films possess not only a high uniform thickness but also a multilayer structure[28]-[30]. The interfaces between layers in polyion films are not sharp, and partial interpenetration (30-40% of their thickness) between neighboring polymeric layers takes place [29][30]. A distinct spatial component separation may be reached between the first and the third or fourth neighboring polyion layers. In the neutron reflectivity experiments with the selectively deuterated component (usually d-PSS), it was possible to observe 1-3 Bragg reflections in addition to Kiessig fringes. This observation was not possible in the X-ray reflectivity experiments because of a small scattering contrast of neighboring polycations and polyanions, and because of their large interpenetration. X-ray Bragg reflections from the alternate gold nanoparticle/poly(allylamine) multilayers were observed by Schmitt, Decher and others [39]. They demonstrated that in order to have good spatial separation between gold layers in the film, one needs to make a thicker polyion interlayer (of 3-4 PSS/PAH bilayers). In a similar approach we formed the four-step unit cell multilayers of

myoglobin, deuterated, and "usual" poly(styrenesulfonate): (myoglobin/deuterated-PSS/myoglobin/PSS)$_9$. A Bragg-reflection in the neutron reflectivity curve of this four-step unit cell multilayer was observed (Figure 1-5). The film's total thickness was calculated at 94.0 nm, and the four-unit cell thickness was 11.1 nm.
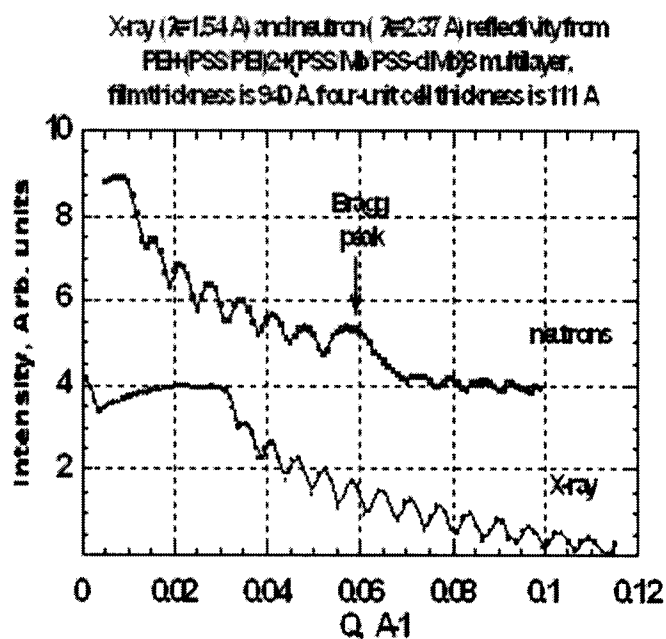
Figure 1-5 Small-angle X-ray and neutron reflectivity curves from (PSS/myoglobin/deuterated PSS/myoglobin)$_8$ multilayer

The polycation/polyanion bilayer thickness depends on the charge density of the polyions. It was shown that more than 10% of polyion side groups have to be ionized for a stable reproducible multilayer assembly via alternate electrostatic adsorption [32]. High ionization of polyions results in a smaller step of film growth (1 - 2 nm) and lower ionization gives a larger growth step (3 - 6 nm). It can be reached either by adding salt to a polyion solution (as discussed above for strong polyelectrolytes, such as PDDA and PSS), or by varying the pH for weak polyelectrolytes (e.g., polyacrylic acid (PAA) and poly(allylamine) (PAH), as was analyzed by Rubner et al [31]). Direct zeta-potential

measurements confirmed a symmetric positive/negative alternation of the polycation/polyanion multilayer's outermost charge with adsorption cycles [32].

1.4 Patterning Techniques

To use LbL-multilayers in devices, we have to provide film ordering not only in a vertical direction but also in the planar direction. This is critical for nanodevice production, such as nanoelectronic chips or NEMS (Nano Electro Mechanical Systems) [55]-[58].

There are works on applications of the layer-by-layer assembly on two-dimensional (2-D) patterns [59]-[63]. They are based mostly on the microprinting of thiol compounds on gold and further assembly of the polyion multilayers on charged patterns, and they were developed by Hammond et al. [59]-[62] This strategy is designed to produce patterns by stamping onto substrates chemicals with different functionalities, i.e. polyion adhesive or resisting. The polyions were directed only to charge "attractive" regions and were repelled from the resistant regions. Whitesides et al [62] crystallized latex particles in capillary channels produced by PDMS micromolding and made 3-D ensembles of 450-nm spheres with resolution of ca.1 μm. In another approach [63], poly(pyrrole) and poly(styrenesulfonate) were LbL-assembled on the 2-D charged micropattern produced on fluoropolymer by plasma treatment. The three methods described were quite successful but restricted in applications by substrate materials (gold, fluoropolymers) or by necessity of special plastic stamps. We presented two approaches to realize 2-D patterning of self-assembled multilayers by silicon based lithographical technology, which is a well-established industrial process.

1.5 Photochemical Lithography

Photolithography, literally meaning *light-stone-writing* in Greek, is the process by which patterns on a semiconductor material can be defined using light. It is the means by which the small-scale features of integrated circuits are created. Before the resist is applied to the substrate, the surface is cleaned to remove any traces of contamination from the surface of the wafer such as dust or organic, ionic and metallic compounds. The cleaned wafer is subject to priming, to aid the adhesion of the resist to the surface of the substrate material. A resist is applied to the surface using a spin-coating machine. This device uses a vacuum to hold the wafer of semiconductor. A small quantity resist is dispensed in the center of the spinning wafer. The rotation causes the resist to be spread across the surface of the wafer with the excess being thrown spun off. Close to the centre of the wafer, the variation in the thickness of resist is around 30 nm. Preparation of the resist is concluded by a pre-bake, where the wafer is gently heated in a convection oven and then a hotplate to evaporate the resist solvent and to partially solidify the resist.

The photomask is created by a photographic process and developed onto a glass substrate. The cheapest masks use ordinary photographic emulsion on soda lime glass, while chrome on quartz glass is used for the high-resolution, deep UV lithography. Alignment of the mask is critical and must be achieved for x-y as well as rotationally. Industrial photolithography machines use automatic pattern recognition to achieve the registration alignment. Depending on the design of the photolithography machine, the mask may be in contact with the surface, very close to the surface, or used to project the mask onto the surface of the substrate. These methods are called, not surprisingly, contact, proximity and projection, respectively. Figure 1-6 shows a schematic diagram of

these methods. The projection system is the most complex method but does mean the projection of the mask can be scaled. The limit of the feature size is limited by the diffraction limit and depends on the size of the wavelength of light used to illuminate the mask. Systems using UV light are limited to feature sizes of $1 \mu m$.

An alternative to using a mask is to directly expose the resist using an excimer laser, electron beam or ion beam. These systems do not require a mask. Such methods are known as Direct Write to Wafer methods (DWW). With the density of features steadily increasing, keeping up with the Moore law, finer lithographic techniques will be required. During the exposure process, the resist undergoes a chemical reaction. Depending on the chemical composition of resist, it can react in two ways when the light strikes the surface. The action of light on a positive resist causes it to become polymerized where it has been exposed to the light. A negative resist has the reverse property. Exposure to UV-light causes the resist to decompose. After the developing process, a negative of the mask remains as a pattern of resist. Although not necessary for all processing, to further harden and remove any residue of the developer, the wafer undergoes a post-bake process. During this process, the resist temperature can be controlled to cause a plastic flow of the resist, which can be desirable for tailoring sidewall angles. After either deposition of semiconductor layers or metal or etching down to selectively remove parts of the SiO_2, the resist can be removed. For positive photoresists, accetone, trichloroethylene and phenol-based strippers may be used, while negative resists are generally removed using Methyl Ethyl Ketone (MEK) or Methyl Isobutyl Ketone (MIBK). Figure 1-6 shows the process schematically using a proximity mask.
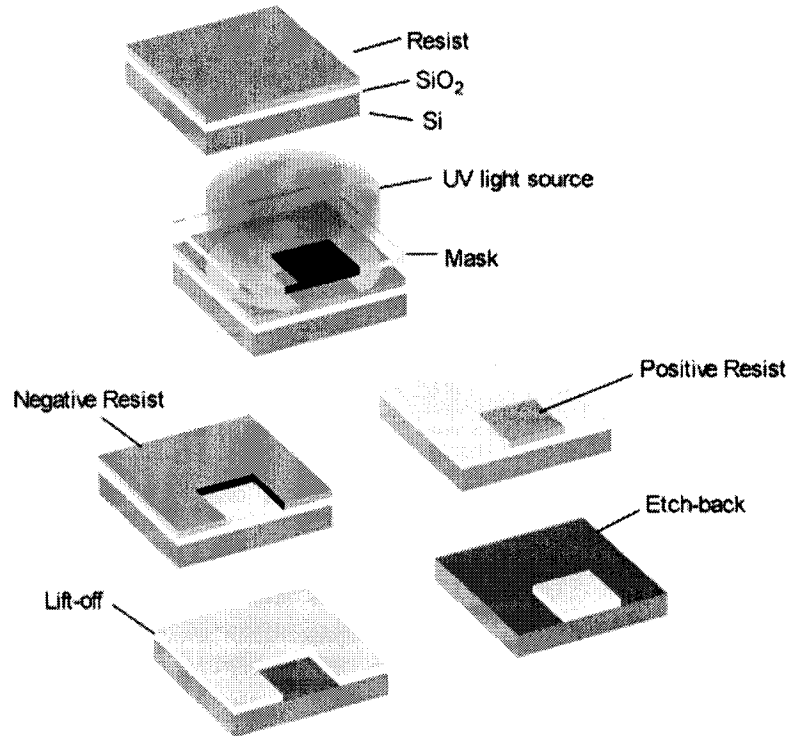
Figure 1-6 The main processes in the photolithography[64]

CHAPTER TWO

TEMPERATURE EFFECT ON LBL SELF-ASSEMBLY

2.1 Introduction

Research into polyelectrolyte multilayer (PEM) thin films has seen a massive escalation since the layer-by layer assembly technique [65] was first applied to polymer films in the early 1990s [66][67]. The assembly of multilayer thin films is driven by Coulombic attraction between two multiply-charged species: the substrate surface and the polymer adsorbate. This electrostatic binding of multiple charge sites provides for robust and quasi-irreversible adsorption of each individual polymer layer [68][69]. Moreover, these individual layers can be successively deposited to create multilayer heterostructures. Because these multilayers are versatile in terms of the type of charged species that can be incorporated into the system [23][70], a wide variety of complex structures is possible. Due to this tremendous structural versatility, as well as the simplicity of the deposition procedure, the alternate assembly is now extended to functional polymers [70], conducting and dielectric layers [71], organic and inorganic nanoparticles [72]-[74], and biospecific complexes [75]. The regular alternate immersion of a wafer in oppositely charged solutions allows complete automation of the process. It is likely to open up a new field to diversities of functional devices fabricated with nanoblocks by batch production.

22

The ability to rationally design functional materials and devices based on layer-by-layer self-assembled multilayers depends on a thorough knowledge of the factors that control the deposition and structural evolution of these films. Similarly, the ability to predict the behavior of these materials under various conditions depends on a clear understanding of environmental influences on self-assembled microstructure. However, an accurate physical model has not been established to reveal the mechanism of the electrostatic colloidal adsorption onto the substrate. Moreover, in order to produce a workable device, tens or even hundreds of monolayers have to be coated layer-by-layer. Therefore, efficiency will be one of the important issues for economical consideration.

Ultrathin polymer films may be deposited on a substrate by exposing it, in an alternating fashion, to solutions of oppositely charged polyelectrolyte [76]-[78]. Each immersion cycle contributes a reproducible and, eventually, constant increment to the film thickness. Several key experimental variables control the buildup of multilayered films in these systems [78]. For a given pair of strongly dissociated polycations and polyanions, the concentration of salt in the deposition solution appears to exert the strongest influence on the thickness of each polymer layer, which is approximately proportional to salt concentration [79]. Variables of lesser impact include salt composition, molecular weight, polymer concentration, and deposition time [79]. Previous studies have shown that film growth is mainly affected by factors such as polyelectrolyte charge density and pH [80].

2.2 Silica Multilayers

As an example of the nanoparticle architecture, let us analyze a 45-nm silica assembly by alternate adsorption with polycation poly(dimethyldiallylammonium

chloride), (PDDA) [80][81]. In situ quartz crystal microbalance (QCM) monitoring of alternate PDDA and SiO_2 adsorption gave the kinetics of the assembly process. In the first step, PDDA was adsorbed onto a Ag-electrode. The QCM frequency decreased during the first 60 seconds, after which a slower change was observed as adsorption saturation set in. Then, the resonator was immersed in pure water for washing. Next, the film was immersed in SiO_2 dispersion and silica adsorption saturation occurred within several seconds. After subsequent water rinsing, the film was immersed again in a PDDA solution, and so on. Each growth step was reproducible, and the adsorption process reached 90% saturation in 10 seconds for SiO_2 and 30 seconds for PDDA. The film assembly was not possible simply by the multiple immersion of the substrate in the silica solution. An alternation with an oppositely charged polyion was necessary. At every assembly step the component monolayers were formed, as was recorded by QCM, scanning electron microscopy (SEM) (Figure 2-1).

The average density of SiO_2/PDDA multilayers is $<\rho> = 1.43 \pm 0.05$ g/cm^3. SiO_2/PDDA film volume composition is 60% SiO_2 + 10% polycation + 30% air-filled pores. These pores are formed by closely packed 45-nm SiO_2 and have a typical dimension of 20 nm. The films have controlled pores, which can be varied by the selection of the nanoparticle diameter. We estimated the diffusion limitation for surface coverage $A(t)$ by adsorption from solution of particles with the diffusion coefficient D from $A(t) = 2/\pi\, C\, \sqrt{Dt}$. For t = 2 s, C = 10 mg/cm^3, and assuming for 45-nm silica D = 1.1×10^{-7} cm^2/s, $A \approx 3 \times 10^{-6}$ g/cm^2 and the layer thickness: $L = A(t)/<\rho> \approx 21$ nm. This result is reasonably close to the experimental silica monolayer thickness of 24.6 nm. Thus, 2 seconds corresponds roughly to the diffusion-limited time for the SiO_2

monolayer adsorption; this time is the fastest nanoparticle monolayer formation rate that we have achieved.
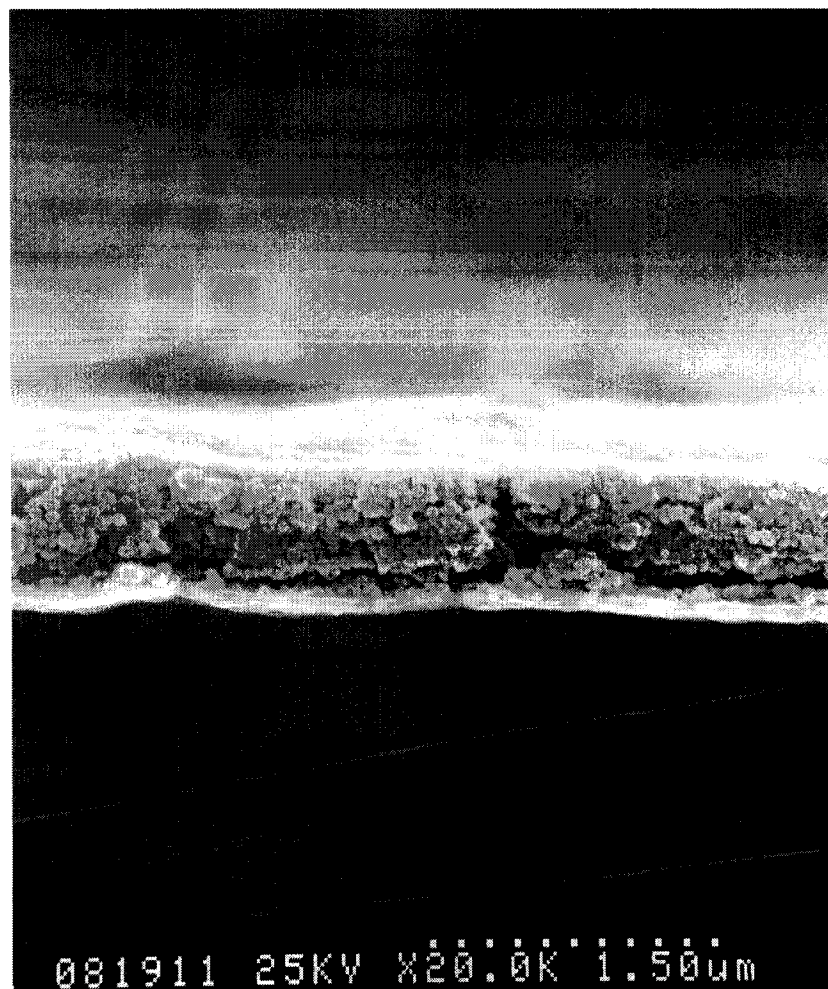
Figure 2-1 SEM image of multilayer containing 18 monolayers of 45-nm diameter silica alternated with polycation PDDA

2.3 Latex Assembly

Charged latex is a good building block for an electrostatic layer-by-layer assembly. Positively or negatively charged monodisperse lateces with diameters of 30, 40, 45, 50, or 75-nm and with different colors are commercially available, for example, from Seradyn Inc or IDC-Ultraclean Uniform Latex Inc. For the first time a multilayer assembly of negative latex spheres (carboxyl-modified or sulfate polystyrene) in

alternation with positive latex (amidine-modified polystyrene) was reported by Bliznyuk and Tsukruk [82]. They have described a strong tethering of charged nanoparticles to the surface, which prevents surface diffusion and the rearrangement required for formation of perfect lateral ordering. This situation is different from the one with the formation of the ordered 3D-mesocrystals by slow crystallization of the monodispersed aqueous colloids [83]. In the nanoparticle/polyion multilayers, one loses the crystal-like ordering, but gains control of the process, preparing multilayers of close-packed nanoparticles with a precisely known number of monolayers.

2.4 The Effect of pH

The thin films prepared using the layer-by-layer method are most frequently composed of strong polyelectrolytes because they remain fully charged over a wide pH range [84].

When weak polyelectrolytes are used as constituents of multilayers, the amount of charges in the multilayers can vary with the solution acidity and/or concentration of small ions; changes in pH/ionic strength might trigger changes in film structure and stability [85]. Ionizable polymers are often used to build multilayers, and pH modulation allows additional manipulation of molecular organization in these systems by the control of the thickness of each deposited polymer layer [85][86]. In their pioneering work, Möhwald and co-workers found that permeation of the chemicals through the shell of the multilayered capsules could be modulated by pH [87].

More recent studies have shown that preparing multiplayer thin films from weak polyelectrolytes can produce systems with a rich suite of properties because the behavior of this class of polyelectrolytes is sensitive to its pH [88]. In fact, it was recently shown

that even a single weak polyelectrolyte layer embedded at the bottom of a 10-layer film is greatly influenced by the local environment at the surface layer [89]. Rubner et al. [90] have recently reported pH-induced changes in stability and morphology of films deposited on a flat substrate.

Many of the polyelectrolytes employed for multilayers are either weak acids or their salts (such as carboxylates) [91]-[93] or protonated forms of weak bases (for example, poly(allylamine), poly(ethylene imine), and other polyamines) [78]. The use of one or more polymers bearing weak acid/base functionality affords the possibility of controlling the average charge per repeat unit and thus the extent of interaction between charged polymers. Most of the initial work, and a substantial number of continuing studies, are performed under pH conditions, which ensure that the polyelectrolyte remains in its most highly charged form (for example, protonated poly- (allylamine), PAH). A number of recent studies, notably those of Rubner et al. [91]-[93], have probed the complex behaviors for weak polyacid/polybase pairs that occur over a wide range of "pH space." Depending on the pH, both polyanion and polycation can be weakly or strongly charged, leading to fine control over the thickness of each deposited polymer layer [92][94]. Under certain deposition conditions, phase separation of multiplayer components yields unusual microporous ultrathin films [93].

2.5 Ionic Strength

Less attention has been paid to the influence of salt concentration (ionic strength) on the buildup of weak polyacid/base-containing multilayers. In a study employing polymers on carboxylate and oligo(ethylene glycol) functionalized monolayers was strongly dependent on the ionic strength of the deposition solution. Selective deposition

of polyelectrolytes on substrates offers the possibility of pattern formation and processing using multilayers [78]. In certain applications, selective (or nonselective) deposition would ideally be followed by quantitative removal of the thin film, preferably in ambient under mild conditions. An additional benefit would be realized if processing were to be based solely on aqueous solutions.

Castelnovo and Joanny [95] investigated the formation of multilayer films in polymeric systems. They find that the first polymer layer differs from subsequent layers and that the thickness of all layers increases monotonically with the solution salt concentration, in agreement with experimental observations [23].

More recently, Park et al. [96] reexamined the layer-by-layer deposition of charged polymers, accounting for "charge regulation," or the sensitivity of the degree of charging to pH. They find that the adsorbed layer thickness is molecularly thin when the polyelectrolytes are fully charged, while thicker, brush-like layers are obtained when the chains are not fully dissociated.

It was found that, as may be expected, the thickness of an adsorbed layer of rigid macroions on an oppositely charged substrate increases monotonically with the substrate-to-macroion charge ratio. The layer thickness decreases with the solution salt concentration and increases with its hydrophobicity, as manifested by a decrease in its dielectric constant.

2.6 Other Factors

In a system with electrostatically driven self-assembly, Schlenoff contrasted the effects of pH and ionic strength on the multilayer stability [97]. In a different system, in which self-assembly was driven by hydrogen bonding, it has been shown recently that

multilayers can be controllably "erased" by changes in pH, ionic strength, or electric field [98]. The control over film decomposition offers new possibilities in making drug release devices. Patterned surfaces created by the selective removal of specific multilayer films [99] are also possible.

For the time-dependent control of adsorption and monitoring of the assembly in situ, the quartz crystal microbalance method is quite suitable [100]. The kinetics of the adsorption process could be delineated by the QCM-technique, which is indispensable for establishing proper assembly conditions (e.g., a saturation adsorption time).

The multilayer assemblies are characterized by means of quartz crystal microbalance technique in two ways: 1) after drying a sample in a nitrogen stream we measured the resonance frequency shift and calculated an adsorbed mass by the Sauerbrey equation; or 2) by monitoring the resonator frequency during the adsorption process onto one side of the resonator which was in permanent contact with polyion solutions. While performing experiments in permanent contact with the polyion solution, we touched the surface of solutions with one side of the resonator, while the upper electrode was kept open to air, and the upper contact wire was insulated from the solution by a silicone paint covering.

The fitting of adsorption to an exponential law yields a first-order rate of adsorption for poly(styrenesulfonate) (PSS) τ= 2.5 ± 0.2 minutes and for polyallylamine (PAH) τ= 2.1 ± 0.2 minutes. This means that during the first 5 minutes about 87% of the material is adsorbed onto the charged support and t = 8 minutes (t = 3τ gives 95% full coverage. Typically, in most publications on polyion assembly, adsorption times of 5 to 20 min are used. One does not need to maintain an adsorption time with great

precision: a minute more or less does not influence the layer thickness if we are at the saturation region. For other species, poly(dimethyldiallylammonium chloride) (PDDA), polyethyleneimine (PEI), montmorillonite clay, myoglobin, lysozyme, and glucose oxidase, the first-order rate of adsorption onto an oppositely charged surface was found to be 2, 3, 1.8, 3, 4 and 5 min respectively. Interestingly, 5 - 20 minutes is essentially greater than the diffusion-limited time (mass transport limitation), which is necessary for complete surface covering (for the used linear polyion concentrations, it is a few seconds). Only for 45-nm silica / PDDA assembly do we have an example when 2 seconds time corresponds to the diffusion limited time for the SiO_2 monolayer adsorption.

One could suppose that linear polyion adsorption occurs in two stages: quick anchoring to a surface and slow relaxation. To reach a surface charge reversion during linear polyion adsorption one needs a concentration greater than 10^{-5} M [100]. The dependence of polyion layer thickness on concentration is not great: thus, in the concentration range of 0.1 - 5 mg/mL poly(styrenesulfonate)/poly(allylamine) (PSS/PAH) pair yielded a similar bilayer thickness. A further decrease in polyion concentration (using 0.01 mg/mL) decreases the layer thickness of the adsorbed polyion. An increase in the component concentrations to 20-30 mg/ml may result in the non-linear (exponential) enlargement of the growth rate with adsorption steps, especially if an intermediate sample rinsing is not long enough [101].

2.7 Temperature Effect

Though the ionic strength and pH dependence of multilayer assembly has been studied extensively, the temperature dependence has been comparatively neglected.

Recent work by Büscher et al. [102] has shown that increasing the temperature of the deposition solution tends to increase the thickness of electrostatically deposited films of poly(allylamine) hydrochloride (PAH) and poly(styrenesulfonate) (PSS).

In my work the temperature dependence of PEM film thickness has been further explored in an effort to identify the mechanism by which heat promotes polyelectrolyte adsorption. Electrostatically grown, multilayer films containing two strong polyelectrolytes, poly(diallyldimethylammonium chloride) (PDDA) and PSS, have been prepared under various conditions and characterized ellipsometrically. Moreover, the effect of temperature on alternate layer-by-layer (LbL) self-assembly of inorganic and organic nanoparticles was investigated. Compared to bigger particles, temperature has more effect on the adsorption rate of smaller particles. High temperature can enhance the efficiency dramatically. Based on this, temperature can be used as one of the alternative parameters to optimize this layer-by-layer electrostatic self-assembly. The significance of this study mainly relies on the batch-production feasibility of LbL self-assembled devices based on NP thin films.

Materials involved are (1) poly(dimethyldiallyl ammonium chloride) (PDDA) aqueous solution, MW 200 to 300 K, 3 mg/ml, 0.5 M NaCl, (2) sodium ploy(styrenesulfonate) (PSS) aqueous solution, MW 70 K, 3 mg/ml , 0.5 M NaCl. Both of them were obtained from Aldrich Sigma. SiO_2 colloidal dispersions in water (231 mg.ml^{-1}, Nissan Kagaku, Japan) were diluted to provide a concentration of 5 mg/ml, and SiO_2 particles were 45 and 300 nm in diameter. The 04644-Series Digital Hot Plate/Stirrer was from Cole & Parmer. The WYKO RST white light interferometer microscope used to measure the thin film surface roughness was made by WYKO. Silver

Plated QCM resonators, 9 MHZ were from Sanwa Tsusho Co. Ltd and the frequency counter from Itsuwa Electric Co.,Ltd.

A series of experiments were designed and implemented to monitor the adsorption rate and quality of the multilayer films at various temperatures. The quartz crystal microbalance (QCM) technique was adopted to measure the mass change during the assembling process. QCM frequencies decrease proportionally upon mass increase. The QCM resonators are covered by evaporated silver on both sides as the electrodes. The resonance frequency was 9 MHz (AT-cut). The resonator was soaked into the polyelectrolyte solution for a period of time and dried by a nitrogen gun, and the frequency change was registered. The QCM frequency in air was stable within ±2Hz during 1 hour [103]. At the beginning, the base film containing several polyion layers (in the alternate mode) was assembled onto the resonators with the outermost positive PDDA layer. Following the above procedure, the resonator was alternately immersed for 10 minutes in an aqueous solution of SiO_2 and PDDA with intermediate distilled (DI) water rinsing and drying by a nitrogen stream. The frequencies were measured after washing and drying periodically. The relationship here is obtained between the adsorption mass M (g) and the frequency shift ΔF (Hz) by taking into account the characteristics of the quartz resonators, which is the so-called Sauerbrey equation

$$\Delta f = -2\Delta m n f_0^2 / (A\sqrt{\mu_q \rho_q})$$ (2-1)

Where n is the overtone number, f_0 is the fundamental frequency, A is the electrode area, m_q is the shear modules of quartz, and r_q is the density of quartz. For our QCM resonator the thickness can be expressed by the following equation:

$$d(nm) = 0.022(-\Delta F(Hz)) \qquad\qquad (2\text{-}2)$$

For each type of particle the experiment was carried out at 0°C, 22°C, 45°C, 60°C, and 90°C, respectively. The QCM resonator must be cleaned in the solution (KOH 1% + alcohol 39% + DI water 60%) with an ultrasonic treatment for 30 seconds. At every temperature the adsorption was in a sequence of PDDA (20 minutes) + PSS (10 minutes) + PDDA (10 minutes) + PSS (10 minutes) + [PDDA (10 minutes) + SiO_2 (2.5 minutes)]$_5$. Intermediate DI water rinsing of 40 seconds and drying by a nitrogen stream was necessary. The original frequency of each QCM was recorded as well as the frequency after each step. It took a period of time for the frequency to stabilize and the frequency was recorded after one minute. Therefore the frequency shift of each step was obtained and temperature dependent curves were made from a series of adsorption curves at various temperatures.

Three layers of monolayers composed of the same particle were also deposited on the silicon wafer under an identical condition. The roughness of each thin film was measured by WYKO RST white light interferometer microscope.

2.7 Results and Discussions

The LbL self-assembled nano-blocks can grow in the vertical direction in a presetting sequence at about 2 nm every growth step. This provides the way to construct well-ordered and tight structures composed of various substances, as shown in Figure 2-2 and Figure 2-3.

As the first simple system, we have analyzed the assembly between PSS and PDDA. Figure 2-4 illustrates the frequency and thickness shift against the assembly step, when a QCM was alternatively immersed into the PDDA and PSS solution at different

temperature. The amount of polyions assembled increased upon increasing the solution temperatures. Table 2-1 shows both the polycation(PDDA) and polyanion(PSS) have the same trend. In addition, the similar amount of polycations were adsorbed on the QCM when it is assembled with silica nanoparticles (300nm) as shown in Figure 2-4(b).
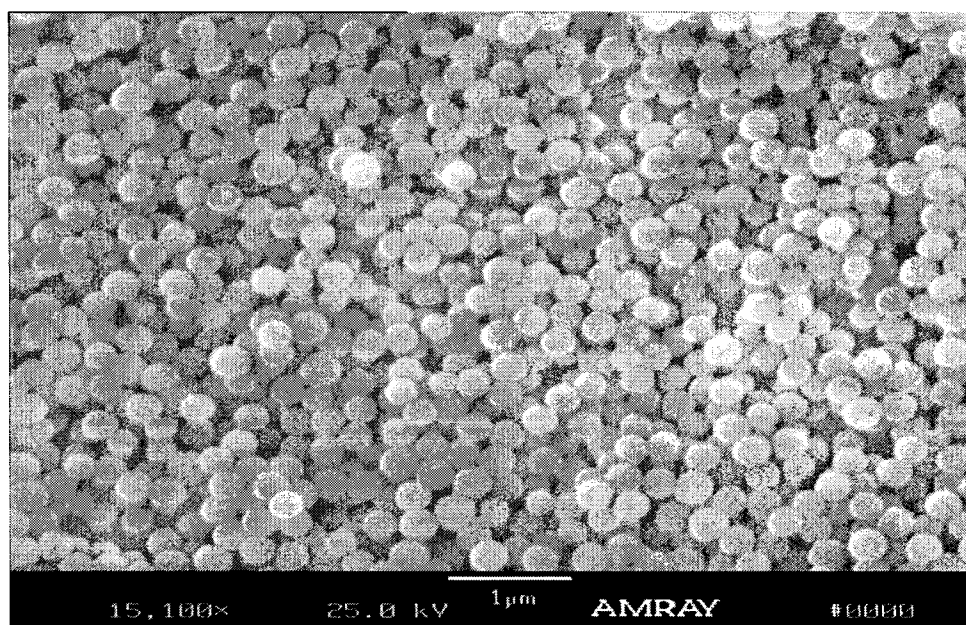
Figure 2-2 SEM picture of silica particle thin film (particle size: 300 nm)
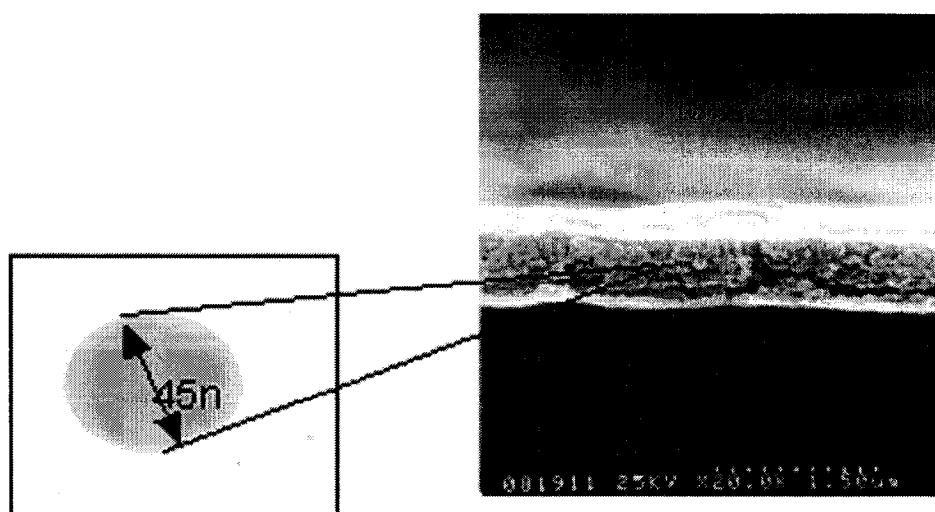
Figure 2-3 TEM picture of silica particle thin film (particle size: 45 nm)

Figure 2-5 & Figure 2-6 illustrate the stepwise assembly of PDDA and silica

nanoparticles onto the QCM surface at 2°C, 22°C, 45°C, 60°C, and 90°C, respectively.

The higher temperature results in the larger amount of adsorption substances on the

surface, which is possibly due to the enhancement of the energy of the particles at

increased temperatures.
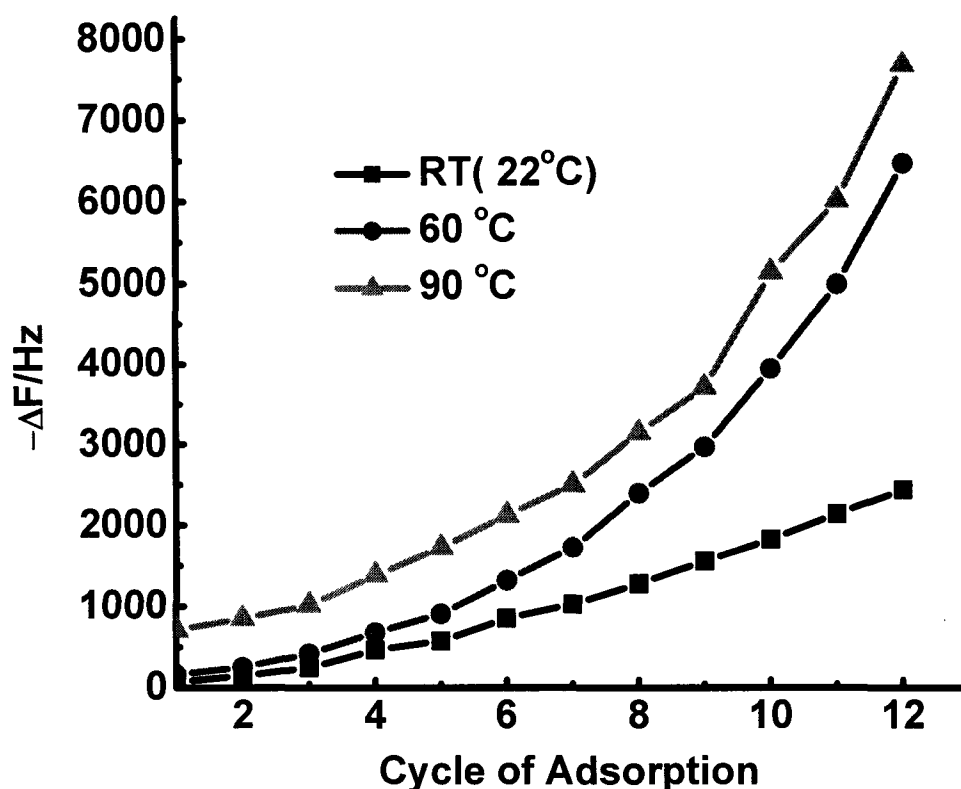
Figure 2-4 Frequency shift for PDDA(PSS/PDDA)$_{2-12}$ at different temperatures

The adsorption rate (the amount of adsorption per step) is related to the

probability for a particle to get into the attractive region, which relies on the energy of the

particles. The role of temperature is to adjust the thermal energy or velocity of the

particles. The particles with more energy will have more opportunities to search for a site

to reside. In addition, the polyions (here PDDA) also gain more thermal energy and

probably go through the gaps among the nanoparticles and then fill in the gaps, resulting

in more adsorption of polyions. As observed in Figure 2-4, a stronger electric field is created and more oppositely charged particles are needed to neutralize it. Consequently, all of these factors contribute to increase the thickness of every step.

Table 2-1 The mean frequency shift in the above figures

Temperature / Adsorption(Hz)		RT(22°C)	60°C	90°C
PSS/PDDA Figure 2-4	PDDA,1st	76	496	823
	<PDDA>	188	401	425
	<PSS>	265	688	826
PDDA/Silica(300nm) Figure 2-5	<PDDA>	195	423	300
	<Silica>	2233	3151	5969

PDDA, 1st : the frequency shift for first assembly step

<PDDA> : the mean frequency shift for each assembly step of PDDA

<PSS>: the mean frequency shift for each assembly step of PSS

<Silica>: the mean frequency shift for each assembly step of Silica (300nm)

It is also shown in Figure 2-6 that the temperature has much more effect on smaller particle than on bigger ones. The frequency shift at every step for the smaller particles was more from room temperature (RT) to 90°C, compared to the bigger particles, illustrating that the gap between the curves at RT and 90°C is wider for smaller particles, as shown in Figure 2-5. Compared to bigger particles, smaller particles are more sensitive to temperature adjustment. On one hand, its thermal velocity varies greatly under the same momentum change due to its smaller mass. On the other hand, the

larger amount of smaller particles is needed to neutralize the opposite charges of the polyion layers because it carries less electrical charges.

Another important phenomenon is the threshold of temperature effect. The experiment demonstrates that the deposition performance is the same at 0°C and room temperature. It means that temperature does not influence the deposition process until it exceeds the threshold temperature (here it is about room temperature). Under the threshold value, the increase of temperature is not considerable because the thermal velocity of the particle and the probability of being adsorbed onto the substrate are not increased greatly.

Above the threshold value, the temperature changes the deposition rate dramatically. For example, it takes almost 5 cycles of immersions for the 45 nm particle thin films to reach 200 nm thick at room temperature, but it takes only one cycle at 90°C. If one cycle takes 15 minutes, then 1 hour is saved. The LbL self-assembled monolayer is usually at the magnitude of a nanometer so that tens of layers of different materials are necessary to realize certain thickness. By dipping the substrate at higher temperatures, a great quantity of time can be saved if batch fabrication is under consideration in the future.

A control system (with nothing on the QCM) was designed to investigate the temperature effect on the QCM itself. Figure 2-7 shows this frequency shift of QCM after being kept in the solution at different temperature for 20 minutes and then another 10 minutes. The frequency shift is small comparing to former study in Figure 2-5 and Figure 2-6, and it is almost kept unchanged during the following adsorption steps, indicating the temperature effect on QCM can be omitted in our studies

Figure 2-5 Adsorption of Silica particle on QCM surface (the first 4 steps are base layers), thickness versus cycles of adsorption (particle size: 300 nm)

Another conjecture is temperature effect on the pH of the solution. However, the pH has little effect on the adsorption behavior of PDDA, while has some influence on the assembly of PSS. In our first simple system, the frequency shift for the first adsorption of PDDA also increases dramatically as the temperature increases, suggesting that the temperature can directly affect the assembly.

The surface roughness prepared under different temperature was inspected, as shown in Figure 2-8, Figure 2-9 and Figure 2-10. It is found that raising the temperature will have little effect on the multilayer film prepared by the smaller particles. However, when the bigger particles were utilized, the surface roughness was degraded, which may be caused by the big size of the particle. In other words,

these observations suggested that this temperature effect would be most suitable for

the particles with smaller dimensions if the film quality is critically required.

Figure 2-6 Adsorption of Silica particle on QCM surface (the first 4 steps are base
layers), thickness versus cycles of adsorption (particle size: 45 nm)

Figure 2-11 shows the similar result for LATEX particles. Comparing the curves

for SiO_2 and LATEX, we can see that high temperatures can affect the adsorption of the

LATEX more,nprobably because the dimension of LATEX particle is much larger than

that of the silica. So when the possibilities of the adsorption to the surface are increased,

the thickness increased more.

Frequency(Hz)

5400
4400
3400
2400
1400
400
-600

—◆—Frequency after 20min

—■—Frequency after another 10min

0°C   22°C   45°C   60°C   90°C
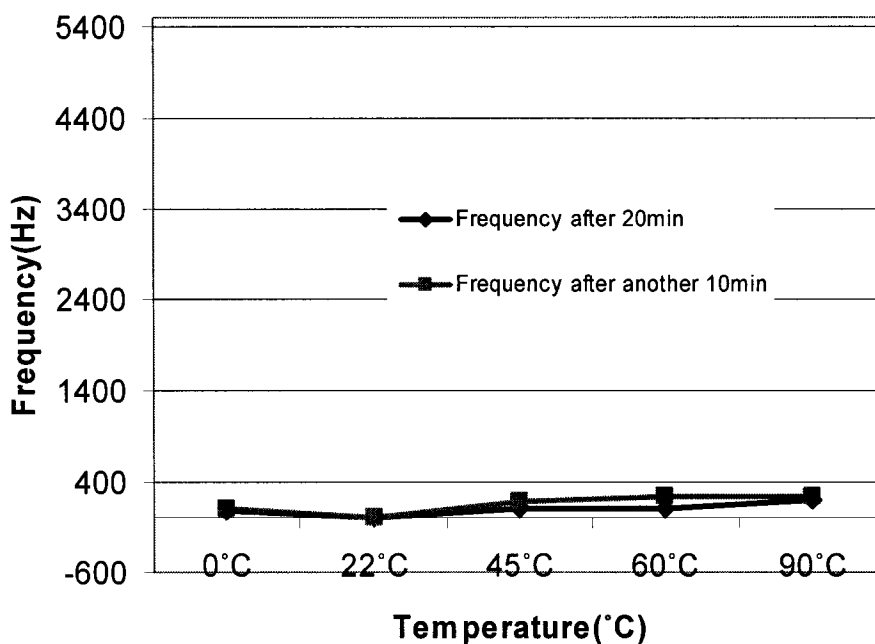
Temperature(°C)

Figure 2-7 Frequency shift versus the temperature for the control system. The shift is negligible comparing to our results in Figure 2-5 and Figure 2-6

A new phenomenon in layer-by-layer self-assembly of linear polyions and nanoparticles, 100–200% increase of growth step with temperatures, was found, and it has to be taken into account in the applications of LbL technique. The possible mechanism may involve the temperature effects of polymer conformation, dielectric constant of medium, electrostatic interaction, enthalpy/entropy balance in charge shielding, the surface coverage of polymers and the aggregation of polymers at greater temperatures due to dehydration.

WYKO   Mag: 20.0 X   **Surface Data**   Date: 08/05/02
       Mode: VSI   Time: 16:50:33

Surface Statistics:
Ra: 4.35 nm
Rq: 7.46 nm
Rz: 324.71 nm
Rt: 968.53 nm

Set-up Parameters:
Size: 368 X 236
Sampling: 850.00 nm

Processed Options:
Terms Removed:
Tilt
Filtering:
None

Title:
Note:
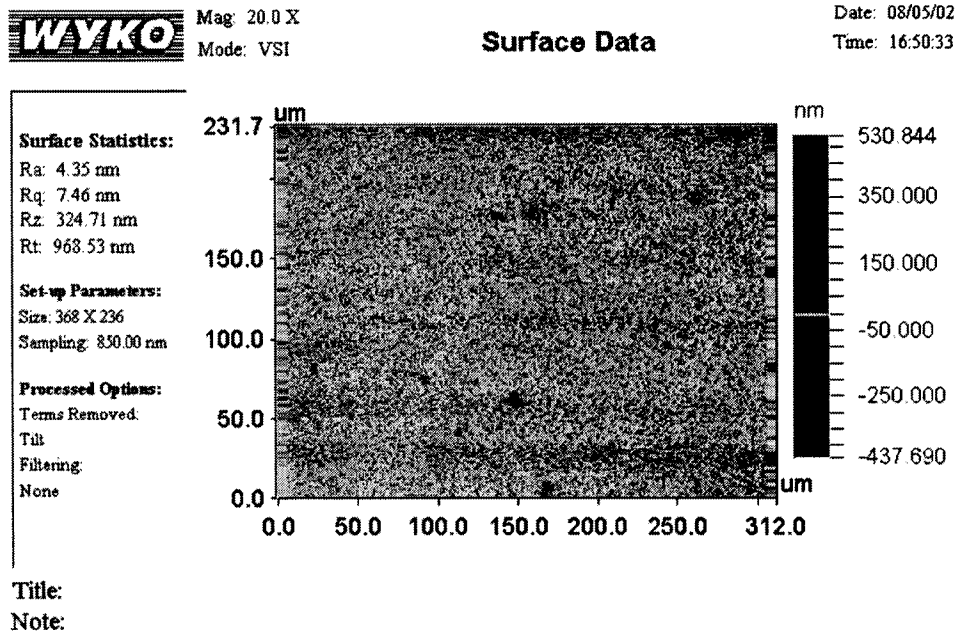
Figure 2-8 Surface Roughness of the multilayer film at RT(22°C) for 45 nm silica

WYKO   Mag: 20.0 X   **Surface Data**   Date: 08/06/02
       Mode: VSI   Time: 14:19:23

Surface Statistics:
Ra: 6.07 nm
Rq: 8.43 nm
Rz: 186.03 nm
Rt: 493.24 nm

Set-up Parameters:
Size: 368 X 236
Sampling: 850.00 nm

Processed Options:
Terms Removed:
Tilt
Filtering:
None

Title:
Note:
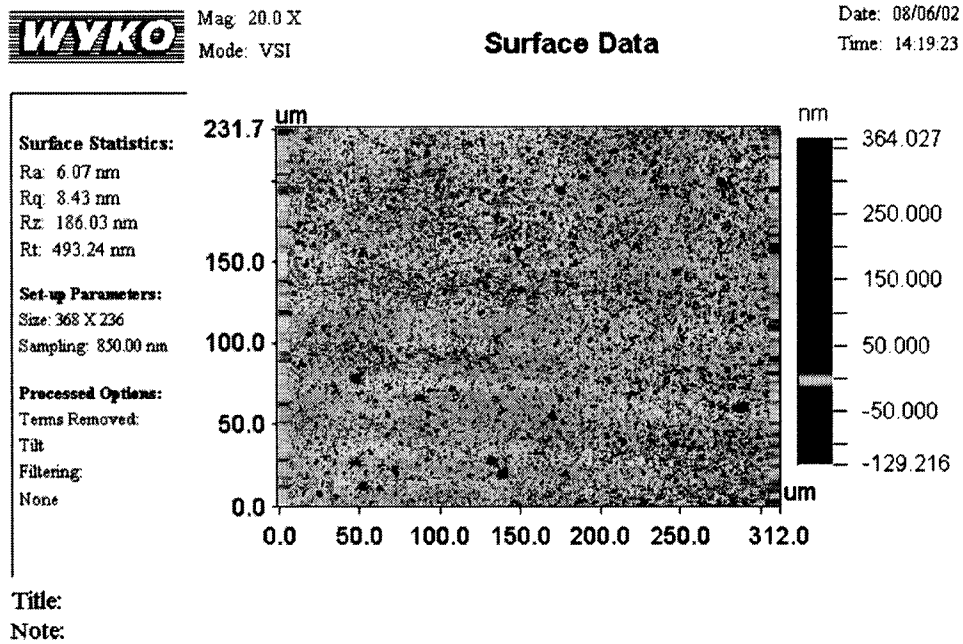
Figure 2-9 Surface Roughness of the multilayer film at RT(90°C) for 45 nm silica
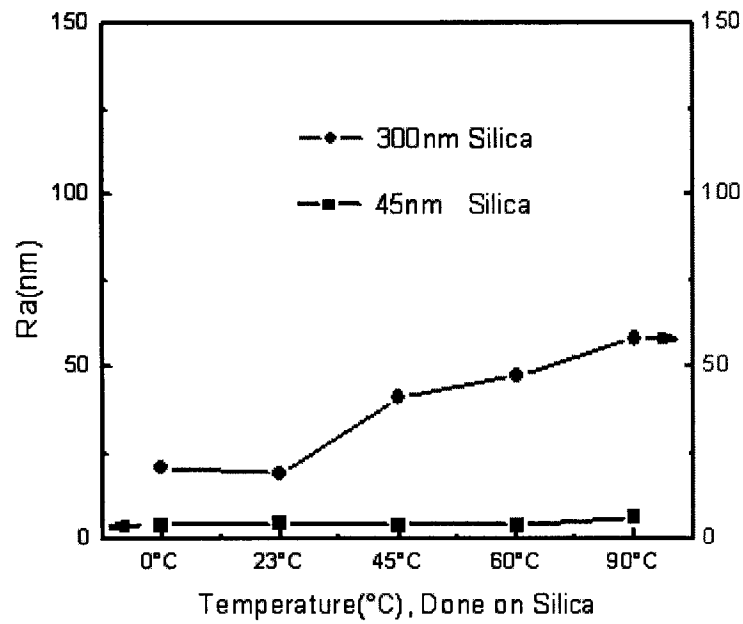
Figure 2-10 Surface Roughness of the multilayer film at various temperatures for 45 nm nanoparticles and 300 nm nanoparticles
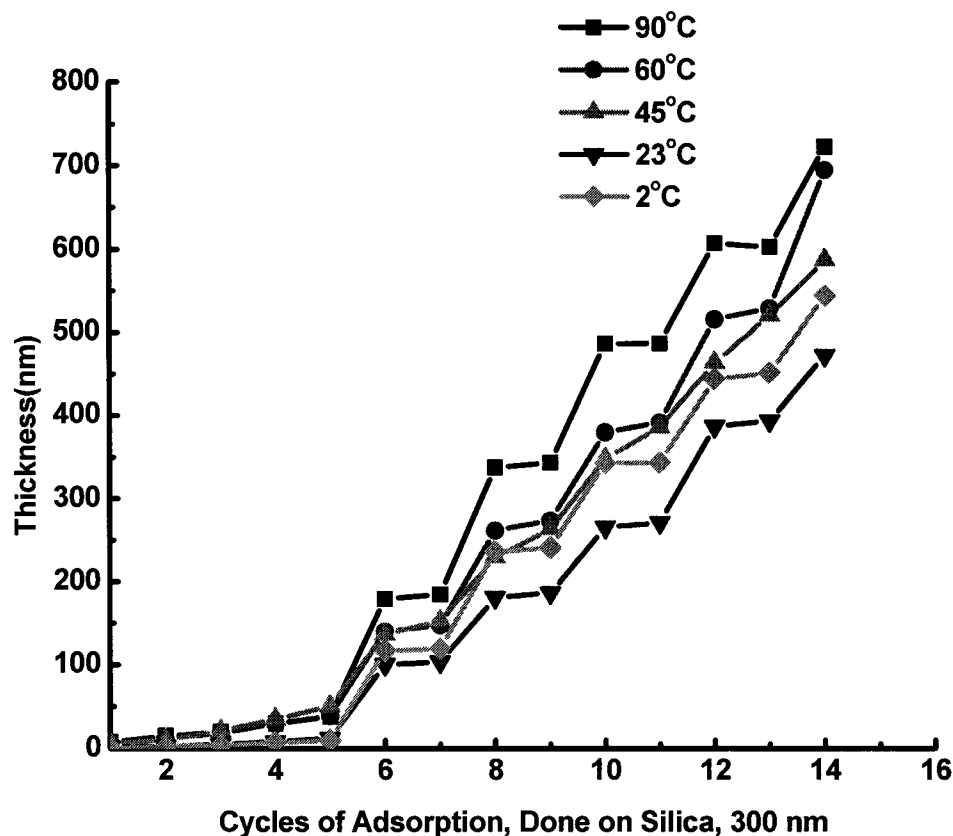
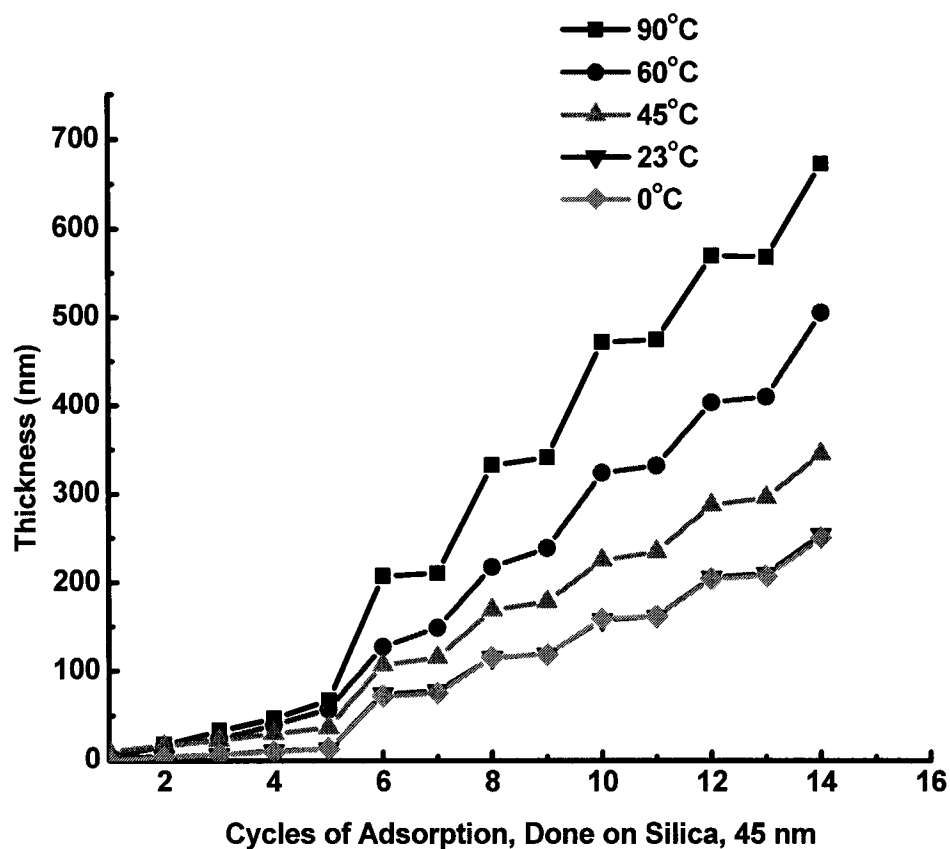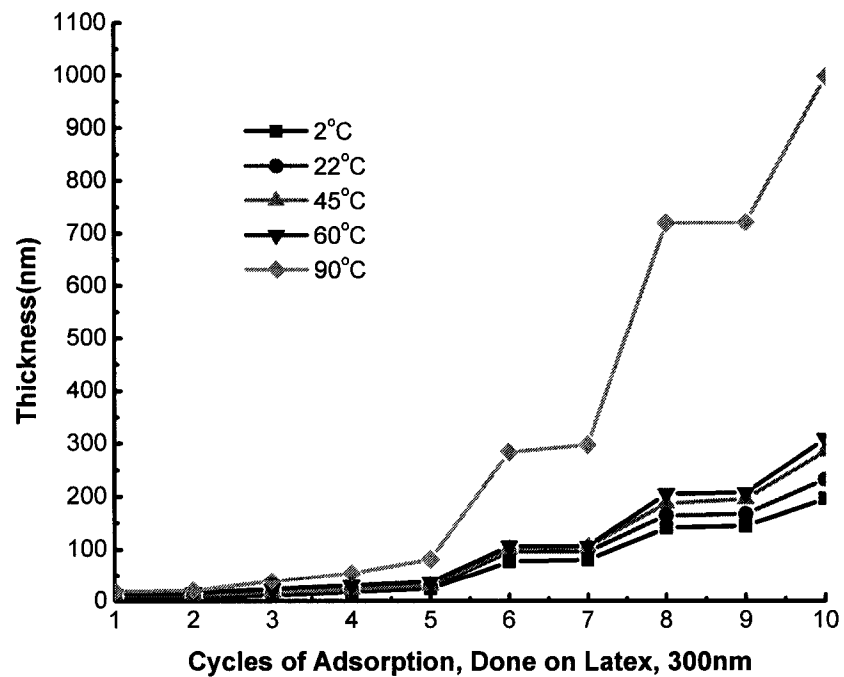

Figure 2-11 Adsorption of LATEX particles on QCM surface (the first 4 steps are base layers), thickness versus cycles of adsorption (particle size: 300 nm)

CHAPTER THREE

FABRICATION OF INDIUM RESISTOR

3.1 Introduction

The electrical resistance of a material is a measure of how difficult it is for electric current to flow through the atomic structure of a material. A resistor is an electronic circuit element with a fixed amount of resistance to current flow. Resistors are used to create a voltage drop to meet the voltage requirements of the electrical device through which the electric current is flowing.

A microelectronic resistor is commonly formed by creating a thin ribbon of semiconducting material, doped with either negative "N-type" or positive "P-type" charge carriers, in a region doped with charge carriers of the opposite type [104].

With the increasing demand for ever-smaller devices, much recent research has focused on the fabrication and characterization of "self-organizing" nanoscale systems. This charge reveals a shift away from "top-down" approaches, such as those based on photolithography, to "bottom-up" approaches that should not only permit the fabrication of much smaller devices but also allow facile, and yet highly reproducible assembly.

Nanoparticles based nanostructured films are currently under intense investigation since they offer the potential for applications in various fields such as semiconductors,

43

molecular electronics, photovoltaic, chemical and biological sensing and catalysis [105]-[107].

These particles are of interest for several reasons: first, it is possible that new energy levels become available because of the reduced dimensionality of the system; this is particularly relevant to semiconductor particles [108]. For metallic nanoparticles, it is not so much that the energy levels change but rather that the reduced dimensions of the particles become smaller than the electron mean free path. This charge leads to increased electron scattering and, hence, affects both the electronic and optical properties of the nanoparticles. Further, by reducing the size of such particles, one also reduces the capacitance associated with charging them, which, in turn, can lead to interesting conductivity behavior, for example, room-temperature single electron transport [109].

3.2 LbL in Solid State Devices

In solid state devices inorganic multilayer films have already attracted great interest as a way to control surface properties. In particular, the introduction of nanostructured materials inside a lamellar structure has been of great interest as a way to develop specific nanosize effects, in particular with colloidal particles [21]. Several attractive combined properties including mechanical, electrical, optical, and magnetic ones have been developed with different inorganic nanoparticles such as, for example, TiO_2, Fe_3O_4, CdTe, and MoS_2 [110].

Different technical approaches exist for hybrid materials; all of them are based on a sequential way to control the multilayer deposition. These techniques are based mainly on van der Waals type interactions, as in the classical Langmuir–Blodgett (LB) approach, covalent bonding in self-assembly monolayers (SAMS), or electrostatic interactions using

layer-by-layer assembly [7]. This last technique, using oppositely charged polymers, has been successfully developed during these past years [23]. It has recently been demonstrated that the growth of lamellar systems containing inorganic charged nanoparticles can be controlled [111]. This process is an alternative to the already developed semiamphiphilic LB technique with ionic surfactants used, in particular, for specific molecular magnetic systems [112].

Recently the layer-by-layer (LbL) growth of polyelectrolyte/ gold nanoparticle films has also been reported [113][114] using the electrostatic method popularised by Decher [23]. These works have demonstrated that depending on the polyelectrolyte structure and nanoparticle morphology as well as conditions of self-assembling, the final properties of charge transport and permeability within the assembly can be varied from a film with bulk metal conductivity [113] to a film exhibiting electronic charge transport from electrode through the film via an electron hopping from nanoparticle to nanoparticle. A tunable mobility of electrolyte ions moving through the film (necessary for electroneutrality) has also been described [114]. On the other hand, it has been also demonstrated that electronic charge transport within LbL self-assembled multilayers of polyelectrolytes can occur by electron hopping between adjacent molecular redox centers that are covalently grafted on the polyelectrolyte backbone. Such systems involved redox polyelectrolytes assemblies such as poly(butanylviologen)/poly(styrenesulfonate) [115], poly(allylamine)ferrocene or osmium complex-derivatized poly(allylamine)/glucose oxidase [116] or viologenfunctionalized poly(vinylpyridinium)/nitrate reductase [117].

3.3 Conductivity of an LbL Polyelectrolyte Multilayer

Despite these advantages, early ionic conductivity results were disappointing. The dielectric and ion conduction properties of LbL films were first investigated by Durstock and Rubner [118], following limited earlier studies on cast polycation/polyanion complexes [119].

The first LBL investigation evaluated films of poly- (allylamine hydrochloride) (PAH) with poly(styrene sulfonate) (SPS) and poly(acrylic acid) (PAA). These composites demonstrated ionic conductivity with a maximum of 2×10^{-7} S/cm at room temperature and high hydration [118], which is too low for most electrochemical applications. The low ionic conductivity of typical electrostatic LBL films can be explained using the general relation.

$$\sigma = \sum_{i=1}^{all\ ion\ types} n_i q_i \mu_i \qquad (3\text{-}1),$$

where σ is ionic conductivity, i is the ion type, n is the number of mobile ions, q is the ion charge, and μ is the ion mobility. The ion number and mobility are potentially limited by the LbL technique.

The limited number of mobile ions is due to the large extent of polyion pairing and rejection of residual small ions from the LbL film bulk, which is especially notable in strong polyion systems such as poly(diallyl dimethylammonium chloride) (PDAC)/SPS [119]. In general, an electrostatic LbL film cannot contain as many dissociable small counter ions as a neat film of either polyion, which would contain one counter ion per monomer unit. In addition, hydrophobic aspects of common model polyelectrolytes such as PAH, PDAC, or SPS limit the potential for residual or added salt to dissolve into the film.

Limited mobility is due to an inherently high crosslink density, which has been shown to decrease ionic conductivity in polyether networks [121]. The underlying mechanism of such poor conductivity is the constraint of small-segment polymer dynamics, which are widely recognized as being coupled to ion mobility [122]. Furthermore, each ion pair within a LbL film can behave as a "coulomb trap", slowing migration by temporary association with the migrating ion.

3.4 Conductivity of Inorganic Nanoparticles/Polyelectrolyte Multilayer

Recently, technologies for the production of metallic, semiconducting, and insulating nanocrystals are able to provide nanoparticles that function similarly to the high-grade materials used by the modern microelectronics industry [122][123]. Due to their unique properties and versatility, nanoparticles have become the focus of material research for applications in microelectronics, optoelectronics, and catalysis and for fundamental research in solid state physics.

A number of studies have been performed specifically investigating the buildup of nanoparticle/polyelectrolyte composites, with many different combinations of materials possible. Some common nanoparticle components in these films have been SiO_2 [124], TiO_2 [124][125], iron oxide [125], and gold [126]. These materials have been combined with polymers such as poly(styrene sulfonicacid) [124][125], poly(allylamine hydrochloride), and poly(diallyldimethylammonium chloride) [125].

Among various nanoparticle/polyelectrolyte composites, metal nanoparticles and nanostructures have been the subject of many extensive scientific and practical studies [127][128]. There are a number of conductor applications requiring medium to low resolution lines (10 μm and up) including solar cells, microwave circuits et. al.

3.5 Manufacturing Method

The optimum deposition approach is one that minimizes capital investment while reducing ancillary processing. Direct writing of inks to form conductor lines has inherent processing advantages over screen-printing and vapor deposition in that no post-printing thermal treatments or photolithographic processing are required. However, they have some special requirements for the ink. These inks must function to produce adherent and electrically connected layers at suitable processing temperatures. In addition, high purity may be required to attain satisfactory conductivity in the deposited layers [129]. Liquid embossing overcomes these limitations through two critical differences from other techniques. The first is that the patterned material remain a liquid throughout the embossing, requiring no chemical reaction or phase change to occur during the actual patterning. The second is that the emboss pushes through the thin liquid film and contacts the substrate beneath, enabling the additive fabrication of electrically isolated features and the direct formation of vias, both without the etching required for contact-printing and imprint schemes. But it still depends on the template fabrication [130]. The master is fabricated using microlithography techniques such as photolithography, micromachining, e-beam writing, or by using available relief structures such as diffraction gratings [131].

We developed lift-off and metal mask technique based on LbL self-assembly and traditional lithography [132]-[136]. Self-assembled monolayer or multilayers were utilized to generate the devices such as capacitor [135], FET. Because layer-by-layer self-assembly and lithography techniques are mature processes, and lithography is widely applied in the modern semiconductor industry, a combinative technique will be economical and suitable for mass production. By just following the traditional process,

the nanostructures composed of nano-building blocks can be realized. As it is used in the semiconductor industry, the process results in such a high reproducibility that distinct patterns (in this experiment precise 10μm) can be created in almost all of the dies on the wafer.

As we all know well, microelectronic devices consist of a conducting layer, insulating layer, and a semiconducting layer. For our devices, both the semiconducting layer and the insulating layer can be fabricated by LbL self-assembly. For both methods, the conducting layers were fabricated by evaporation or sputtering [135]. To our knowledge, few conducting layers were generated by LbL self-assembly with inorganic nanoparticles. In our work, LbL self-assembly techniques were employed in order to form metal nanoparticle/polyions multilayers. Indium nanoparticles were utilized as building blocks to obtain conducting line.

<div align="center">3.6 Conductive Materials</div>

For bulk materials, gold, platinum and copper are all good as conductive components. Accordingly, their nanoparticles were used in our work. However, the results were disappointing. The multilayer made of gold nanoparticles/PDDA didn't show any resistor-like characteristics. The multilayer of Cu nanoparticles/PDDA and Pt nanoparticles/PDDA multilayer showed fairly poor conductance as well. SEM (Scanning Electron Microscopy) images were taken on these multilayers.

From Figure 3-1a, b and c we can see those nanoparticles do not at all or barely contact each other. Polyelectrolytes filled the gap between the nanoparticles. Their conductance was proven to be very low. Therefore, instead of common materials, indium nanoparticles were utilized. These particles showed desired characteristics, and the SEM

image reveals the reason (Figure 3-1(d)). Unlike the previous pictures, these

nanoparticles have good connection with each other. Further treatment by RTA (Rapid

Thermal Annealing) results in even better properties.

(a)

(b)

(c)

(d)
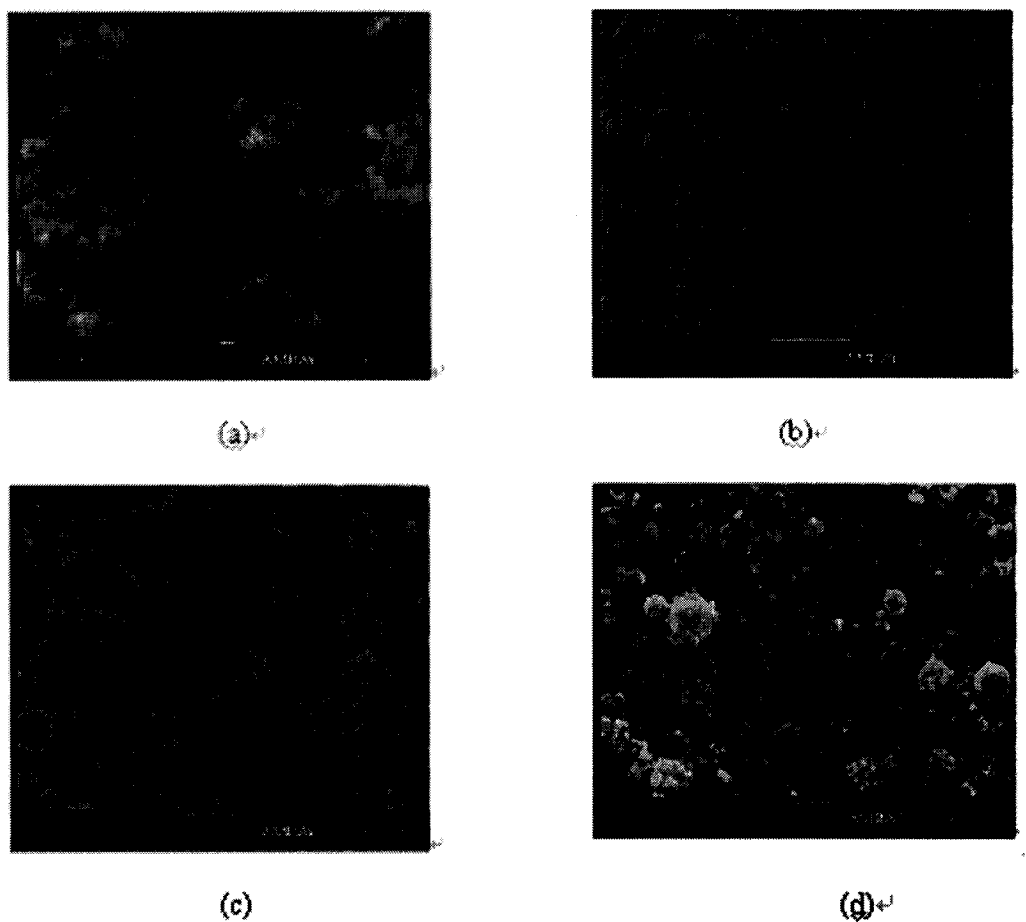
Figure 3-1(a) SEM image of $(PDDA/PSS)_2+(Au/PDDA)_7$,(b) SEM image of $(PDDA/PSS)_2+(Pt/PSS)_7$,(c) SEM image of $(PDDA/PSS)_2+(Cu/PDDA)_7$,(d) SEM image of $(PDDA/PSS)_3+(In/PSS)_{10}$

3.7 Fabrication of the Indium Resistor

Materials involved are poly(dimethyldiallyl ammonium chloride) (PDDA) aqueous solution, MW 200 to 300K, 3mg/ml; 0.5M NaCl and sodium ploy(styrenesulfonate) (PSS) aqueous solution, MW 70K, 3mg/ml; and 0.5M NaCl. Both of them were obtained from Aldrich Sigma. Dispersion of In nanoparticles, 0.15g/ml,

10-80nm in diameter was also taken from Aldrich Sigma. RTA facilities (RTA-600S, Modular Process Technology Corp) were used for post-treatment.

A 4-inch silicon wafer was immersed in H_2SO_4 and H_2O_2 solution (volume ratio 7:3) at 70°C for 1 hour. Then, it was "hardbaked" at 115°C on hotplate for 5 minutes. A layer of 1 μm photoresist was spun on the silicon wafer. The speed was 1500 rpm, ramp was 200 r/s, and time 40 seconds. It was baked on hotplate at 115°C for 1 minute. It was exposed under UV light for 7 seconds, and the desired pattern on photomask was transferred onto the surface of photoresist by developing. The developer was MF-319, and the time was 40 seconds.

The substrate was dipped into PDDA, PSS solutions alternatively, in the sequence of PDDA(20 minutes) +(PSS(10 minutes)+ PDDA(10 minutes))$_2$+ PSS(10 minutes). The substrate was rinsed by DI water for 1 minute and dried by spinning between two alternate immersions. The speed was 1300 rpm, ramp was 300 r/s and time 40 seconds. Indium nanoparticles were adsorbed alternately with PSS in the sequence of (Indium (2.5 minutes) +PSS(10 minutes))$_{10}$ and dried by parallel nitrogen flow between two alternate immersions.

The substrate was put into acetone solution with ultrasonic treatment for 7 seconds to remove the photoresist. Finally, the patterned thin film went through Rapid Thermal Annealing (300°C, 3 seconds)

<div align="center">3.8 Results and Discussions</div>

Figure 3-2 shows the lift-off method used to fabricate the functional devices and microscopic configuration of the conducting line. It can work well on the thin film made of indium nanoparticle. A lear image can be seen in Figure 3-3.

Figure 3-4 shows the electrical characteristics of fabricated devices. The electrical properties were determined by standard four-probe measurements (Figure 3-5). From this figure, we can see RTA (rapid thermal annealing) has significant effects on conductance of the fabricated devices. The measurement was made on the 10um wide, 220um long line. From the results obtained by RST, the thickness of the film was around 543nm. By combing the measured resistance R of the resistor with its geometry (h, w and l), the resistivity of the patterned Indium was calculated using the formula $\rho = \dfrac{Rs}{l}$.

The resistivity before annealing was calculated as 2.4×10^5 $\Omega \cdot cm$. It was reduced dramatically after annealing as around 0.9 $\Omega \cdot cm$. In air, the conductance of the devices decreases. The performance of the devices degraded as the current goes through. It might be caused by the heat generated when the voltage was applied. One of the possible reasons for the conductance decrease is the oxidation of the nanoparticles. Indium can be oxidized to In_2O_3 when it is heated in the air, and then it will become more insulating. The other possible reason is that the multilayer may adsorb H_2O contained in the air, so that the conductance was reduced.

The degradation gets less significant as we continued to apply voltage on the device. At some value, it becomes stable. The reason is not very clear yet. It is predicted that only some amount of indium nanoparticles can be oxidized. The stable value comes after maximum oxidation happens. Therefore, this device can function relatively consistently if the current is kept going through for some time before it begins working.

Figure 3-6 presents the two AFM images before and after RTA, respectively. Before annealing, the nanoparticles are separately distributed. They do not contact well. RTA made it possible to form the cluster of indium nanoparticles. The melting point of

indium is around 140°C, and our annealing temperature is around 300°C. Therefore, when the nanoparticles are heated, they might melt and aggregate as shown in Figure 3-5(b). The other possible reason is the removal of polyions by annealing. RST (Roughness Surface Tester) results show that the thickness of the multilayer decreased lightly after annealing.
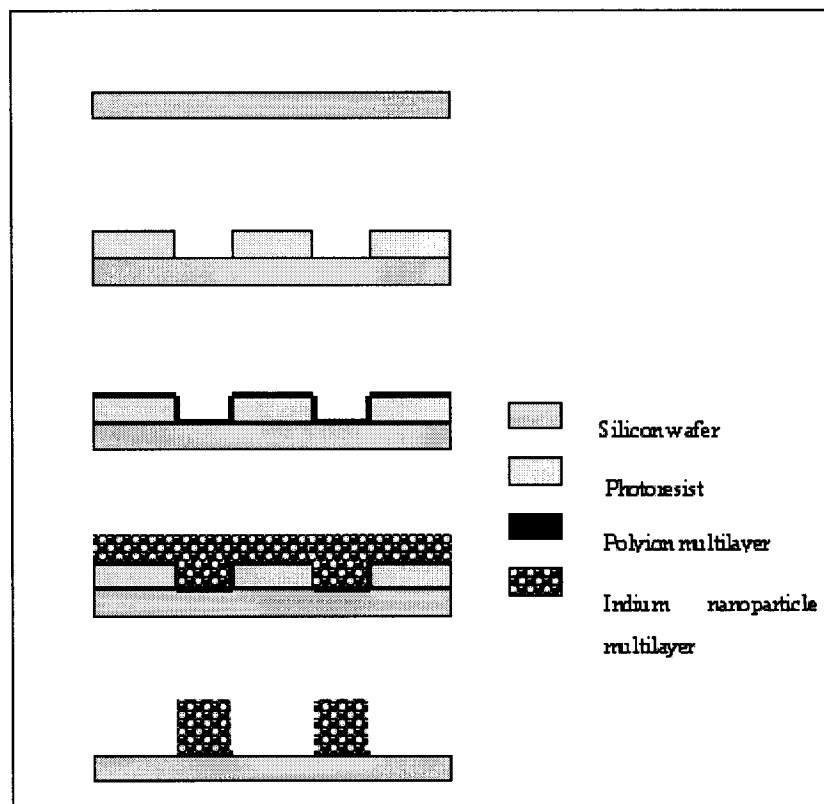
Figure 3-2 Scheme of patterning nanoparticle thin films with lift-off method

Several different types of metal nanoparticles were investigated, such as gold, platinum and copper nanoparticles. All of them have lower resistivity than indium as bulk materials. But even for the noble metals like Au, they didn't show good conductivity when we tried the same fabrication process on them as we did on indium nanoparticles. The possible reason is all of them have much higher melting temperature, so we couldn't get the good contact even through RTA.
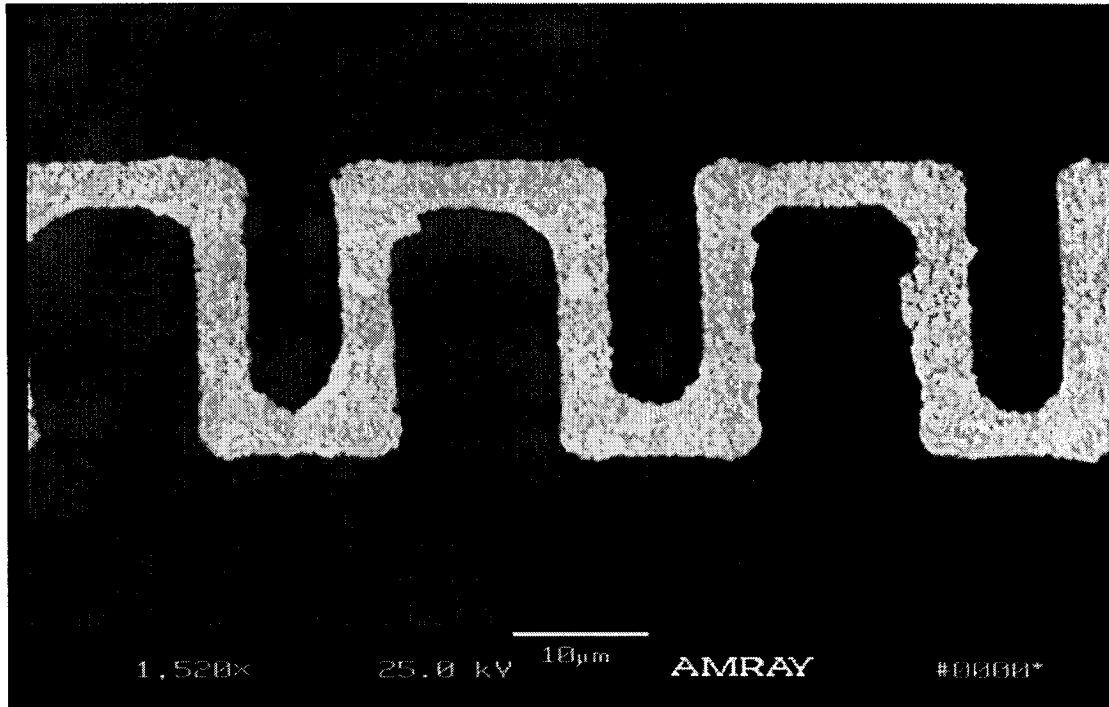
Figure 3-3 Patterned conducting line made of indium nanoparticle (the first 6 steps are platform layers)

A resistor based on multiplayer thin film made of indium nanoparticles and polyions was fabricated by LbL self-assembly and traditional lithography techniques. It has the lowest resistivity ever realized by LbL technique and can work as a conductive layer in the microelectronic devices. RTA annealing can improve the conductance dramatically. One of the possible reasons is the aggregation of indium nanoparticles through rapid thermal annealing due to its low melting point. Degradation is a problem for this device. However, one can still have relatively good and stable performance by applying voltage on it for some time. This device will have potential applications in microelectronic devices and MEMS with an advantage of lower cost and a simpler process.

Figure 3-4 Schematic diagram of set-up for I-V and C-V measurement
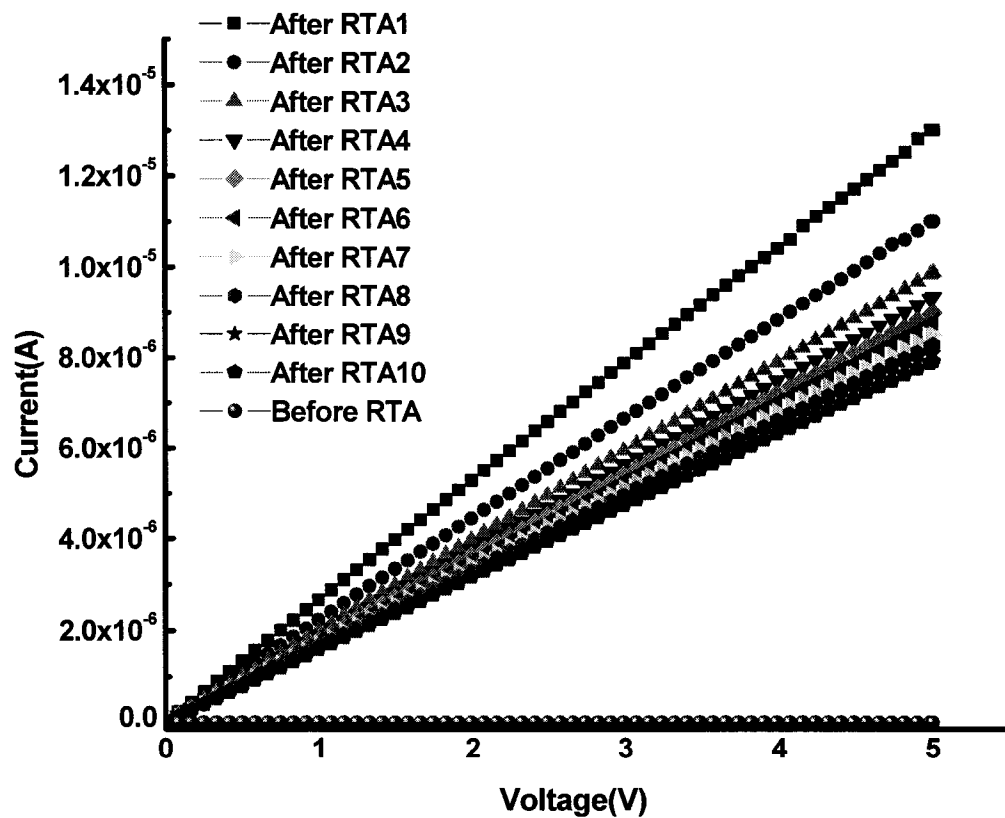
Figure 3-5 Typical I-V curves measured on patterned LBL Indium nanoparticle thin film (before and after RTA). After RTA 1,2, 3… refer to the measuring sequences
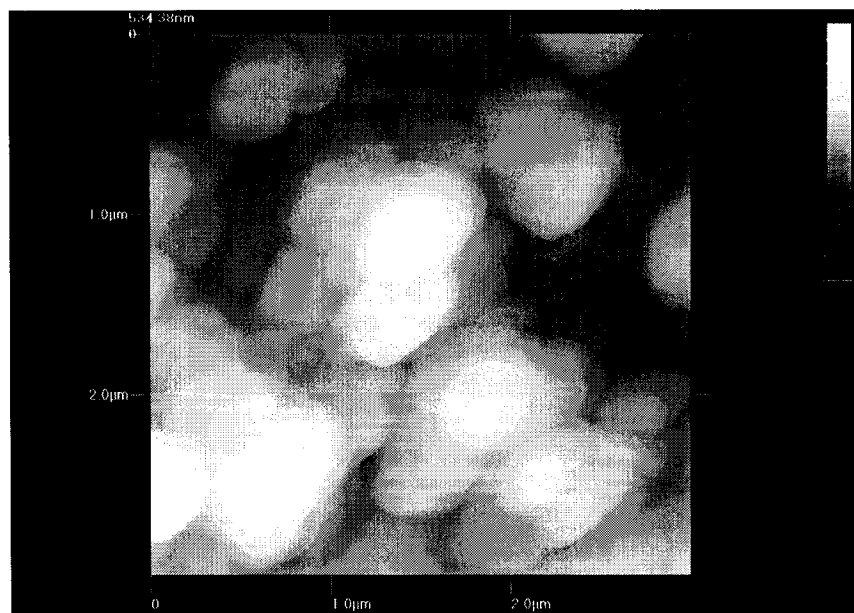
(a)
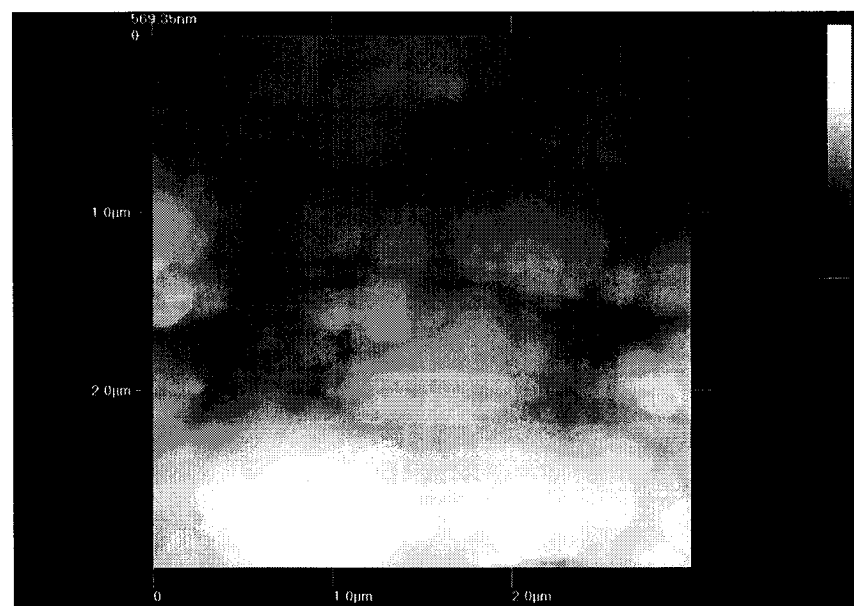
(b)

Figure 3-6 AFM micrograph taken on multiplayer thin film of indium nanoparticles and ployions a) Before RTA b) After RTA

CHAPTER FOUR

LBL NANOASSEMBLY COMBINED WITH HOT-EMBOSSING

4.1 Introduction

Nowadays, nanoscale electronics is a fast developing field and is predicted to play a significant role in future device technology [24]. Useful and interesting properties have been reported in the case of nanowires of metallic alloys [137] and semiconductors [138]. Many interesting problems have been thrown up because of unusual properties exhibited by these materials [21][139]. The drive to develop nanostructures has prompted a creative surge in technologies bridging the gap between the bottom-up nanoassembly and top-down micromanufacturing due to the high density of structures that can be produced with precise control over architecture at the nanoscale. Layer-by-Layer (LbL) self-assembly is a prospective nanofabrication technique to produce multilayer structures with precision of one nanometer through alternate adsorption of oppositely charged components (polymers, enzymes and nanoparticles) primarily via electrostatic attraction. When combined with nanopatterning techniques, this approach will make it possible the formation and study of conducting, semiconducting, and insulating nanowires.

Hot embossing is a reasonably fast and moderately expensive technique used to replicate mold structures into thermoplastics. It is a simple process, where the polymer and the tool are heated above the glass transition temperature (Tg) of the thermoplastic

57

and a controlled force is applied under vacuum. With the force still applied, the assembly is cooled below the Tg and they are de-embossed. Though the process cannot be fully automated, it is widely used to replicate microstructures on thermoplastics having different glass transition temperatures due to low start-up costs and ease of fabrication. Hot embossing offers the advantage of a relatively simpler replication process with few variable parameters and high structural accuracy. The hot-embossing technique can be employed to form the stamps with a nanoedge or nanotip. Our final goal is employing LbL self-assembly technique to fabricate metallic, semiconducting, and insulating nanowires with the aid of the stamps we already made.

<div align="center">

4.2 Fabrication and Discussion

</div>

4.2.1 Fabrication of Silicon Mold

A 4-inch silicon wafer with 1um silicon was immersed in H_2SO_4 and H_2O_2 solution (volumn ratio 7:3) at 70°C for 1 hour. Then, it was "hardbaked" at 115°C on hotplate for 5 minutes. A layer of 1 μm photoresist was spun on the silicon wafer. The speed was 1500 rpm, ramp was 200 r/s, and time 40 seconds. The wafer was baked on hotplate at 115°C for 1 minute. It was exposed under UV light for 17 seconds, and the desired pattern on photomask was transferred onto the surface of photoresist by developing. The developer was MF-319, and time was 40 seconds. Following the above steps, BOE (NH_4F: HF = 5.4:1) etching was done for 12 minutes in order to transfer the pattern on SiO_2. KOH wet etching (45% KOH) was carried with SiO_2 as mask for 1h. The resulted mold was shown in Figure 5-1. In this step, the KOH etching speed will substantially affect the quality of fabricated microstamp. Reducing the etching rate could get the best results.
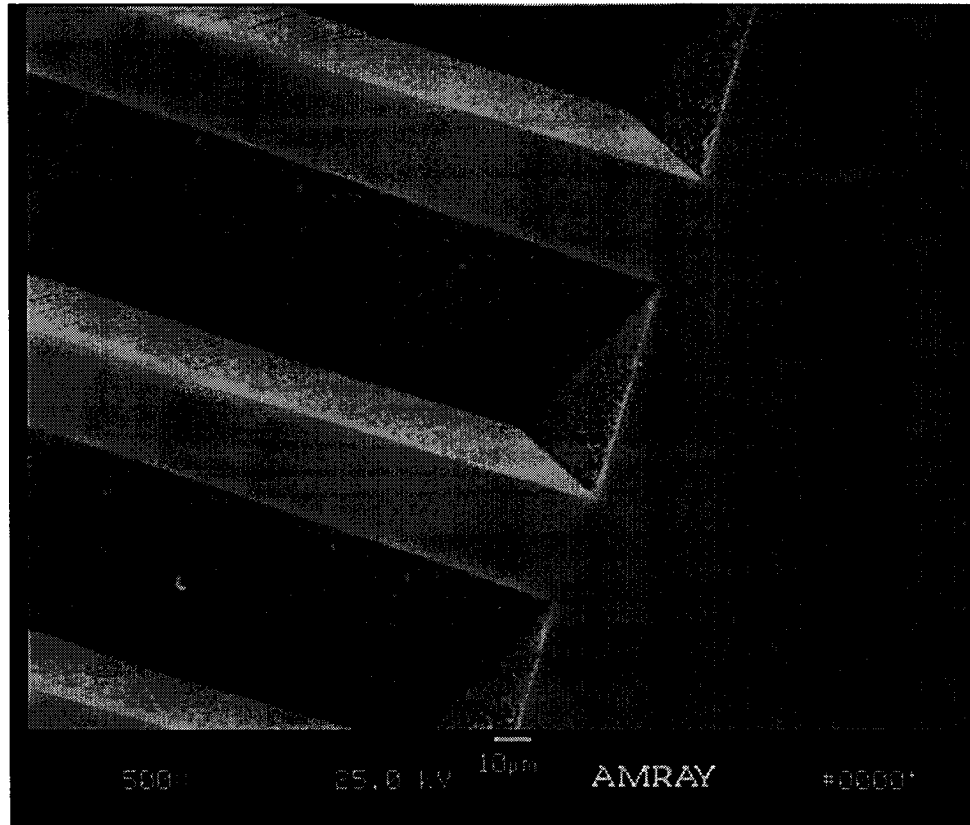
Figure 4-1 Silicon mold after KOH etching

4.2.2 Fabrication of PDMS Stamps

The elastomeric stamp is prepared by cast molding [140]: A prepolymer of the elastomer is poured over a master having a relief structure on its surface, then cured and peeled off. The master was fabricated as described. Figure 4-2 illustrates the procedure for fabricating PDMS stamps. The PDMS elastomer that we usually use is Sylgard™ 160 obtained from DowCorning. It is supplied as a two-part kit: a liquid silicon rubber base (i.e. a vinyl-terminated PDMS) and a catalyst or curing agent (i.e., a mixture of a platinum complex and copolymers of methylhydrosiloxane and dimethylsiloxane). Once mixed, poured over the master, and heated to elevated temperatures, the liquid mixture becomes a solid, cross-linked elastomer in a few hours via the hydrosilylation reaction between vinyl (SiCH=CH2) groups and hydrosilane (SiH) groups [141].

Pouring PDMS or Hot-embossing to get PDMS or PMMA stamp

Feature size should be in nanoscale (not shown in figure)

Stamping
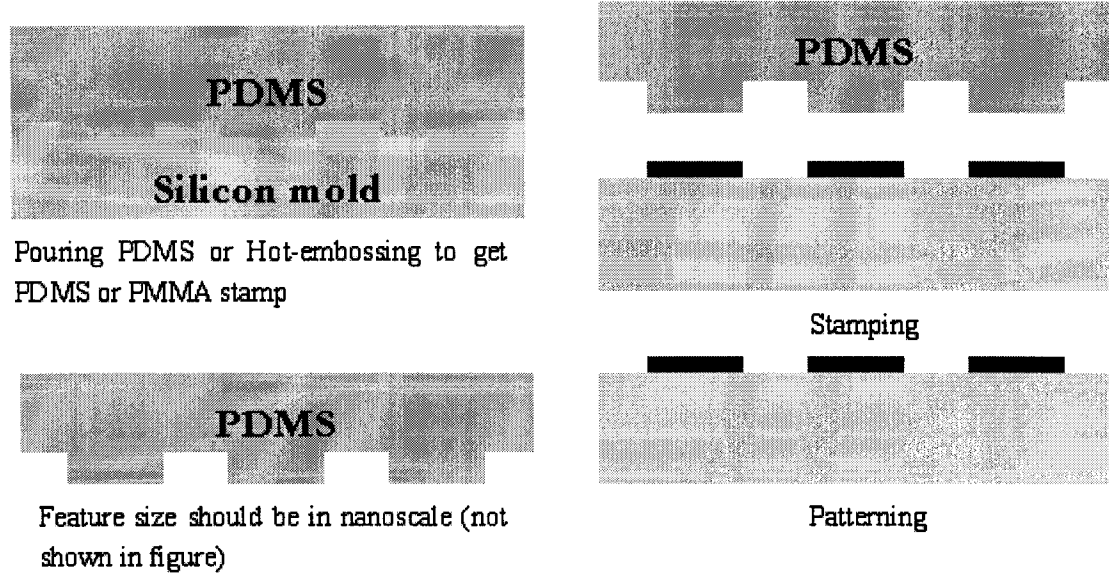
Patterning

Figure 4-2 Fabrication process of nanopatterning

4.2.3 Fabrication of PMMA Stamps
by Hot-embossing

Hot embossing system HEX 01/LT is used in our experiment, a commercial system from Jenoptik Mikrotechnik Company in Germany. The PMMA sheet is 0.5 mm thick with a glass transition temperature of 98°C. The entire fabrication procedures and parameters are as follows: (1) Open chamber and put PMMA on the substrate stage, (2) Close chamber and evacuate it down to 3 mTorr, (3) Lower the mold tool down to barely touch on the PMMA with the touch force 300 N, (4) Heat mold and PMMA in the same time to 130°C and keep the temperature for about 5 minutes, (5) Insert the mold into PMMA under force around 35000 N and keep it for 1 minute, (6) Cool down the mold and PMMA to 85°C, (7) Vent chamber and then demolding. The whole processing cycle is about 20 minutes. The sharp edges were accomplished after this. A good result obtained under the above process is shown in Figure 4-3
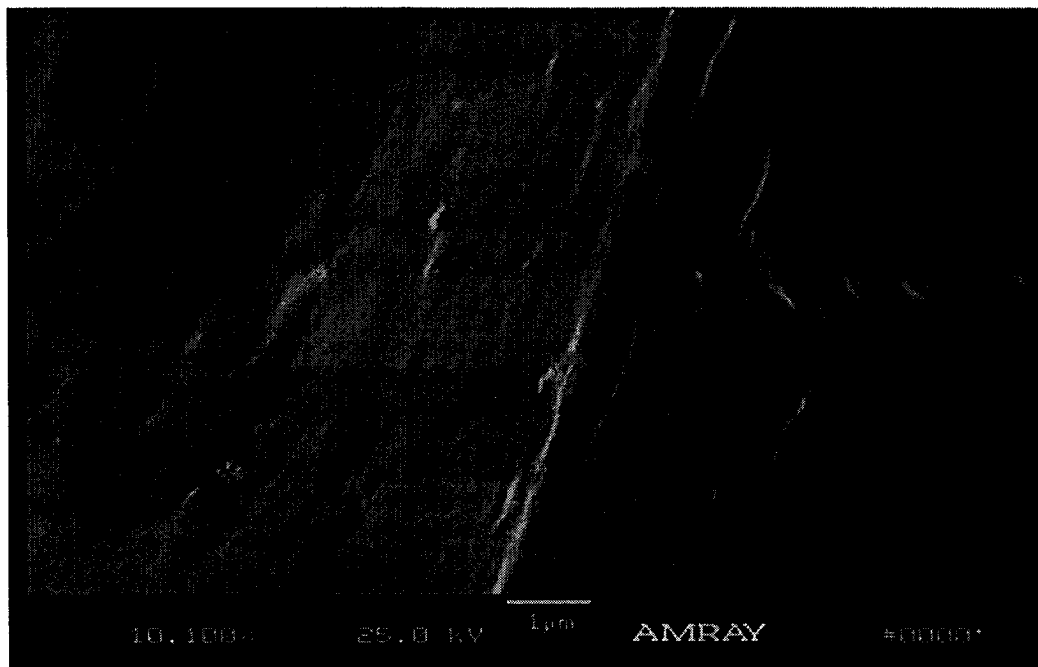
Figure 4-3 PMMA stamp made by hot-embossing

4.2.4 LbL Self-assembly and Discussion

LbL assembly of 45 nm silica particles was implemented on the silicon wafer. The sequence of the alternate immersion was [PDDA (10 min) + PSS (10 min)]$_2$ + [PDDA (10 min) + silica (10 min)]$_6$. The intermediate rinsing and drying after each immersion was necessary. The rinsing was done by purging the wafer in DI water flow for 1 minute. The wafer was placed on a spinner and spun to remove water by centrifugal force. The maximum rotation speed was set at 1300 rpm for a time of 45 seconds.

During the fabrication, we found the molecular weight of silicon elastomer has a critical effect on the formation of PDMS stamp. Silicon elastomer 184 (lower molecular weight) was used, and the formed stamp was shown in Figure 4-4(a). From this figure, we can see the edge is not as sharp as expected. It is not in nanoscale. Figure 4-4(b) shows the stamp formed by the silicon elastomer 160 (higher molecular weight). It almost

has the same structure of the silicon mold. The PMMA stamp with nanoscale feature size

can also be fabricated by hot-embossing techniques.
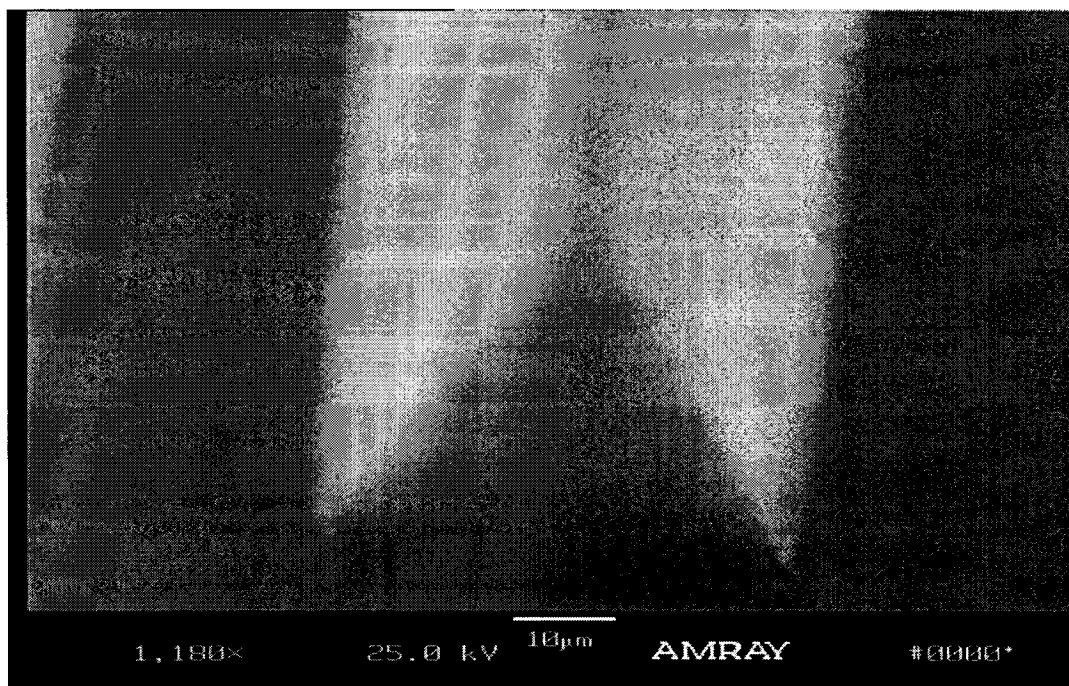
(a)
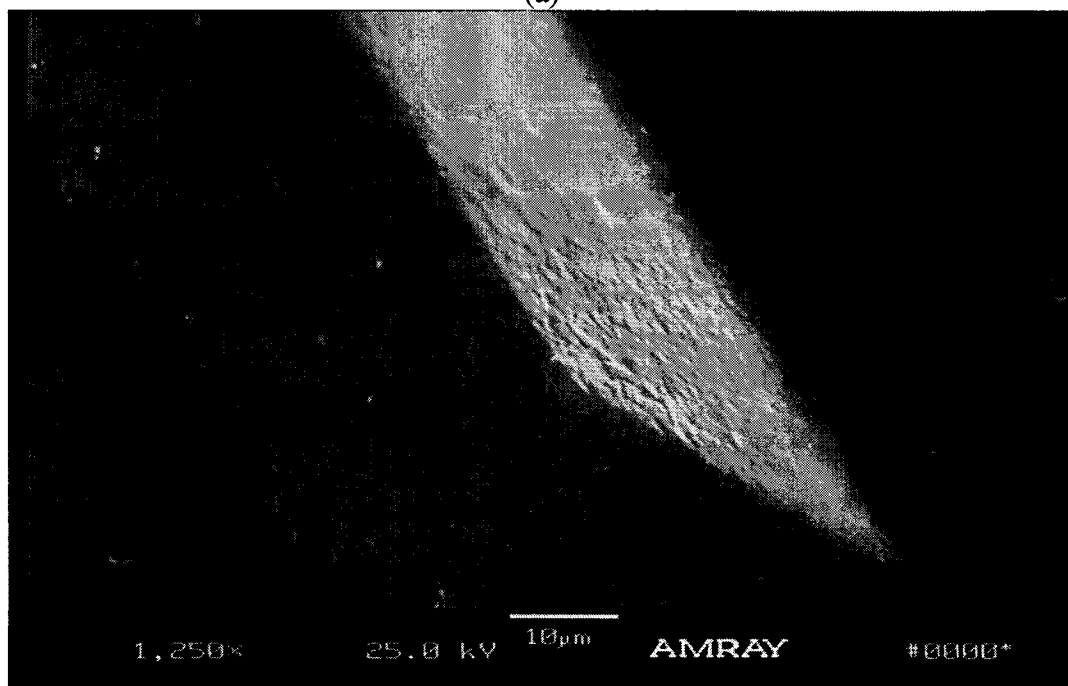
(b)

Figure 4-4(a) PDMS stamp made of silicon elastomer 184; (b) PDMS stamp made of silicon elastomer 160

CHAPTER FIVE

MICROCANTILEVER ARRAY BY LBL NANOASSEMBLY

5.1 Introduction

In the last decade, emerging MEMS technology and micromachining techniques have been popular in the miniaturization of sensors. Recent advances in designing and fabricating microcantilever beams capable of detecting extremely small forces, mechanical stresses, and mass additions offer the promising prospects of chemical, physical, and biological sensing with unprecedented sensitivity and dynamic range [142][143]. The cantilevers are microscopic bars free to move at one end and fixed at the opposite end, the bases are produced using standard silicon microfabrication techniques. The cantilevers are the simplest microelectromechanical systems devices that can easily be micromachined and mass-produced. Microcantilever-based sensors can be operated as surface stress sensors. Microcantilever-based surface stress sensors have been successfully used to monitor different bio-interactions in liquid environment like unspecific protein adsorption [144][145], DNA hybridisation [146], and antibody/antigen interaction [147]. The basis for the detection as surface stress sensor is that, when the target substance adsorbs onto the cantilever, the surface stress of that cantilever side changes. The change then generates a difference in the surface stress between both sides of the cantilever, which induces a permanent bending. It is this

63

cantilever bending which is ultimately detected and recognized as indicating the presence of the target analyte. The bending of the cantilever is detected using an optical lever method, by focusing the light from a low power laser diode onto the free end of the cantilever and recording the deflection by monitoring the displacements of the reflected laser light with a position sensitive detector.

Compared to traditional microsensors without moving parts, microcantilevers present some interesting properties such as good sensitivity and compactness. A cantilever array that enables multiple experiments to be performed simultaneously will expedite the experimental process and thereby rapidly provide a large database to study the underlying physics. A cantilever array also offers the opportunity to cancel cantilever drift and effects of external unrelated stimuli by subtracting the deflection signal of a functionalized cantilever from a nonfunctionalized one [148]. LbL was used for the construction of the microcantilevers for chemical/bio sensing. It is expected that these microarray assays will be able to provide massive, parallel platforms for data gathering. The advantage of the LbL method over the existing solid silicon or metal microcantilevers is that it allows remarkable nanometer-level control over the thickness and the vertical structure of the resulting multilayer. The thickness, hardness and other physical or chemical properties can be tuned through the number of layers that are deposited and the types of nanoparticles that are used. The thickness of microcantilevers fabricated in our experiments is 230nm, which is much thinner than regular solid or metal microcantilevers.

Primary technologies used in microarray manufacture include photolithography, ink-jetting, mechanical microspotting, and derivatives thereof [149][150]. In our work,

traditional microfabrication techniques such as lithography, ICP, and wet etching were employed in order to form multiple microcantilevers and provide the possibility of direct experimental determination of many physical properties of the LBL films of fundamental significance.

5.2 Fabrication of Microcantilever Array

Poly(dimethyldiallyl ammonium chloride), MW 200-300K (PDDA, Aldrich); and sodium poly (styrenesulfonate), MW 70,000 (PSS, Aldrich), were used at a concentration of 1.5 - 3 mg/ml. Dispersion of montmorillonite clay (Sigma) and Fe_3O_4/Fe_2O_3 powder were prepared by ultrasonificating for 30minutes. Both of the concentrations are 5 mg/ml. Fe_3O_4/Fe_2O_3 nanoparticles were bought from PolySciences Incorp. Buffered Oxide Etch (BOE) solution (6 parts 40% NH_4F and 1 part 49% HF) and positive photoresist S1813 (SHIPLEY) were employed in the fabrication process. An Inductively Coupled Plasma Etch System (Alcatel) was used for dicing the wafer, and a DC-RF Magnetron Sputter Deposition System (Uni-Film Technology) was used for the deposition of titanium and gold on the surface of the microstrip. For analysis of the microcantilever structures, we used a Scanning Electron Microscope (SEM, AMRAY), and Optical microscope (Olympus Japan).

A 4-inch silicon wafer (with 2μm SiO_2) was placed in nano strip solution at 80°C for 1 hour. The wafer was completely rinsed by DI water and baked on a hotplate at 115°C for 7 minutes. Positive photoresist (PR1813, Shipley) was coated on a silicon wafer with 2μm oxide. The photoresist was subsequently exposed to UV light through a mask. After developing and removing the exposed oxide, inductively coupled plasma (Alcatel) etching was done on this patterned wafer to form trenches to easily divide the

wafer. Photoresist was again applied on the wafer, and a second mask was utilized to transfer channels onto the photoresist. The photo resist was irradiated again through the third mask to project the image of the cantilever beams on the photoresist. LbL assembly of clay and magnetite nanoparticles was performed on this patterned substrate. Two precursor bilayers of PDDA and PSS were deposited to provide a uniformly charged surface. The subsequent coating of clay was optimized to make the multilayer strong and flexible. The sequence of assembly being [PDDA (10 minutes) +PSS (10 minutes)]$_{2\text{ cycles}}$ +[PDDA (10 minutes) + Fe_3O_4-Fe_2O_3 (15 minutes) +PDDA (10 minutes) +Clay (8 minutes)]$_{8\text{ cycles}}$. The intermediate rinsing and drying after each immersion was necessary. Subsequently, 20nm titanium, and 20nm gold were deposited on the multilayer. The wafer with the stratified layers of polyelectrolyte, magnetic nanoparticles, clay powder, titanium and gold was soaked in the developer solution to remove the photoresist and the multilayers above it. The wafer was then placed in acetone for 24 hours to obtain free-standing cantilevers. Finally, the wafer was divided to obtain cantilever bodies (Figure 5-1). An example of a thin film assembled to build up multilayers with alternating montmorillonite (clay) nanoparticles and cationic PEI or PDDA is shown in Figure 5-2.

5.3 Results and Discussion

The size of the microcantilevers is 200μm×100μm (Figure 5-3 and Figure 5-4). And the thickness of the microstrip was measured to be 230nm (Tencor Profiler). The cantilevers are highly flexible and can bend over 90 degrees by moving a permanent magnet of 400 Oe, 0.5cm above them and can be restored immediately once the magnetic field was removed.

ICP etching

LbL deposition

Channel formation

Lift-off

Cantilever image

Cantilever release

1500um

3500um
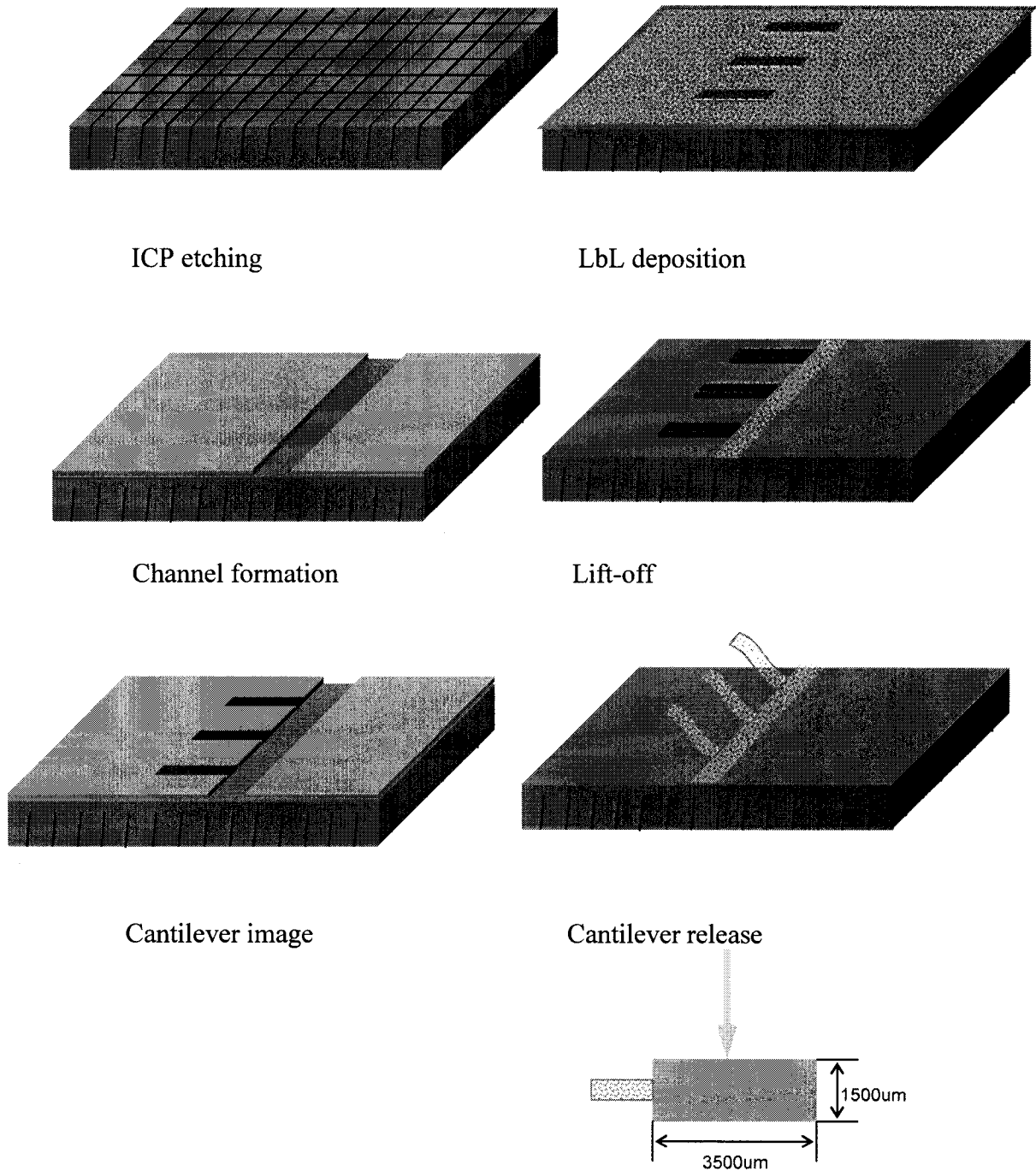
Figure 5-1 Fabrication procedure of microcantilevers by lithography and LbL assembly
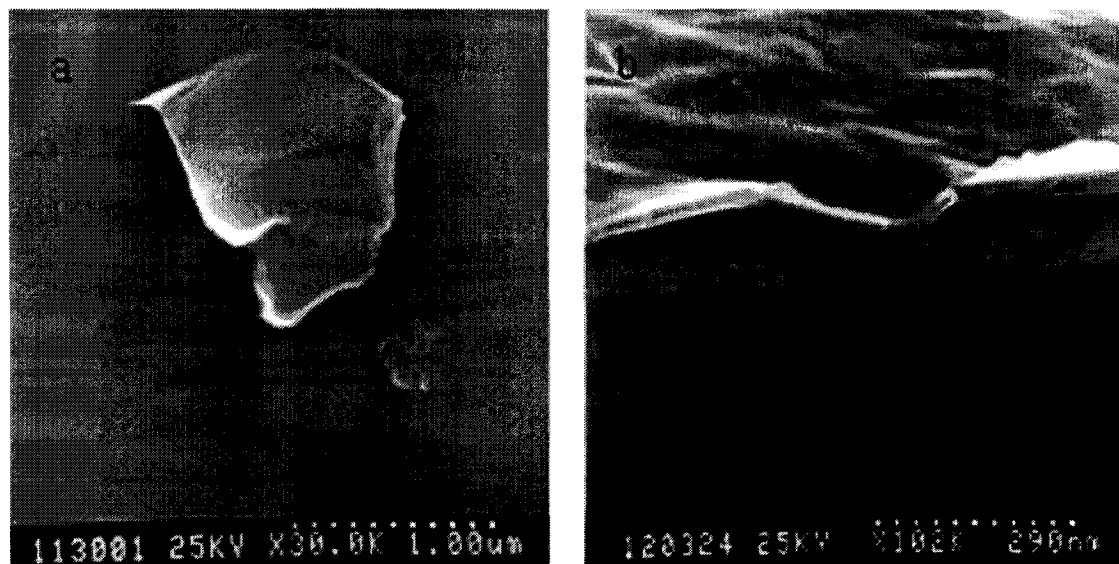
Figure 5-2 SEM image of a single Montmorillonite sheet and cross-section of the composite Montmorillonite/PDDA multilayer used for cantilever preparation

The apparatus used for deflection measurements is shown in Figure 5-5. The experiments were carried out in a flow-through glass fluid cell that holds the microcantilever. The volume of the glass cell is 0.3 cm^3, which ensures the fast replacement of the solution. The deflection of the microcantilever was measured utilizing an AFM head by monitoring the position of a laser beam reflected off the surface of the cantilever onto a four-quadrant photodiode (position-sensitive detector) [151]. The inset in Figure 5-4 shows the real picture when the cantilever was incorporated into the system. Once the molecules (in preliminary experiments – glucose oxidase) are absorbed through LbL assembly onto the cantilever surface, glucose oxidase will react with glucose in the solution. The cantilever will bend due to the stress induced by the reaction, and then the deflection can be detected.
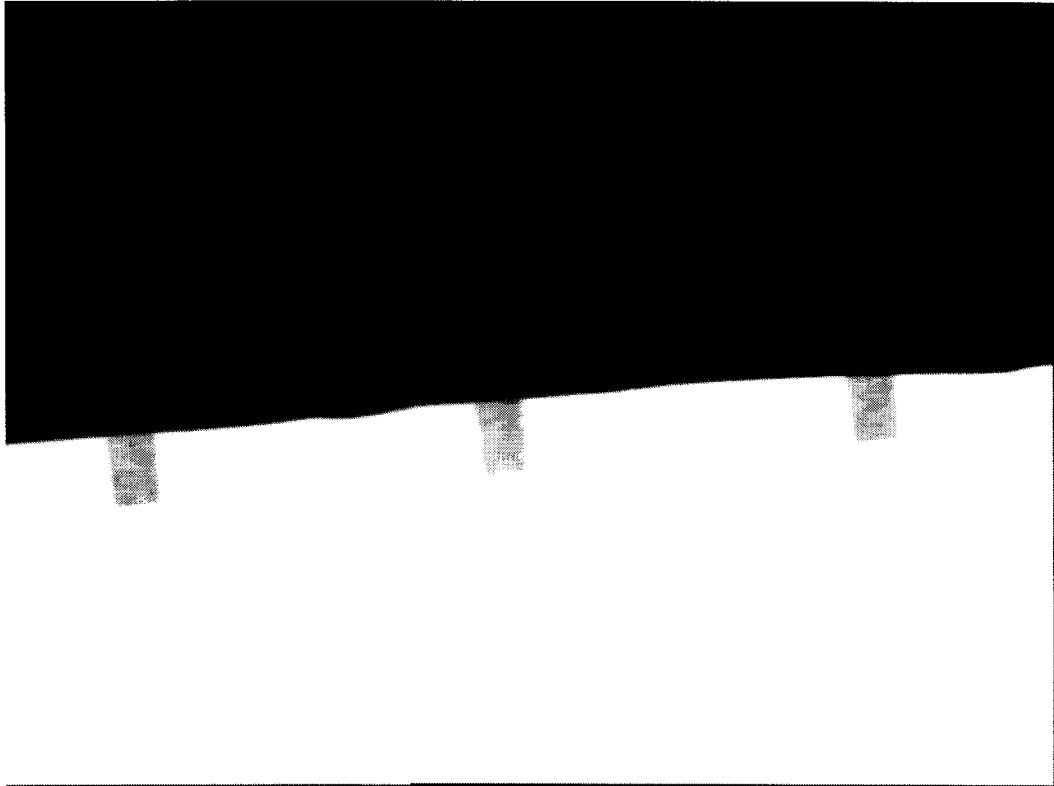
Figure 5-3 Images of free-standing microcantilever array in water
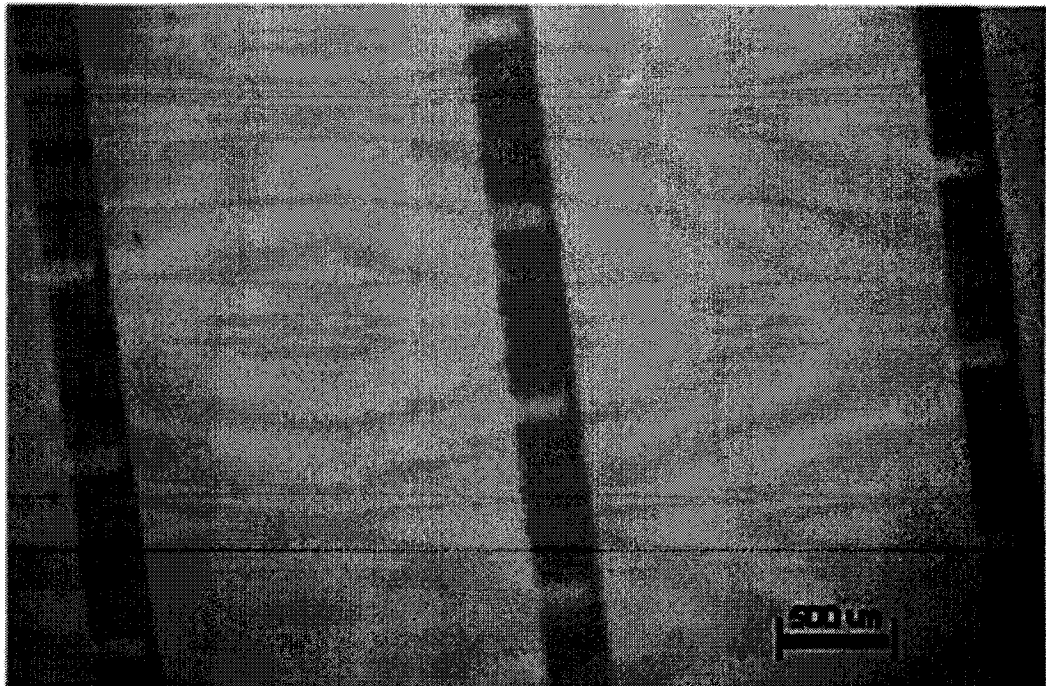
Figure 5-4 (left) and optical microscope image of microcantilever array (right)

The realization of the deflection measurement requires strong reflectivity of the cantilever surface. However, the property of the multilayer made from nanocomposite materials is inferior. The morphology of the microcantilever surface was investigated using the SEM (Figure 5-6). Although LbL self-assembly provided the nanostructured, precisely ordered ultrathin structure for the microcantilevers, the surface roughness was added while each layer of nanoparticles was deposited. Total integrated theory [152][153] provides the premise that rougher surfaces scatter more light, relating the surface roughness to the intensity of either diffuse or specular reflectivity. From equation 5-1 the R_{spec}/R_{total} value of close to one will be desirable for our work. In order to obtain this, δ (RMS roughness) has to be as small as possible. For instance, the average surface roughness of wafer doesn't exceed 5Å, and they will be able to provide sufficient reflectivity after sputtering the 20nm thick gold with all the other parameters in the equation kept same.

$$\frac{R_{spec}}{R_{total}} = \exp^{-\left(\frac{4\pi\delta \cdot \cos\theta_i}{\lambda}\right)^2} \qquad (5\text{-}1)$$

λ=wavelength

δ=RMS roughness

θ_i=angle of incidence

R_{spec}=total specular intensity

R_{total}=total reflected intensity (specular+diffuse)
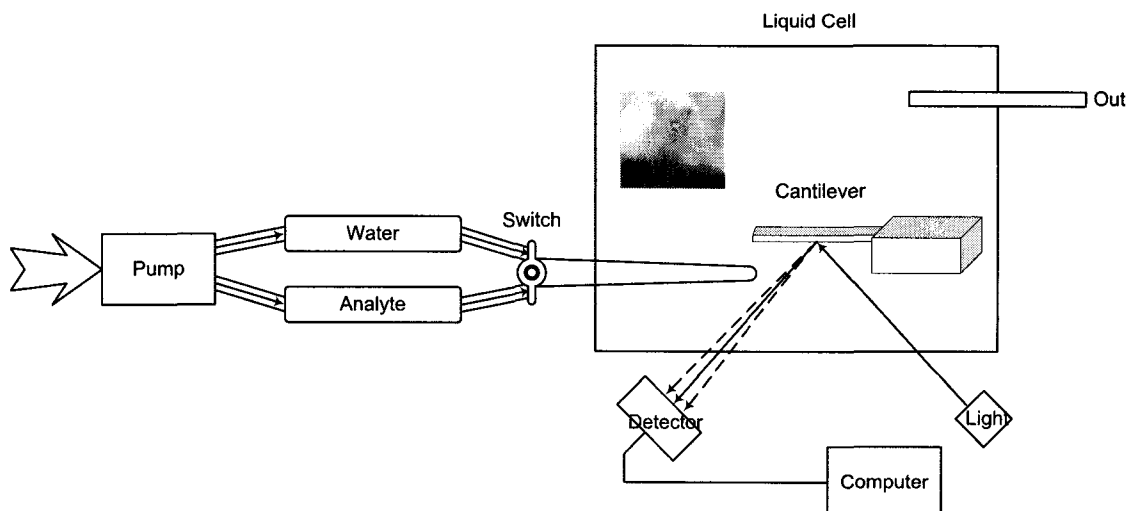
Figure 5-4 Schematic representation of the instrument showing the method of measuring cantilever deflection and the scheme for introducing solutions onto the cantilever
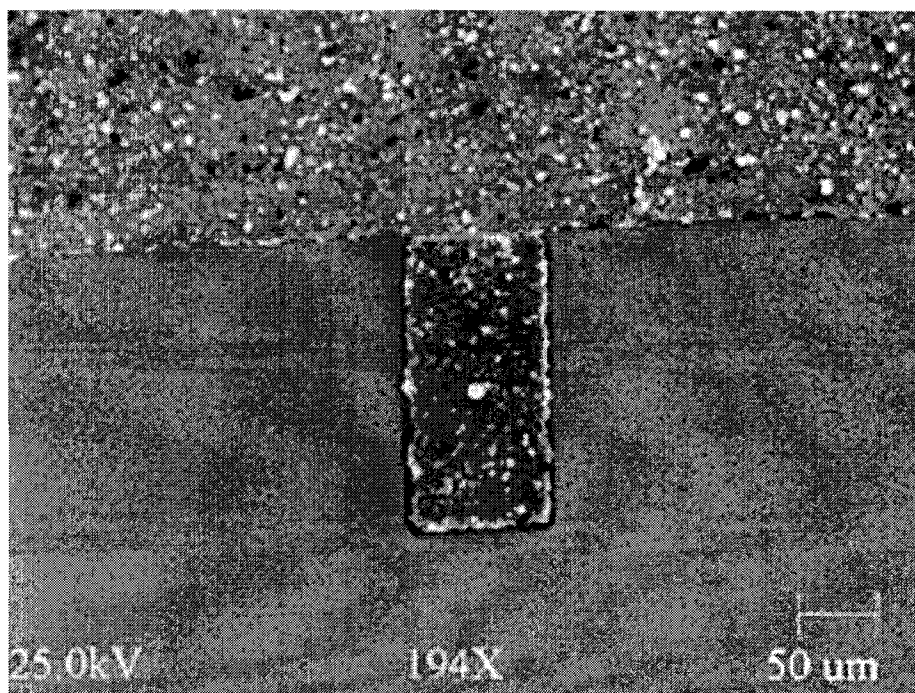
Figure 5-5 SEM image of one single microcantilever after sputtering deposition of 20nm titanium and 20nm gold

Veeco
Mag: 20.5 X
Mode: VSI

Surface Data

Date: 07/22/2004
Time: 03:25:33

Surface Statistics:
Ra: 398.92 nm
Rq: 445.95 nm
Rz: 5.96 um
Rt: 3.98 um

Set-up Parameters:
Size: 736 X 480
Sampling: 410.36 nm

Processed Options:
Terms Removed:
Tilt
Filtering:
None

Title:
Note:

Veeco
Mag: 20.5 X
Mode: VSI

Surface Data

Date: 07/22/2004
Time: 03:23:14

Surface Statistics:
Ra: 496.82 nm
Rq: 645.54 nm
Rz: 5.35 um
Rt: 5.94 um

Set-up Parameters:
Size: 736 X 480
Sampling: 410.36 nm

Processed Options:
Terms Removed:
Tilt
Filtering:
None

Title:
Note:

Figure 5-6 The surface roughness of modified nanocomposite multiplayer by deposition of (PDDA/PSS)$_{10}$, Upper, before modification; Bottom, after modification

Therefore, the surface has to be tailored to form a uniform multilayerd ultrathin strip. Polyelectrolytes have been utilized to modify surfaces and colloids [23][70]. In our experiments, multilayer buildup of PDDA and PSS was deposited on the microcantilever

surface before gold/titanium coating through spin-assembly [154]-[156]. It was expected that the surface smoothness would increase. The surface morphology was changed after modification. From the Figure 5-7, we can see the polyelectrolytes formed islands on the surface of originally fabricated multiplayer, which, however, provided insufficient reflectivity in the following characterizing experiments. Adjustment of fabrication processes will be required to provide better reflectivity.

Nanocomposite microcantilever arrays were fabricated using tradiational lithography and LbL techniques. These microcantilevers are highly flexible due to the special properties of nanocomposite materials, providing a new route of constructing particularly sensitive chemical sensors to detect desired or undesired chemicals in the solutions. Measurements of cantilever deflections will be performed by detecting the reflected laser beam from the top of the microcantilever using a four quadrant photodiode. Further work will be done to modify the surface of microcantilever by LbL self-assembly for various chemical sensing.

CHAPTER SIX

CONCLUSIONS AND FUTURE WORK

LbL nanoself-assembly has been described as an approach to design organized films that contain different polymer, protein, dye, and nanoparticle monolayers in precise locations perpendicular to the surface. It can be further investigated and combined with various microfabrication techniques such as RTA, photolithography, hot-embossing and ICP to form microelectronic and MEMS devices. The LbL nanoself-assembly is an easy and general fabrication process. It does not demand a high purity of components. It can be automated and scaled-up for mass production.

The temperature effect of LbL self-assembly was studied. In addition to ionic strength, pH, it can be another factor to adjust the adsorption rate. Increasing temperature can enhance the efficiency of this technique. With further knowledge about this method, a resistor was fabricated by combining photolithography and LbL self-assembly. The RTA technique was employed to achieve higher conductivity. Microstamps with nanoedge were formed by hot-embossing, and they could be applied to attain nanopattering on LbL self-assembled multilayer. Through integrating nanoassembly, photolithography, wet etching and ICP, microcantilever arrays were accomplished. Provided less surface roughness is achieved, the multiple microcantilevers can be utilized for chemical/biosensing.

Different materials such silica nanoparticles can replace magnetic nanoparticles as the main component for the construction of microcantilevers array. Since they have more uniform size distribution than Fe_2O_3/Fe_3O_4 nanoparticles, smoother surfaces will be expected. Another approach is to adjust the fabrication process. If the evaporation or sputtering of gold layer can be done before the deposition of nanoparticle multilayers, it will not be affected by the rough surface made by LbL self assembly. Once this obstacle is cleared, these microcantilever arrays can be developed into various chemicals/biosensors by simply modifying the top surface with selective chemicals.

APPENDIX A

MOS-CAPACITOR BASED ON LBL SELF-ASSEMBLY

1 Introduction

Nanoparticles (NPs) are exciting materials because they exhibit unique electronic, catalytic, and optical properties, sometimes different from those of the same bulk material. A great deal of attention has been attracted for applications of nanoparticles as building blocks to microelectronics, optoelectronics, and catalysis.

The relatively new layer-by-layer (LbL) self-assembly, based on alternate adsorption of oppositely charged components (polymers, nanoparticles, or proteins), is becoming an increasingly popular technique. At the beginning of the process, three layers of linear polyions are adsorbed onto the substrate to make the surface uniformly charged. Next, negatively charged nanoparticle layers are assembled step by step in alternation with an oppositely charged polycation solution.

In addition to the thin film deposition, an approach must be developed to readily generate complex and distinct patterns on the LbL self-assembled multilayer films. In our early reports, two methods, based on the combination of traditional lithography and LbL assembly, were presented to pattern nanoparticle films. One is referred to by the authors as the "modified lift-off", and the other as the "metal-mask method". In our experiment, the capacitor arrays were patterned by the "modified lift-off" as illustrated in Figure 1.

76

These capacitors can be fabricated onto integrated circuit chips. Metal-oxide-semiconductor (MOS) capacitors, with thermal SiO_2 as the gate oxide, have become the prime structure to carry out digital functions in silicon integrated circuits. However, the fabrication of a MOS capacitor using the conventional silicon MOS technology demands sophisticated facilities. High process temperature also needs to be balanced to avoid the damage to subsequent processes. And the growth rate of the thermal silicon dioxide is usually very low. Hereby an approach to fabricate the basic MOS capacitor with a technique combining traditional lithographic technique and LbL self-assembly was developed because dielectric layer consisting of silica and polyion can be self-assembled easily and rapidly. The insulating layer is made of 6 layers of LbL self-assembled silica nanoparticle thin film. Capacitors are fabricated on 4 inch P-type and N-type silicon wafers. The measured CV curves are in compliance with typical MOS capacitors. Compared to the traditional process, this has the advantages of low temperature, low cost, and short processing time. LbL self-assembly is also called molecular beaker epitaxy because it just requires several beakers to realize the "dipping in" adsorption. The lithographic technique is already a mature process, widely used in the microelectronic industry. The combination of traditional lithography and LbL self-assembly guarantees an extremely high reproducibility in fabrication of semiconductor devices. The regular dipping also enables the automation of this process if it is applied to mass production. The self-assembled thin film of silica nanoparticle is stable enough to withstand the ultrasonic wave. The simplicity and reliability of this process to fabricate the simple MOS capacitor provides a new way to fabricate other microelectronic or optoelectronic devices by traditional lithography and LbL self-assembled building blocks.

2 Experimental Methods

Poly (diallyldimethylammonium chloride), MW 200-300K (PDDA, Aldrich), and

sodium poly (styrenesulfonate), MW 70,000 (PSS, Aldrich), were commercially

available and used without further purification at a concentration of 1.5 - 3 mg/mL. The

pH of the solutions was adjusted by adding aqueous NaOH or HCl. PDDA is a

quarternary ammonium linear polycation and PSS (pK_a 1) is a linear polyanion.

Polyions were used in solutions at pH 8. SiO_2 colloidal solutions (231 mg/mL, Nissan

Chemical, Ltd) were diluted in water to provide concentrations of 10 mg/mL at pH 9.

The diameter of the silica particles was 45 ± 5 nm.
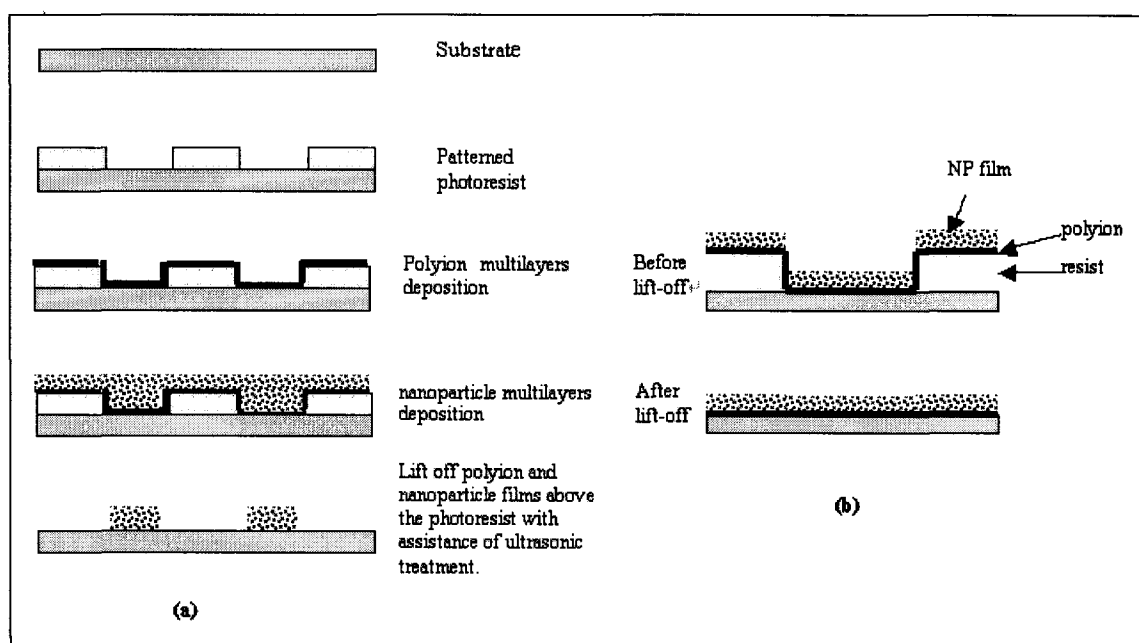
Figure1 (a) Scheme of patterning nanoparticle thin films with ultrasonic treatment (b)
Scheme of patterning nanoparticle thin films without ultrasonic treatment. NP and
polyion films can not be lifted off because of the linkage between polyion molecules

A QCM equipment produced by USI System in Japan was used to monitor the

assembly process. The resonators used were covered by evaporated silver electrodes on

both sides. The resonance frequency was 9 MHz (AT-cut). The QCM resonator was

immersed for a given period of time in a polyelectrolyte solution and dried in nitrogen

stream. The frequency changes were then measured. The QCM frequency was stable within ± 2 Hz during 1 hour. All experiments were carried out in an air-conditioned room at about 22 °C.

In the first stage, a well-defined precursor film with a thickness of about 10 nm was assembled from PDDA and PSS onto resonators or mica. The precursor films contained 3 polyion layers in the alternate mode: PDDA /PSS, and the terminal layer was "positive" PDDA. Then a substrate was alternately immersed for 10 min in aqueous dispersions of SiO_2 and in aqueous PDDA with intermediate water washing. This process was periodically interrupted for the purpose of measuring QCM resonance frequency.

The following relationship is obtained between adsorbed mass M (g) and frequency shift ΔF (Hz) by taking into account the characteristics of quartz resonators used:

$$\Delta F = -1.83 \times 10^8 \, M/A \tag{1}$$

where A is the apparent area of quartz microbalance placed between QCM electrodes. This is 0.16 ± 0.01 cm^2 in our system. Then, one finds that 1 Hz change in ΔF corresponds to 0.9 ng in weight. The thickness of the alternate layer corresponding to QCM frequency shift was determined by SEM observation of the film cross-section from SEM images of cut resonators coated with silicon/polycation films, which gives the following relationship with ±5 % error:

$$d \, (nm) = 0.022 \, (-\Delta F) \, (Hz) \tag{2}$$

A resonator with an assembled film was cut and coated with 20 Å thick Pt by use of an ion-coater (Hitachi E-1030 ion sputter, 10 mA/ 10 Pa) under argon atmosphere.

Scanning electron micrographs were obtained with a Hitachi S-900 instrument at an acceleration voltage of 25 kV. SEM images of MOS-capacitors were made with a lower resolution instrument "AMRAY"

The substrates were 4-inch silicon wafers, P type (orientation <100>, > 1 OHM-CM) and N-type (orientation <100>, 1-100 OHM-CM) from Silicon Quest Inc. A double-side mask aligner (EV420 from Electronic Visions, Inc.) was used as the UV light illuminator. Aluminum layers were deposited on a silicon substrate by the DV-502A high-vacuum evaporator from Denton Vacuum, Inc. The WYK RST white light interferometer microscope was used to measure the surface roughness and dimension of the thin film. The electronic characteristic instrument was from Keithley Co., Inc. Ultrasonication was performed with an 8892 Cole-Parmer ultrasonic cleaner.

Initially, the 4-inch silicon wafer was put into sulfuric acid and hydrogen peroxide solution (volume ratio 3:7) at 70°C for 1 hour. The wafer was completely rinsed by DI water and baked on a hotplate at 150°C for 5 minutes to remove the moisture. Then it was placed on a spinner to coat a layer of negative photoresist (NR9-1500P from Futurrex, Inc.). The maximum speed was set at 1000 rpm for 40 seconds. The wafer with photoresist was baked on a hotplate at 150°C for 80 seconds. The resist was subsequently exposed by UV light for 22 seconds to transfer the pattern from the mask onto the resist. Next, it was baked at 100°C for 80 seconds and finally immersed in developer solution for 12 seconds. At this point, the capacitor pattern was transferred onto the resist.

Following the above steps, LbL assembly of 45 nm silica particles was implemented on the silicon wafer. The sequence of the alternate immersion was [PDDA

(10 min) + PSS (10 min)]$_2$ + [PDDA (10 min) + silica (10 min)]$_6$. The intermediate rinsing and drying after each immersion was necessary. The rinsing was done by purging the wafer in DI water flow for 1 minute. The wafer was placed on a spinner and spun to remove water by centrifugal force. The maximum rotation speed was set at 1300 rpm for a time of 45 seconds. Subsequently, the deposition of aluminum was carried out at a pressure of 10-5 mtorr with a deposition rate of 2 Å/s until a thickness of 3000 Å was reached. The wafer was then soaked into acetone solution for 5 minutes to dissolve the photoresist, and an ultrasonic bath was introduced for roughly 3 seconds to improve the lift-off.

The capacitors were made on both P and N type wafers. The capacitance versus voltage curves were obtained under a voltage range from -2V to 2V with a step of 20 mV.

3 Results and Discussions

Figure 2(a) shows an SEM image of the (45-nm silica/PDDA)$_4$ multilayer cross-section. The film has a permanent thickness of 170 nm, leading to 43 nm for every bilayer close to the silica particle diameter. A film mass from QCM and film thickness from SEM gives a density of the SiO$_2$/PDDA multilayers as ρ = 1.43 ± 0.05 g/cm^3. To calculate the silica packing coefficient in the films, it is reasonable to assume that the dry film consists of SiO$_2$, PDDA, and air-filled pores. The mass ratio of PDDA to PDDA/SiO$_2$ bilayer obtained from QCM measurements is 0.08. Taking into account component densities (ρ = 1.43, ρ_{SiO2} = 2.2, and ρ_{PDDA} = 1.1 g/cm^3), the volume ratio is obtained as $V_{PDDA}/V_{bilayer}$ = 0.1. From the equation $\rho_{PDDA}V_{PDDA} + \rho_{SiO2}V_{SiO2} +$

$\rho_{air} V_{air} = \rho V$, where the air-term is very small, $V_{SiO2}/V = 0.7$. This is very close to the theoretical dense-packing coefficient for spheres (0.63), and corresponds to details in the SEM-micrographs. SiO_2/PDDA film volume composition is: 70 % SiO_2 + 10 % polycation + 20 % air-filled pores. These pores are formed by closely packed 45-nm SiO2 and have a typical dimension of 15 nm. Therefore, the dielectric constant of our silica/PDDA multilayer is different from silica due to about 30% of inclusions, such as air, polyion layers, etc. In the analysis of the MOS devices, it is found that the dielectric constant was slightly higher than the one for thermal silica. In our group, it is possible to produce ultrathin multilayers of silica nanoparticles in the thickness ranging from 100 nm to hundreds of nm with precision of about 10 nm. These films have a porous structure related to the close packing of silica spheres in the layer.

As shown in Figure 3, clear patterns of the capacitor arrays with sharp borders were created on a silicon wafer. The arrays consist of round and square capacitors with various sizes. All 45 nm SiO_2 spheres were closely packed to form a dense structure. The surface roughness of the capacitor was 6.5 nm measured by RST. The growth step can be easily estimated by measuring the frequency shift of the quartz crystal microbalance resonator, and the monolayer thickness can be calculated accordingly by the Sauerbrey equation. Figure 2(b) gives the QCM monitoring of alternate PDDA and SiO_2 adsorption where the thickness was calculated from frequency shifts with formula 2. As recorded by QCM, at every assembly step, the component monolayer was formed. It shows that at the sixth cycle, the thickness of the SiO_2 layers is 260 nm. When added to the 300 nm aluminum electrode, the height of the whole device is 567 nm, in well compliance with the 2-D profile of Figure 3(b).
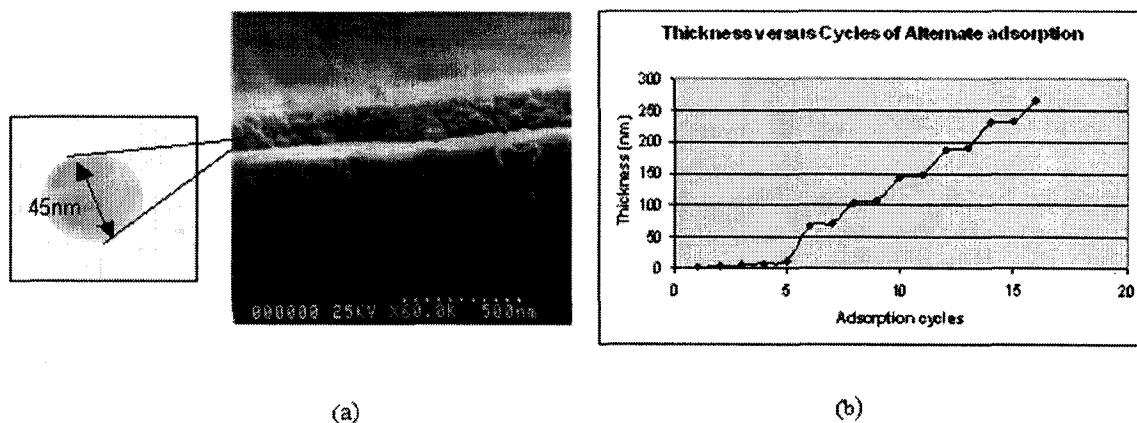
(a)

(b)

Figure 2 (a) SEM image of cross-section of (45-nm silica / PDDA)4 multilayer on silver electrode (b) QCM monitored 45-nm silica growth

The fabricated device demonstrates the C-V curve of a typical MOS capacitor with distinct accumulation, depletion, and inversion regions, as shown in figure 4. The MOS structure is basically a capacitor with the silica as the dielectric material. If the silicon were a perfect conductor, the parallel-plate capacitance would be determined by the oxide capacitance as it is in the accumulation region. However, it always deviates from the oxide capacitance due to the voltage dependence of the surface space-charge layer in silicon. The space-charge occurring at the interface of silicon and oxide acts as another capacitance in series with the oxide capacitor, giving an overall capacitance that is smaller than the pure oxide capacitance. Since the inversion of a P-type MOS capacitor happens at a positive voltage and an N-type one at a negative voltage, the C-V curves move in opposite directions for P and N type MOS capacitors. If the layer of silicon dioxide was produced by conventional thermal oxidation, the dielectric constant would be 3.9. Given the size of each square device 200 μm by 200 μm and 267 nm high, the oxide capacitance is calculated as 5.2 pF, reasonably close to the experimental data, 8 pF. The slightly larger value means a larger dielectric constant of the LbL self-assembled insulator layer. The precursor and intermediate polyion multilayer is the root for the

higher dielectric constant because the dielectric constant of the polyion films is normally ten times higher than silica[18]. The experimental results also show that the capacitance of each device is strictly proportional to the area of electrode, implying an extremely high reproducibility of the processes.

In our process, a conventional lithographic technique, such as lift-off, was used to pattern the capacitors on multilayer films. However, because the LbL self-assembled nanoparticle films are unlike the conventional thin films in many respects, modification and optimization of the traditional process is required.

During the lift-off it was better to introduce ultrasonic treatment for 3 seconds when the wafer was soaked in developer solution. Inside the structure of nanoparticle film, polyion multilayers such as PDDA and PSS were sandwiched between the nanoparticle film and photoresist as a kind of "chemical glue". The structure of the polyion is like a long thread which strongly links to each other. It is hard to break them up during the lift-off, so at some areas the nanoparticle and polyion multilayer can not be removed when the photoresist is dissolved. They just drop down and re-attach to the film underneath, as shown in Figure 1(b). The ultrasonic treatment is introduced to disconnect the linkage between polyion branches and obtain a more distinct pattern with higher reproducibility.
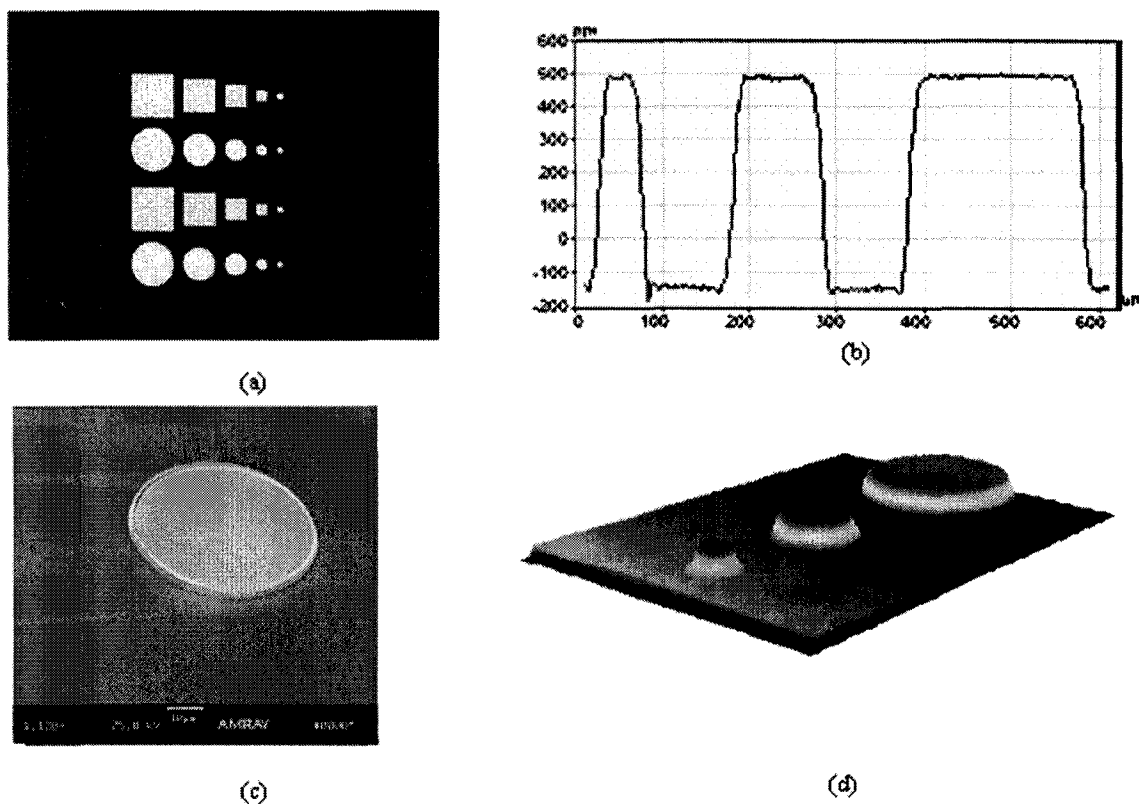
Figure 3 (a) optical image of the capacitor arrays, the minimum diameter or size is 50 μm (b) 2-D profile (c) SEM image of layers of 45-nm silica particle thin film (d) 3-D plot of the capacitors

Other dielectric materials such as montmorillonite had also been tested as the insulating layer. They did not perform as well as the silica nanoparticle although the monolayer thickness can be more precisely controlled. There are many other nanoparticles suitable for LbL self-assembly which may function differently for various devices.

4 Conclusions

Layer-by-layer (LbL) self-assembled thin films were introduced to the fabrication of basic MOS devices. The corresponding patterning technique was also developed to process the LbL assembled thin film. The resulted geometry and electronic characteristics indicate the extension of this technique to fabricate other semiconductor or

optoelectronic devices. The combination of LbL assembly with the mature lithography process offers us the opportunity to fabricate devices rapidly with inexpensive beakers at room temperature. The additive thin films can be coated on almost any material in nature. It also provides a remarkable reliability and possibility of automation for batch production.

A wide array of potential applications exists for the fabrication of conventional devices using nano-bricks, as well as lowering the price and reducing the complexity of the traditional processes. More sophisticated devices such as MOS field effect transistors made by this technique are under investigation.
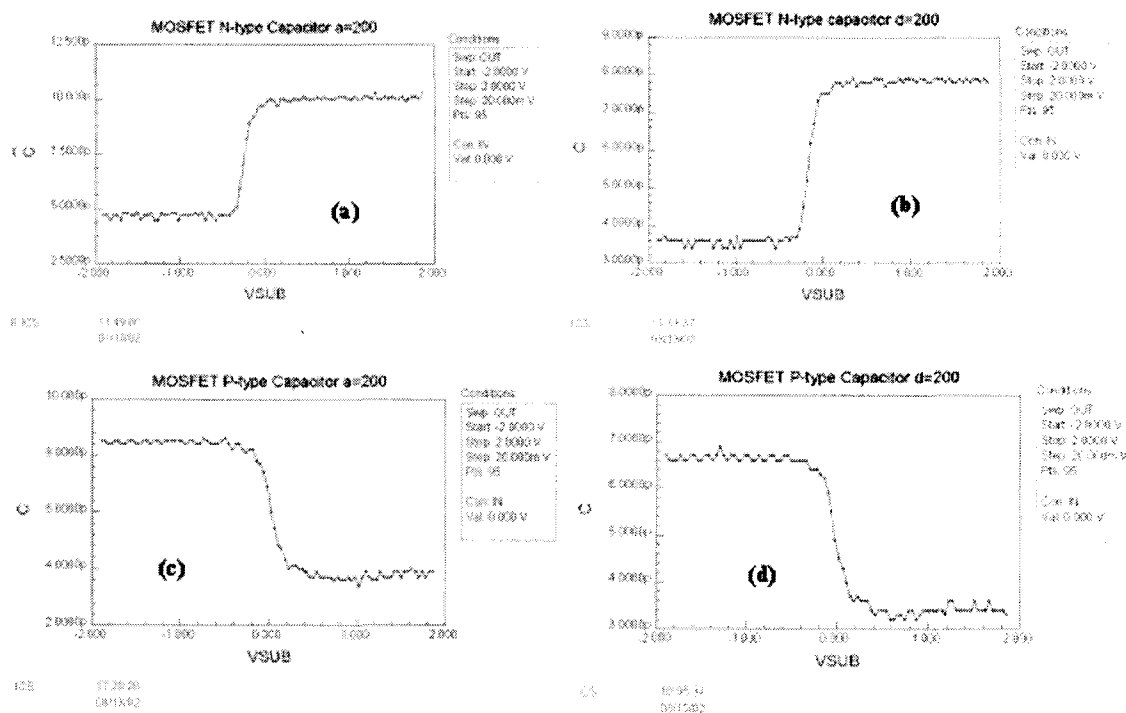

Figure 4 capacitance versus voltage curves of MOS P and N type capacitors (a) N type square capacitor with size of 200 μm (b) N type round capacitor with diameter of 200 μm (c) P type square capacitor with size of 200 μm (d) P type round capacitor with d

APPENDIX B

OFET CONTAINING LBL SELF-ASSEMBLED SILICA

1 Introduction

Organic field-effect transistors (OFETs) have attracted great interests since the last decade due to their low cost, flexibility, and easy processability for the applications to large-area displays and low-end electronic devices like smart cards.

To be the potential solutions for those applications, OFETs must provide substantial performance and processing advantages compared with the conventional technologies. The main important parameters of device performances are charge carrier mobility, threshold voltage, on/off current ratio. Among the various OFETs based on organic semiconductors, pentacene OFETs were demonstrated to have the highest mobility and sufficiently high on/off current ratios up to date. Moreover, the low-cost and batch fabrication process is extremely necessary to benefit the various advantages of the OFETs. Furthermore, the low-temperature process is required due to the thermal properties of the organic materials. SiO_2 is the most widely used gate dielectric. However, the deposition of SiO_2 in the previous works was done either by the high-temperature thermal oxidation, or through LPCVD, PECVD, or sputtering requiring complex equipments.

87

In recent years, the layer-by-layer nano-assembly has gathered a lot of attention in the fabrication of nanometer scale electronic devices because it is a very easy and low-temperature process requiring no expensive and complex facilities. The vertical dimension of the self-assembled thin film can be precisely controlled as well as the molecular order. Unlike the conventional process, the LbL self-assembly allows one to obtain the thin films for a semiconductor device with a dramatically lower temperature, lower cost and shorter processing time. In this paper, a simple, low-temperature, and low-cost fabrication procedure of pentacene OFETs is presented. Self-assembly technology was used to deposit the gate dielectric layer formed with SiO_2 nanoparticles.

2 Experiments

Figure 1 shows the electrical characteristic of the Au/self-assembled SiO_2/heavily doped Si structure shown as the inset of Figure 1. The SiO_2 layer 0.45 μm thick was self-assembled and a gold electrode 80 nm thick was sputtered. Since the breakdown field was larger than 0.44 MV/cm from the analysis of electrical characteristics shown in Figure 1, it indicates that the self-assembled SiO_2 can be used as a gate dielectric instead of silicon dioxide based on thermal oxidation or other deposition techniques.

For the pentacene OFETs with self-assembled SiO_2 (SA-SiO_2) as the gate dielectric, shown in Figure 2(b), a heavily doped silicon wafer (resistivity of about 0.001 $\Omega\cdot$cm) was used as the gate electrode and the substrate. Next, the dielectric layer was self-assembled with SiO_2 nanoparticles 45 nm in diameter. Figure 3(a) shows the schematic diagram of the device with 4 layers of self-assembled SiO_2 nanoparticles, and Figure 3(b) illustrates the self-assembled SiO_2 thin film. After the cleaning of the silicon wafer surface and H_2SO_4-H_2O_2 treatment for 1 hour, the silicon substrate was immersed

into a 50 ml poly(dimethyldiallylammonium chloride) (PDDA) solution for 20 minutes. Following that, it was rinsed in DI water for 1 minute, and dried by a nitrogen flow. It was then immersed in a 50 ml polystyrene (PSS) solution for 10 minutes, rinsed and dried as in the previous step. Then the immersion into PDDA was repeated for 10 minutes. The sequence was done as {PDDA (20 minutes) + [PSS (10 minutes) + PDDA (10 minutes)]$_2$}, i.e. dipping in PSS and PDDA were carried again after the first three steps. The intermediate rinsing and drying are necessary. Thus up to date the outermost layer was positively charged PDDA. After the precursor mutilayer, the substrate was immersed in 50 ml diluted SiO_2 (45 nm in diameter) colloidal dispersions (231 mg/ml, Nissan Kagaku, Japan) with a concentration of 5 mg/ml for 5 minutes, rinsed and dried, followed by another cycle of PDDA (10 minutes). Therefore the complete sequence of adsorption is {PDDA (20 minutes) + [PSS (10 minutes) + PDDA (10 minutes)]$_2$} + [SiO_2 (5 minutes) + PDDA (10 minutes)]$_{10}$. After 10 layers of SiO_2 nanoparticles self-assembled, the thickness of the final SiO_2 layer is about 450 nm.

Upon finishing the self-assembly of SiO_2 layer as the gate dielectric, a layer of Au 80 nm thick was sputtered on top of gate dielectric, and then patterned to form the source and the drain electrodes, as shown in the Figure 2(b). Finally, the pentacene OFETs were completed with the deposition of a layer of pentacene about 200 nm thick as the organic semiconductor. Pentacene, consisting of five fused benzene rings with the structure shown in Figure 2(a), was thermally evaporated through a shadow mask with a slow deposition rate and a working pressure of 6×10^{-7} Torr. Pentacene was used as purchased from the company without any purification. During the evaporation of pentacene, the substrate was held at room temperature. With the purification of the pentacene material

and the moderation of the substrate heating as described in previous work, the electrical characteristics of the fabricated FETs could be much improved as expected. The electronic characteristic instrument was from Keithley Co., Inc.
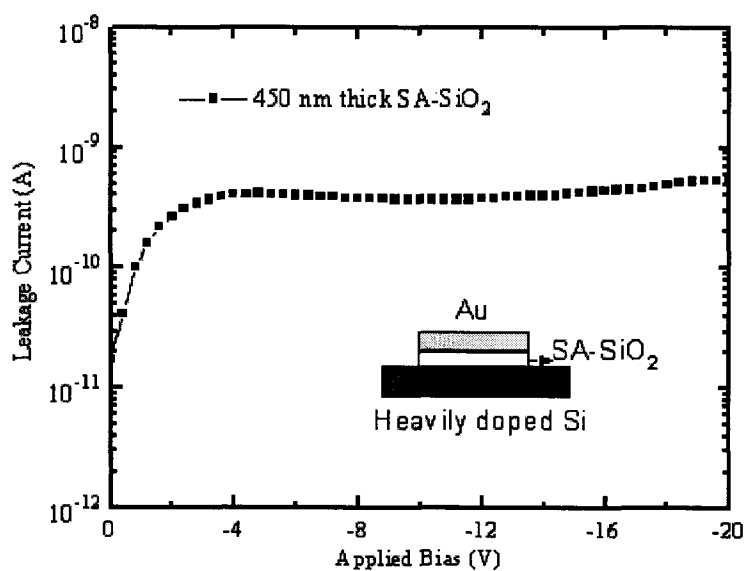

Figure 1 Gate leakage characteristic of the Au/self-assembled SiO_2/heavily-doped Si structure
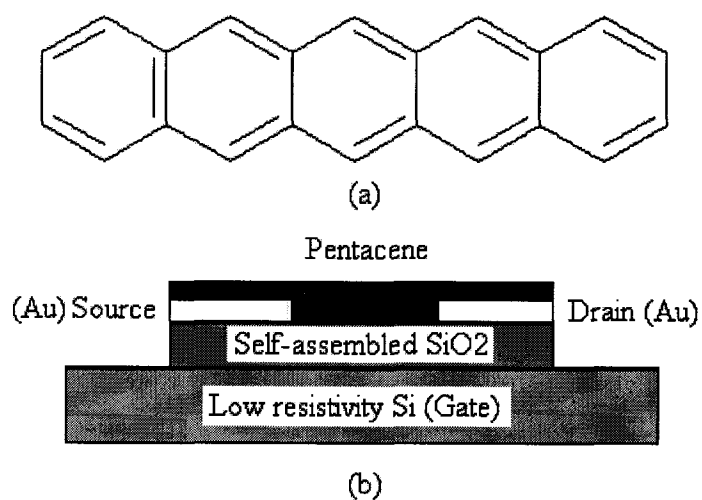

(a)

Pentacene

(b)

Figure 2 Schematic structures (a) chemical structure of pentacene molecular, (b) Organic FET

3 Results and Discussions

By assuming that the MOS theory of the traditional MOSFETs is still effective for the organic FETs, the drain current in the linear region and the saturation region can be expressed by the following equations.:

$$I_D = \frac{W\mu_{FET}C_{ox}}{L} V_{DS}(V_{GS} - V_{th}) \tag{1}$$

$$I_{Dsat} = \frac{W\mu_{FET}C_{ox}}{2L} (V_{GS} - V_{th})^2 \tag{2}$$

where W and L are the channel width and length, respectively, μ_{FET} is the field-effect mobility of the charge carrier in the pentacene channel, $C_{ox} = \varepsilon_{ox}/d_{ox}$ is the gate dielectric capacitance per unit area (ε_{ox} and d_{ox} are the dielectric constant and the thickness of the self-assembled SiO_2 gate dielectric layer, respectively), and V_{GS}, V_{DS}, V_{th} are the gate-source voltage, the drain-source voltage, and the threshold voltage, respectively.

The I_D-V_{DS} drain characteristics of a typical pentacene FET fabricated with self-assembled SiO_2 as the gate dielectric are shown in Figure 4. This device has a channel length and width of 25 and 500 μm, respectively, and a gate dielectric layer 450 nm thick.

The average density of SiO_2 / PDDA multilayers is $<\rho> = 1.43 \pm 0.05$ g/cm^3. SiO_2 / PDDA film volume composition is: 70 % SiO_2 + 10 % polycation + 20 % air-filled pores. These pores are formed by closely packed 45-nm SiO_2 and have a typical dimension of 20 nm. The films have controlled pores, which can be varied by the selection of the nanoparticle diameter.

If the layer of silicon dioxide were produced by conventional thermal oxidation, the dielectric constant would be 3.9.
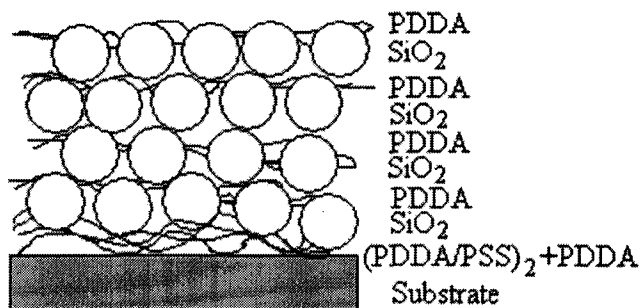
(a)
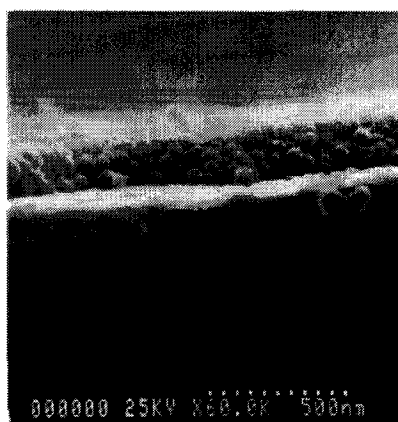
(b)

Figure 3 (a) Schematic diagram of self-assembly of SiO_2 nanoparticles on a silicon substrate, (b)nano-assembled SiO_2 nanoparticles 45nm in diameter

The following relationship is obtained between adsorbed mass M (g) and frequency shift ΔF (Hz) by taking into account the characteristics of quartz resonators used:

$$\Delta F = -1.83 \times 10^8 \, M/A \qquad (3)$$

where A is the apparent area of quartz microbalance placed between QCM electrodes. This is $0.16 \pm 0.01 \text{ cm}^2$ in our system. Then, one finds that 1 Hz change in ΔF corresponds to 0.9 ng in weight. The thickness of the alternate layer corresponding to QCM frequency shift was determined by SEM observation of the film cross-section from SEM images of cut resonators coated with silicon/polycation films, which gives the following relationship with ± 5 % error:

$$d\ (nm)\ =\ 0.022\ (-\Delta F)\ (Hz) \tag{4}$$
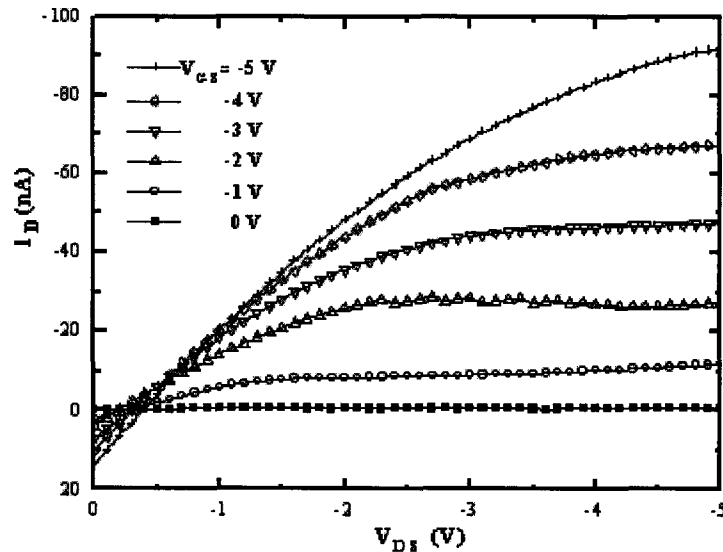
Figure 4 Drain characteristics of pentacene FET on SA-SiO$_2$ with L/W=25/500

In pentacene organic FETs, the current between the drain and the source I$_D$ is controlled by the applied gate-source voltage V$_{GS}$. Since pentacene is a p-type polymeric semiconductor, pentacene FETs generally operate in the accumulation mode with the negative bias on drain-source and the gate-source electrodes. The negative gate bias will enlarge the conduction channel due to the formation of a hole accumulation layer. Thus, the conductivity of the channel between the drain and the source is increased with the negative gate bias.

Figure 5 shows the measured gate transfer characteristics of the same pentacene organic FET described above. The field-effect mobility is generally determined in the region where the drain current saturates according to the equation (2). From the slope of the square root of the saturation current as a function of the gate voltage as shown in Figure 5, a field-effect mobility of 0.064 cm^2/Vs was extracted at the small V$_{DS}$ of -3 V. By linearly extrapolating the curve to the V$_{GS}$ axis, the threshold voltage V$_{th}$ can be

extracted to be 0.3 V. When the V_{DS} of -3 V was applied and the gate voltage were swept from 2 V to -10 V, the threshold slope was obtained to be about 1.4 V/decade, and the on/off current ratio was about 10^3.
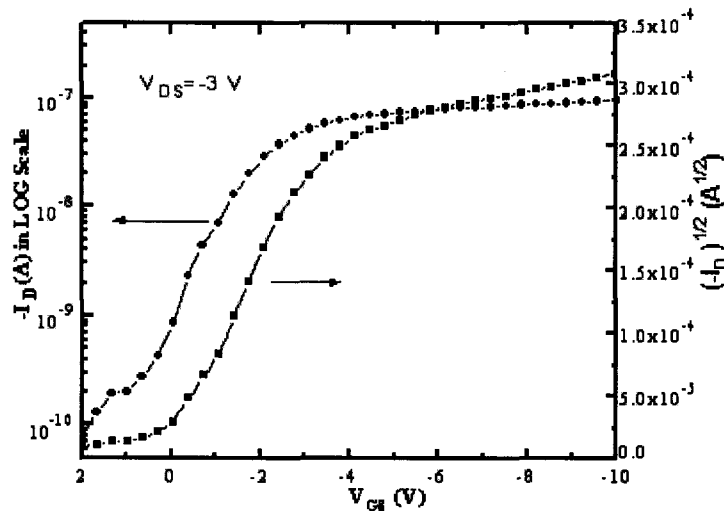
Figure 5 Gate characteristics of pentacene FET on SA-SiO2 with L/W=25/500 um

4 Conclusions

In summary, we have demonstrated the low-cost and low-temperature fabrication process of organic field-effect transistors (OFETs) using self-assembled SiO_2 as a gate dielectric material and pentacene as a semiconductor. 10 layers of SiO_2 nanoparticles 45 nm in diameter were self-assembled to form the dielectric layer, which has a breakdown field larger than 0.44 MV/cm. The fabricated transistors have a threshold voltage of 0.3 V, a field-effect mobility of 0.064 cm^2/Vs, and an on/off current ratio of about 10^3. Due to the low-cost and low-temperature advantages of the fabrication process, self-assembly is particularly suitable for the fabrication of OFETs.

APPENDIX C

PUBLICATIONS

<u>1 Journal Papers</u>

(1) F. Hua, **J. Shi**, Y. Lvov, and T. Cui, "Patterning of Layer-by-layer Self-assembled Multiple Types of Nanoparticle Thin Films by Lithographic Techniques", *Nano Letters*, Vol.2, No.11, 2002: pp1119-1222.

(2) **J. Shi**, F. Hua, T. Cui, and Y. Lvov, "Temperature Effect on Layer-by-Layer Self-Assembly of Linear Polyions and Silica Multilayer", *Chemistry Letters*, Vol.32, No.4, 2003: 316-317.

(3) F. Hua, **J. Shi**, Y. Lvov, and T. Cui, "Fabrication and Characterization of MOS-Capacitors Based on Layer-by-Layer Self-Assembly Thin Films", *Nanotechnology*, Vol.14, No.4, 2003: 453-457.

(4) **J. Shi,** T.Cui "Fabrication of indium resistors by layer-by-layer nanoassembly and microlithography techniques", *Solid State Electronics*, Vol. 47, No. 11, 2003:2085-2088

(5) T. Cui, G. Liang and **J. Shi**, "Organic Field-Effect Transistors Containing SiO2 Nanoparticle Thin Film as the Gate Dielectric", *Journal of Nanoscience and Nanotechnology*, Vol. 3, No.6, 2003.

<u>2 Conference Papers</u>

(6) Invited Presentation: Tianhong Cui, Yuri Lvov, Feng Hua, and **Jingshi Shi**, "Novel Lithography-based Approaches to Pattern Layer-by-layer Self-Assembled Thin Films", *ASME* International Mechanical Engineering Congress & Expositions, New Orleans, November 17-22, 2002.

(7) Tianhong Cui, Feng Hua, **Jingshi Shi**, and Yuri Lvov, "Lithographic Approach to Pattern Multiple Nanoparticle Thin Film Prepared by Layer-by-Layer Self-Assembly for Microsystems", submitted to *TRASDUCERS'03*, 2002.

(8) Tianhong Cui Guirong Liang, and **Jingshi Shi**, "Fabrication of Pentacene Organic Field-Effect Transistors Containing self-assembled SiO2 Nanoparticle Thin Film as the Gate Dielectric,"*IEDM* (2003).

(9) Yuri Lvov, Feng Hua, **Jingshi Shi**, Tianhong Cui, "Marriage" of LbL-Nanoassembly and Traditional Lithography for Microelectronics Element Production," *226th National American Chemical Soc. Meeting*, New York, September 7, 2003.

(10) Feng Hua, **Jingshi Shi**, Yuri Lvov, and Tianhong Cui, "Patterning of Nanoparticle Thin Films by Layer-by-Layer Self-assembly for Microelectronic Devices", *the 1st International Symposium on Nanomanufacturing*, MIT, Cambridge, Ma, on April 24-26, 2003.

(11) Dinesh Kommireddy, **Jingshi Shi**, Haifeng Ji, Yuri Lvov, "Electrostatic Layer-by-Layer Nano-Assembly: Films, Micropatterns, Cantilevers, Nanocapsules, *SPIE Optics East 2004*.

3 Book Chapter

(12) Invited chapter, Tianhong Cui, Yuri Lvov, **Jingshi Shi**: "Layer-by-Layer Self-Assembly for Polymer Microelectronics", " *Encyclopedia of Nanoscience and Nanotechnology* ", 2004.

4 Disclosure

(13) Tianhong Cui, Yuri Lvov, Feng Hua, and **Jingshi Shi**: "Layer-by-Layer Self-assembled Microelectronics Devices", disclosure to Louisiana Tech University in 2003.

REFERENCES

[1]   C. Joachim, J. K. Gimzewski and A. Avir am, *Nature*, 2000, 408, 541.

[2]   From *the Foundation of American Communication*, Science and Technology.

[3]   N*ational Nanotechnology Initiative*: Leading to the Next Industrial Revolution, pp.15, 2000

[4]   *National Nanotechnology Initiative*: Leading to the Next Industrial Revolution, pp.16-20, 2000

[5]   M. Bockrath, *Science*, 1997, 275,1922.

[6]   H. Doumanidis, *Nanotechnology*, 2002, 13, 248.

[7]   A. Ulman, *An Introduction to Ultrathin Films, from Langmuir-Blodgett to Self-Assembly*; Academic Press: Boston, 1991, p.1-440

[8]   Bornside, *J. Imaging Technology*, 1987,13, 122.

[9]   G. M. Whitesides and B. Grzybowski, *Science*, 2002, 295, 2418.

[10]   G. M. Whitesides, J. P. Mathias and C. T. Seto, *Science*, 1991, 254 1312

[11]   J. S. Lindsey, *New J. Chem.*, 1991, 15, 153.

[12]   K. B. Blodgett, *Phys. Rev.*, 1937, 51 964.

[13]   D. F. Evans and H. Wennerstrom, *The Colloidal Domain: Where Physics, Chemistry, Biology and Technology Meet* 2nd edn (New York: Wiley–VCH), 1999.

[14]   S. Chen, Langmuir, 2001,17, 2878.

[15]   Y. Tian and J. H. Fendler, *Chem. Mater.*, 1996, 8, 969.

[16]   F. Feng, T. Miyashita, Y. Amao and K. Asai, *Thin Solid Films*, 2000, 366, 255.

[17]   J. Cha, Y. K. See, J. Lee and T. Chang, *Synth. Met.*, 2001,117, 149.

[18]   C. J. Brinker, Y. Lu, A. Sellinger and H. Fan, *Adv. Mater.*, 1999, 11 579.

[19]   T. Thurn-Albrecht, R. Steiner, J. DeRouchey, C. M. Stafford, E. Huang, M. Bal, M. Tuominen, C. J. Hawker and T. P. Russell, *Adv. Mater.*, 2000,12, 787.

[20]   K. Nagayama, *Colloids Surf. A*, 1996, 109, 363.

[21]   R. K. Iler, *J. Colloid Interface Sci.*, 1966, 21, 569.

[22]   S. Keller, H-N. Kim and T. Mallouk, *J. Am. Chem. Soc.*, 1994,116, 8817.

[23]   G. Decher, *Science*, 1997, 227, 1232.

[24]   G. Decher and J. Schlenoff, *Multilayer Thin Films: Sequential Assembly of Nanocomposite Materials*, John Wiley Publ., NY, Berlin, 2003, p. 1-543

[25]   P. Bertrand, A. Jonas, A. Laschevsky, and R. Legras, *Macromol. Rapid Commun.*, 2000, 21, 319.

[26]   Y. Lvov and G. Decher, *Crystallography Reports*, 1994, 39, 628.

[27]   G. Decher, J. Schmitt and B. Struth, *Curr. Opin. in Colloid & Interface Science*, 1998, 3, 32.

[28]   J. Schmitt, T. Grünewald, K. Krajer, P. Pershan, G. Decher and M. Löshe, *Macromolecules*, 1993, 26, 7058.

[29]   M. Leasche, J. Schmitt, G. Decher, W. Bouwman and K. Kjaer, *Macromolecules*, 1998, 31, 8893.

[30]   M. Tarabia, H. Hong, D. Davidov, S. Kirshtein, R. Steitz, R. Neumann and Y. Avny, *J. Appl. Phys.*, 1999, 83, 725.

[31]   D. Yoo, S. Shiratori and M. Rubner, *Macromolecules*, 1998, 31, 4309.

[32]   N. Hoogeveen, M. Cohen Stuart and G. Fleer, *Langmuir*, 12, 3675, 1996.

[33]   T. Farhat, G. Yassin, S. Dubas and J. Schlenoff, *Langmuir*, 1999, 15, 6621.

[34]   Y. Lvov, M. Onda, K. Ariga and T. Kunitake, *J. Biomater. Sci., Polym. Ed.*, 1998, 9, 345.

[35]   D. Elbert, C. Herbert and J. Hubbell, *Langmuir*, 1999, 15, 5355.

[36]   D. Yoo, J. Lee and M. Rubner, *Mat. Res. Symp. Proc.*, 1996, 413, 395.

[37]   Y. Lvov, S. Yamada and T.Kunitake, *Thin Solid Films*, 1997, 300, 107.

[38]   E. Kleinfeld and G. Ferguson, *Science*, 1994, 265, 370.

[39]   J. Schmitt, G. Decher, W. Dressik, R. Geer, R. Shashidhar and J. Calvert, *Adv. Mater.*, 1997, 9, 61.

[40]   S. Joly, R. Kane, L. Radzilovski, T. Wang, A. Wu, R. Cohen, E. Thomas and M. Rubner, *Langmuir*, 2000, 16, 1354.

[41]   J. Mendelsohn, C. Barrett, A. Pal, A. Mayes and M. Rubner, *Langmuir*, 2000, 16, 5017.

[42]   Y. Lvov, K. Ariga, I. Ichinose and T. Kunitake, *J. Am. Chem. Soc.*, 1995, 117, 6117.

[43]   Y. Lvov and H. Möhwald, *Protein Architecture: Interfacial Molecular Assembly and Immobilization Biotechnology*, Marcel Dekker Publ., 2000, NY, p. 125-136.

[44]   Y. Sun, X. Zhang, C. Sun, B. Wang and J. Shen, *Macromol. Chem. Phys.*, 1996, 197, 147.

[45]   M. Onda, K. Ariga and T. Kunitake, *J. Ferment. Bioengin.*, 1999, 87, 69.

[46]   K. Sirkar, A.Revzin, M. Pishko, *Anal Chem.*, 2000, 72, 2930.

[47]   M. Sano, Y. Lvov and T. Kunitake, *Ann. Rev. Material Science*, 1996, 26, 153.

[48]   Tsukruk, F. Rinderspacher and V. Bliznyuk, *Langmuir*, 1997,13, 2171.

[49]   Y. Lvov, H. Haas, G. Decher, H. Möhwald, A. Mikhailov, B. Mtchedlishvily, E. Morgunova and B. Vainshtein, *Langmuir*, 1994,10, 4232.

[50]   J. Fendler and F. Meldrum, *Adv. Mater.*, 1995, 7, 607.

[51]   T. Cassagneau and J. Fendler, *Adv. Mater.*, 1998, 10, 877.

[52]   T. Cassagneau, J. Fendler and T. Mallouk, *Langmuir*, 2000,16, 241.

[53]   I. Pastoriza-Santos, D. Koktysh, A. Mamedov, M. Giersig, N. Kotov and L. Liz-Marzan, *Langmuir*, 2000, 16, 2731.

[54]   F. Caruso, A. Susha, M. Giersig, and H. Möhwald, *Adv. Mater.*, 1999, 11, 950.

[55]   T. Vossmeyer, S. Jia, E.Delonno, M. Diehl, S.H. J. Kim, *Appl. Phys*, 1998, 84, 3664.

[56]   C. Haynes, Van R. Duyne, *J. Phys. Chem. B*, 2001,105, 5599.

[57]   C. Hulteen, A. Treichel, *J. Phys. Chem. B*, 1999, 103, 3854.

[58]   K. Chen, X. Jiang, L. Kimerling, P. Hammond, *Langmuir*, 2000, 16, 7825.

[59]   X. Jiang, P. Hammond, *Langmuir*, 2000, 16, 8501.

[60]   X. Jiang, H. Zheng, S. Gourdin, P. Hammond, *Langmuir*, 2002, 18, 2607.

[61]   H. Zheng, I. Lee, M. Rubner, P. Hammond, *Adv. Mat.*, 2002, 14, 681.

[62]   E. Kim, Y. Xia, G. Whitesides, *Adv. Mat.*, 1996, 8, 245.

[63]   T. Vargo, J. Calvert, K. Wynne, J. Avlyanov, A. MacDiarmid, M. Rubner, *Supramol. Sci.*, 1995, 2, 169.

[64]   M. A. McCord, M. J. Rooks, *SPIE Handbook of Microlithography, Micromaching and Microfabrication.*

[65]   R. K. J., Iler, *Colloid Interface Sci.*, 1966, 21, 569.

[66]   G. Decher, J. D. Hong, J. Schmitt, *Thin Solid Films*, 1992, 210, 831.

[67]   G. Decher, J. Schmitt, *Prog. Colloid Polym. Sci.*, 1992, 89, 160.

[68]   S. T. Dubas, J. B. Schlenoff, *Macromolecules*, 1999, 32, 8153.

[69]   J. Krý'z, H. J.Dautzenberg, *Phys. Chem. A*, 2001, 105, 3846.

[70]   P. T. Hammond, *Curr. Opin. Colloid Interface Sci.*, 2000, 4, 430.

[71]   J. H. Cheung, A. F. Fou, M. F. Rubner, *Thin Solid Films*, 1994, 244, 985.

[72]   Y. M. Lvov, G. N. Kamau, D. L. Zhou, J. F. Rusling, 1999, *J. Colloid Interface Sci.*, 212, 570.

[73]   J. W. Ostrander, A. A. Mamedov, N. A. Kotov, *J. Am. Chem. Soc.*, 2001, 123, 1101.

[74]   A. Mamedov, J. Ostrander, F. Aliev, N. A. Kotov, *Langmuir*, 2000, 16, 3941.

[75]   Y. Lvov, K. Ariga, I. Ichinose, T. Kunitake, *J. Chem. Soc.*, 1995, 2313.

[76]   X. Arys, A. M. Jonas, A. Laschewsky, R. Legras, In *Supramolecular Polymers; Ciferri, A.,* Ed.; M. Dekker: New York, 2000; p 505.

[77]   G. Decher, J. P. Sauvage, M. W. Hosseini, In *Comprehensive Supramolecular Chemistry*, Pergamon Press: Oxford, 1996; Vol. 9, Chapter 14.

[78]   D. Bertrand, A. Jonas, A. Laschewsky, R. Legras, *Macromol. Rapid Commun.*, 2000, 21, 319.

[79]   S. T. Dubas, J. B. Schlenoff, *Macromolecules*, 1999, 32, 8153.

[80]   Y. Lvov, K. Ariga, I. Ichinose and T. Kunitake, *Langmuir*, 1997,13, 6195.

[81]   Y. Lvov, J. Rusling, D. Thomsen, F. Papadimitrakopoulos, T. Kawakami and T. Kunitake, *Chem. Commun.*, 1998, 1229.

[82]   V. Bliznyuk and V. Tsukruk, *Polymer Prep.*, 1997, 38, 963.

[83]   F. Caruso, A. Susha, M. Giersig, and H. Möhwald, *Adv. Mater.*, 1999, 11, 950.

[84]   G. Decher, M. Eckle, J. Schmitt, B. Struth, *Curr. Opin. Colloid Interface Sci.*, 1998, 3, 32.

[85]   J. J. Harris, M. L. Bruening, *Langmuir*, 2000, 16, 2006.

[86]   T. Cao, J. Chen, Ch.Yang, W. Cao, *Macromol. Rapid Commun.*, 2001, 22, 181.

[87]   G. B. Sukhorukov, A. A. Antipov, A. Voigt, E. Donath, H. Mo"hwald, *Macromol. Rapid Commun.*, 2001, 22, 44.

[88]   D. Yoo, S. S. Shiratori, M. F. Rubner, *Macromolecules*, 1998, 31, 4309.

[89]   A. F. Xie, S. Granick, *Macromolecules*, 2002, 35, 1805.

[90]   J. D. Mendelsohn, C. J. Barrett, V. Chan, A. J. Pal, A. M. Mayes, M. F. Rubner, *Langmuir*, 2000, 16, 5017.

[91]   D. Yoo, S. S. Shiratori, M. F. Rubner, *Macromolecules*, 1998, 31, 4309.

[92]   S. S. Shiratori, M. F. Rubner, *Macromolecules*, 2000, 33, 4213.

[93]   J. D. Mendelsohn, C. J. Barrett, V. V. Chan, A. J. Pal, A. M. Mayes, , M. F. Rubner, *Langmuir*, 2000, 16, 5017.

[94]   S. A. Sukhishvili, S. J. Granick, *Am. Chem. Soc.*, 2000, 122, 9550.

[95]   M. Castelnovo, J. F. Joanny, *Langmuir*, 2000, 16, 7524.

[96]   S. Y. Park, C. J. Barrett, M. F. Rubner, A.M. Mayes, *Macromolecules*, 2001, 34, 3384.

[97]   S. T. Dubas, J. B. Schlenoff, *Macromolecules*, 2001, 34, 3736.

[98]   S. A. Sukhishvili, S. J. Granick, *Am. Chem. Soc.*, 2000, 122, 9550.

[99]   P. Hammond, G. M. Whitesides, *Macromolecules*, 1995, 28, 7569.

[100]   M. Sano, Y. Lvov and T. Kunitake, *Ann. Rev. Material Science*, 1996, 26, 153.

[101]   D. Elbert, C. Herbert and J. Hubbell, *Langmuir*, 1999, 15, 5355.

[102]   K. Bu¨ scher, G. Karlheinz, H. Ahrens, C. A. Helm, *Langmuir*, 2002, 18, 3585.

[103]   Y. Lvov, K. Ariga, M. Onda, I. Ichinose and T. Kunitake, *Langmuir*, 1997, 13, 6195.

[104]   J. D. Meindl, *Microelectronic Circuit Elements*. Scientific American, 1977, September, pp. 70-81.

[105]   A. C. Templeton, W. P. Wuelfing and R. W. Murray, *Acc. Chem. Res.*, 2000, 33, 27.

[106]   J. H. Fendler, *Chem. Mater.*, 2001, 13, 3196.

[107]   A. N. Shipway and I. Willner, *Chem. Commun.*, 2001, 2035.

[108]   J. H. Fendler, *Chem. Mater.*, 1996, 8, 1616.

[109]   M. Dorogi, J. Gomez, R. Osifchin, R. P. Andres, R. Reifenberger, *Phys. ReV. B*, 1995, 52, 9071.

[110]   J. W. Fendler, F. C. Meldrum, *Adv. Mater.*, 1995, 7, 607.

[111]   F. Bertrand, A. Jonas, A. Laschewsky, R. Legras, *Macromol. Rapid Commun.*, 2000, 21 319.

[112]   C. Mingotaud, P. Delhaes, M. W. Meisel, D. R. Talham, *Magnetism, Molecules to Materials*, 2001, 2, 457.

[113]   Y. Liu, Y. Wang and R. O. Claus, *Chem. Phys. Lett.*, 1998, 298, 315.

[114]   J. F. Hicks, Y. Seok-Shon and R. W. Murray, *Langmuir*, 2002, 18, 2288.

[115]   D. Laurent and J. B. Schlenoff, *Langmuir*, 1997, 13, 1552.

[116]   J. Hodack, R. Etchenique and E. Calvo, *Langmuir*, 1997, 13, 2708.

[117]   N. Ferreyra, L. Coche-Guérente, P. Labbe, E. Calvo and V. Solis, *Langmuir*, 2003, 19, 3864.

[118]   M. F. Durstock, M. F. Rubner, *Langmuir*, 2001, 17, 7865.

[119]   S. Toyota, T. Nogami, H. Mikawa, *Solid State Ionics*, 1984,13, 243.

[120]   T. R. Farhat, J. B. Schlenoff, *Langmuir*, 2001, *17*, 1184.

[121]   J. F. LeNest, A. Gandini, *In Second International Symposium on Polymer Electrolytes*; Scrosati, B., Ed.; Elsevier Science Publishing Co., Inc.: New York, 1990; pp 129-141.

[122]   C. Berthier, W. Gorecki, M. Minier, M. B. Armand, J. M. Chabagno, P. Rigaud, *Solid State Ionics*, 1983, 11, 91.

[123]   T. Mimani and K. C. Patil, *Mater. Phys. Mech.*, 2001, 4, 134.

[124]   Y. Lvov, K. Ariga, M. Onda, I. Ichinose, T. Kunitake, *Langmuir*, 1997, 13, 6195.

[125]   N. A. Kotov, I. Dekany, J. H. Fendler, *J. Phys. Chem.*, 1995, 99, 13065.

[126]   S. Dante, Z. Z. Hou, S. Risbud, P. Stroeve, *Langmuir*, 1999, 15, 2176.

[127]   Y. J. Liu, Y. X. Wang, R. O. Claus, *Chem. Phys. Lett.*, 1998, 298, 315.

[128]   A. Otto, I. Mrozek, H. Grabhorn, W. Akemann, *J. Phys.: Condens. Matter*, 1992, 4, 1143.

[129]   W. L. Barners, *J. Mod. Opt.*, 1998, 45, 661.

[130] D. L. Schulz, C. J. Curtis and D. S. Ginley, *Electrochemical and Solid-State Letters*, 2001, 4, C58.

[131] C. A. Bulthaup, E. J. Wilhelm, B. N. Hubert, B. A. Ridley and J. M. Jacobson, *Applied Physics Letters*, 2001, 79, 1525.

[132] Y. Xia, J. Tien, D. Qin, G. M. Whitesides, *Langmuir*, 1996, 12, 4033.

[133] F. Hua, T. Cui, and Y. Lvov, *Langmuir*, 2002 18, 6712.

[134] F. Hua, Y. Lvov, and T. Cui, *Journal of Nanoscience and Nanotechnology*, 2002, 2, 357.

[135] F. Hua, J. Shi, Y. Lvov, and T. Cui, *Nano Letters*, 2002, 2, 1119.

[136] F. Hua, J. Shi, Y. Lvov, and T. Cui, *Nanotechnology*, 2003 14, 453.

[137] P. Bertrand, A. Jonas, A. Laschevsky, and R. Legras, *Macromol. Rapid Commun.*, 2000, 21, 319.

[138] Y. Lvov, G. Decher and H. Möhwald, *Langmuir*, 1993, 9, 481.

[139] S. Keller, H-N. Kim and T. Mallouk, *J. Am. Chem. Soc.*, 1994, 116, 8817.

[140] Haverkorn von Rijsewijk HC, Legierse PEJ, Thomas GE. 1982. *Philips Tech. Rev* 40:287–97

[141] S.J. Clarson, J.A. Semlyen, eds. 1993. *Siloxane Polymers*. Englewood Cliffs, NJ: Prentice Hall

[142] T. Thundat, R. J. Warmack, G. Y. Chen, D. P. Allison, *Appl. Phys. Lett.*, 1994, 64, 2894.

[143] T. Thundat, E. A. Wachter, S. L. Sharp, R. J. Warmack, *Appl. Phys. Lett.*, 1995, 66, 1695.

[144] H.-J. Butt, *J. Colloid Interface Sci.*, 1996, 180, 251.

[145] A. M. Moulin, S. J. O'Shea, R. A. Badley, P. Doyle, M. E. Welland, *Langmuir*, 1999, 15, 8776.

[146] J. Fritz, M. K. Baller, H. P. Lang, H. Rothuizen, P. Vettiger, E. Meyer, H.-J. Gu¨ntherodt, C. Gerber, J. K. Gimzewski, *Science*, 2000, 288, 316.

[147] R. Raiteri, G. Nelles, H.-J. Butt, W. Knoll, P. Skladal, *Sensor Actuat. B-Chem.*, 1999 61, 213.

[148] J. Fritz, M. K. Baller, H. P. Lang, H. Rothuizen, P. Vettiger, E. Meyer, H. -J. Güntherodt, C. Gerber, and J. K. Gimzewski, *Science*, 2000, 228, 316.

[149] A. Blachard, *Genetic Engineering, Principles and Methods*, vol. 20, Plenum Press, New York, 1998.

[150] M. Schena, R. A. Heller, T. P. Theriault, K. Konrad, E. Lachenmeier, R. W. Davis, *M Trends Biotechnol.*, 1998, 16, 301.

[151] G. Y. Chen, T. Thundat, E. A. Wachter, R. J. Warmack, *J. Appl. Phys.*, 1995, 77, 3618.

[152] ASTM Standard E1392-90, *Standard Practice for Angle Resolved Optical Scatter Measurements on Specular or Diffuse Surfaces* (American Society for Testing and Materials, Philadelphia, PA., 1991).

[153] T. V. Vorburger, E. Marx, and T.R. Lettieri, *Applied Optics*, 1993, 32, 3401.

[154] P. A. Chiarelli, M. S. Johal, D. J. Holmes, J. L. Casson, J. M. Robinson, H. L. Wang, *Langmuir*, 2002,18,168.

[155] J. Cho, K. Char, J. D. Hong, K. B. Lee, *Adv. Mater.*, 2001,14, 1076.

[156] P. A. Chiarelli, M. S. Johal, D. J. Holmes, J. L. Casson, J. M. Robinson, J. B. Roberts, H. L.Wang, *Adv. Mater.*, 2001,15, 1167.